JAEA-Research
2007-033

JAEA-Research

Development of ACROSS (Accurately Controlled, Routinely Operated, Signal System) to Realize Constant Monitoring the Invisible Earth's Interiors by Means of Stationary Coherent Elastic and Electromagnetic Waves

Mineo KUMAZAWA, Takahiro KUNITOMO
Takahiro NAKAJIMA, Kayoko TSURUGA*
Yoko HASADA*, Hiromichi NAGAO*
Hiroshi MATSUMOTO*, Junzo KASAHARA*
Naoyuki FUJII and Naotaka SHIGETA

Neotectonics Research Group
Geological Isolation Research and Development Directorate

March 2007

Japan Atomic Energy Agency

日本原子力研究開発機構

本レポートは日本原子力研究開発機構が不定期に発行する成果報告書です。
本レポートの入手並びに著作権利用に関するお問い合わせは、下記あてにお問い合わせ下さい。
なお、本レポートの全文は日本原子力研究開発機構ホームページ（http://www.jaea.go.jp/index.shtml）より発信されています。このほか財団法人原子力弘済会資料センター*では実費による複写頒布を行っております。

〒319-1195　茨城県那珂郡東海村白方白根２番地４
日本原子力研究開発機構　研究技術情報部　研究技術情報課
電話 029-282-6387, Fax 029-282-5920

*〒319-1195　茨城県那珂郡東海村白方白根２番地４　日本原子力研究開発機構内

This report is issued irregularly by Japan Atomic Energy Agency
Inquiries about availability and/or copyright of this report should be addressed to
Intellectual Resources Section, Intellectual Resources Department,
Japan Atomic Energy Agency
2-4 Shirakata Shirane, Tokai-mura, Naka-gun, Ibaraki-ken 319-1195 Japan
Tel +81-29-282-6387, Fax +81-29-282-5920

JAEA-Research 2007-033

Development of ACROSS (Accurately Controlled, Routinely Operated, Signal System) to Realize Constant Monitoring the Invisible Earth's Interiors by Means of Stationary Coherent Elastic and Electromagnetic Waves

Mineo KUMAZAWA※, Takahiro KUNITOMO※, Takahiro NAKAJIMA※
Kayoko TSURUGA[*1], Yoko HASADA[*2], Hiromichi NAGAO[*3], Hiroshi MATSUMOTO[*4]
Junzo KASAHARA[*5], Naoyuki FUJII※ and Naotaka SHIGETA+

Tono Geoscientific Research Unit,
Geological Isolation Research and Development Directorate,
Japan Atomic Energy Agency
Tokai-mura, Naka-gun, Ibaraki-ken

(Received January 30, 2007)

The developmental study made at Tono Geoscience Center under the Earthquake Frontier Research Project since 1996 is reported for a brand new technology system called ACROSS (Accurately Controlled, Routinely Operated, Signal System invented at Nagoya University in 1994). Various technology elements have been combined together under a specific theoretical framework for the underground exploration and monitoring of structures and physical states. The ACROSS is essentially a spectroscopy of the underground space consisted of complex media subjected to environmental noise. The robustness against noise is devised by utilizing coherent elastic and electromagnetic waves with phase controlled very accurately. Demanded hardware technology has been developed successfully and know how has been accumulated for practical applications. Accurate synchronization of transmission and observation systems has provided us with reliable data on the tensor transfer function between the source and receiver, which is

---

+ Horonobe Underground Research Unit
※ Invited Researcher
[*1] The University of Tokyo
[*2] Nagoya University
[*3] Japan Agency for Marine-Earth Science and Technology
[*4] Toyama University
[*5] Japan Continental Shelf Survey, Co. Ltd.

equivalent to Green function within a limited frequency range. Several examples of the field application are demonstrated by the test experiments at Tono Mine site. After the developmental works of 10 years, the ACROSS is brought to be a practical method applied to the remote monitoring of temporal variation of underground states at the Horonobe Underground Research Laboratory and also it is being applied to the expected focal region of the coming Tokai earthquake near Hamaoka in Shizuoka prefecture. Whereas ACROSS technology is not mature enough yet, it is shown to be a potential and versatile methodology applied even for the health monitoring of the construction such as building strongly coupled with the ground in addition to the underground study.

Keywords: ACROSS, Active Monitoring, Earth, Earth Electromagnetism, Earthquake Frontier Research Project, Elastic Wave, Electromagnetic Wave, Frequency Characteristic, Geophysical Exploration, Geophysical Prospecting, Linear Dynamics System, Seismology, Subsurface, Tono Mine, Underground

弾性波および電磁波により地球内部の常時モニタリングを実現するアクロスの開発

日本原子力研究開発機構地層処分研究開発部門
東濃地科学研究ユニット
熊澤　峰夫※, 國友　孝洋※, 中島　崇裕※, 鶴我　佳代子[*1], 羽佐田　葉子[*2],
長尾　大道[*3], 松本　裕史[*4], 笠原　順三[*5], 藤井　直之※, 茂田　直孝†

（2007 年 1 月 30 日受理）

本件は、アクロス（Accurately Controlled, Routinely Operated, Signal System）と呼ばれる新しい地下探査技術の開発に関する成果報告書である。アクロス研究は、1994 年に名古屋大学で開始され、1996 年 4 月から 2006 年 3 月までは、陸域地下構造フロンティア研究プロジェクトとして、東濃地科学センターが主体となって行ってきた。アクロスは、地下の構造と物理的な状態とを探査あるいは監視するために考案された理論体系に基づいて、それを実現するための様々な要素技術を一つの技術体系として統合したものである。本質的には、複合的な媒質から構成された地下空間に対する周波数特性の分析装置であり、精密に位相制御された弾性波や電磁波を常時連続的に送受信することで、ノイズに最も強いシステムとしている。本研究では、その実現のために必要な技術や装置の開発を進め、実践的な応用に関するノウハウを蓄積してきた。アクロスのデータは、送信点と受信点との間のテンソル伝達関数（グリーン関数）として得られ、その信頼性は、送信システムと受信システムとの正確な同期によって担保される。本報告書では、東濃鉱山のテストサイトで行われた様々な研究を中心に紹介する。また、10 年間におよぶ開発成果を応用して、幌延深地層研究センターで地下の時間変化を捉えようとする「遠隔監視システムの開発」や静岡県における東海地震の想定震源域の常時監視研究などが進められている。アクロスの技術としての熟成は、日進月歩で進んでおり、地下の研究に加えて、建造物などのヘルスモニタリングへの適用なども開始されてきている。

核燃料サイクル工学研究所：〒319-1194　茨城県那珂郡東海村村松 4-33
† 幌延深地層研究ユニット
※ 客員研究員
*1 東京大学
*2 名古屋大学
*3 （独）日本海洋研究開発機構
*4 富山大学
*5 日本大陸棚調査（株）

This is a blank page.

Contents

1. Introduction 1

2. Seismic ACROSS 13
2.1 Overview of Seismic ACROSS and its development 13
2.2 Transmitting and receiving technologies of the Seismic ACROSS 29
2.3 Field examples by Seismic ACROSS at the Tono Mine experimental site 41
2.4 A dense seismic array for acquisition of high quality data in the ACROSS observation 55

3. EM-ACROSS 73
3.1 Overview of EM-ACROSS and its development 73
3.2 Long-term operation of the EM-ACROSS and derived transfer function in the diffusion field region 84
3.3 Complex dielectric permittivity spectroscopy using ACROSS measurement system 96

4. Theory of data analysis and modeling 106
4.1 Optimum weighted stacking method for acquisition of the ACROSS transfer functions having the maximum signal-to-noise ratio 106
4.2 Travel time estimation from a transfer function in frequency domain: the revised Sompi event analysis 120
4.3 Numerical computation of wave fields and frequency wavenumber response characteristics of an isolated linear dynamic system 134

5. Target of constant monitoring 144
5.1 Proposal: Detection of transient phenomena due to the structure sensitivity of rocks in the crust and uppermantle 144

Acknowledgement 153

Appendix: Authors of the report 154

目次

1. 緒言 1

2. 弾性波アクロス 13
2.1 弾性波アクロスの概要とその開発 13
2.2 弾性波アクロスにおける送受信技術 29
2.3 東濃鉱山アクロス実験サイトでの観測結果 41
2.4 高品質信号取得のためのアクロス稠密地震計アレイ 55

3. 電磁アクロス 73
3.1 電磁アクロスの概要とその開発 73
3.2 電磁アクロスの長期観測と拡散場領域で得られた伝達関数 84
3.3 アクロス法を用いて測定した複素誘電率スペクトル 96

4. データ解析とモデリングの理論 106
4.1 最適重みつきスタッキング法による最大 SN 比を持つアクロス伝達関数の取得 106
4.2 周波数領域の伝達関数からの走時推定：改良存否イベント解析 120
4.3 孤立線形力学系の周波数・波数応答関数と波動場の数値計算 134

5. 常時監視のターゲット 144
5.1 地殻および上部マントルにおける岩石の構造敏感性を利用した遷移現象の検出 144

謝辞 153

付録：著者リスト 154

List of figures

Figure 1.1.1 Relationship among the different representations of a linear system model.
Figure 1.1.2 Noise processing to reach larger S/N by means of reasonable data stacking.
Figure 2.1.1 Observation site distribution around the transmission site.
Figure 2.1.2 Photograph and schematic of the Seismic ACROSS transmitters at the Tono Mine.
Figure 2.1.3 Layout of the Seismic ACROSS transmission site at the Tono Mine.
Figure 2.2.1 Schematic of the current Seismic ACROSS transmitter.
Figure 2.2.2 Phase angle variation with time of the eccentric mass at 25 Hz rotation.
Figure 2.2.3 Comparison of FM signal waves.
Figure 2.2.4 Continuous switch of rotational direction to obtain time series of transfer function by linear vibration with the signal unit ACROSS transmitter.
Figure 2.2.5 Particle motions of composite record sections of normal and reverse rotation of the Seismic ACROSS transmitter.
Figure 2.2.6 Observed amplitude spectrum in displacement during the 4th transmission.
Figure 2.3.1 An example of transmission force spectrum during the 4th transmission.
Figure 2.3.2 Procedure to switch the rotational direction.
Figure 2.3.3 Location map of the facilities in the Tono Mine ACROSS experimental site.
Figure 2.3.4 Definitions of vibration components at transmission site and at observation site.
Figure 2.3.5 Record sections of whole components during the 2nd transmission.
Figure 2.3.6 Record section of tT and vR components during the 2nd transmission.
Figure 2.3.7 Schematic view of geological cross section at the Tono Mine ACROSS experimental site.
Figure 2.3.8 Record sections overlapping of 576 traces during the 4th transmission.
Figure 2.3.9 Temporal variation of record section of tT component at No. 1 observation point and amount of rainfall per hour in observation area.
Figure 2.3.10 Temporal change of travel times of the direct S waves.
Figure 2.4.1 Flowchart of the data acquisition in the seismic ACROSS.
Figure 2.4.2 The analysis scheme to detect wave elements by SEA and investigate the temporal variations of intensity of the incident waves in a ray parameter space $\boldsymbol{p}(p_x, p_y)$.
Figure 2.4.3 Construction of slant stack processing and relationship of travel times between a slant-stacked time trace and an event time series by SEA.
Figure 2.4.4 Location map of ACROSS observation site.
Figure 2.4.5 Diagrams of the amplitude and phase spectra observed at the source and the receiver.

Figure 2.4.6 Diagrams of the complex spectra of the transfer function Htt and their time traces.
Figure 2.4.7 Space in the ray parameters (p_x,p_y) and an array response function.
Figure 2.4.8 An example of the detections of three wave elements by Sompi event analysis from the slant-stacked spectral data.
Figure 2.4.9 Elapsed time variations of amplitude of wave elements in the space of ray parameter (p_x,p_y).
Figure 3.1.1 Transfer function of the electromagnetic field propagating in the uniform medium.
Figure 3.1.2 Flow chart of the investigation by the EM-ACROSS.
Figure 3.1.3 The signal amplitude of the electromagnetic field emitted by the current dipole.
Figure 3.1.4 The apparent travel time between the source and receiver by the electromagnetic field.
Figure 3.2.1 Tono test site, the arrangement of transmitter and receiver.
Figure 3.2.2 The layout of transmitting electrodes and schematic view of the transmitting and system.
Figure 3.2.3 Amplitude spectrum of the transmitting signal.
Figure 3.2.4 The amplitude spectrum of observed magnetic and electric field.
Figure 3.2.5 The amplitude spectrum of observed electromagnetic field
Figure 3.2.6 Observed transfer function after 181 hours stacking.
Figure 3.2.7 Temporal variation of the phase of the electric field.
Figure 3.3.1 Models of frequency dependence of complex dielectric permittivity
Figure 3.3.2 The electric circuit used for complex dielectric permittivity measurement.
Figure 3.3.3 Method of electrode installation employed in this study.
Figure 3.3.4 Signal and noise in the voltage between the potential electrodes during the complex dielectric permittivity measurements.
Figure 3.3.5 Dielectric dispersion observation.
Figure 4.1.1 Location of Tono Mine and five Hi-net observatories.
Figure 4.1.2 The time series of noise level included in a signal channel.
Figure 4.1.3 Signal level and noise levels at each Hi-net station.
Figure 4.1.4 The growth curve of SNR in the case of seismic ACROSS.
Figure 4.1.5 The time series of electromagnetic noise level.
Figure 4.1.6 The growth curves of SNR in the case of EM-ACROSS.
Figure 4.2.1 The impulse response functions and the corresponding transfer functions.
Figure 4.4.2 Schematic image of a model in the Sompi Event Analysis.
Figure 4.2.3 The synthetic transfer function and the time-domain waveform.
Figure 4.2.4 The frequency dependency of noise amplitude.

Figure 4.2.5 Two-parameter AIC of all models for the previous method and revised method.
Figure 4.2.6 The results of travel-time estimation by the previous method and the revised method.
Figure 4.2.7 The decomposed wave elements and the residual.
Figure 4.3.1 FWR of a uniform medium within the Nyquist range.
Figures 4.3.2 Dispersion relation of particle velocity, travel time curve, and particle velocity.
Figures 4.3.3 FWR on the κ-κ' plane at a certain ω, and dispersion relation.
Figures 4.3.4 Travel time curve of particle velocity, and particle velocity.
Figure 5.1.1 Examples of distribution of structure sensitive bodies.
Figure 5.1.2 Logarithmic distribution spectrum of heterogeneities expected in the crust and upper mantle.

List of tables

Table 2.1.1 Specifications of the seismic ACROSS transmitters at the Tono mine.
Table 2.1.2 Outline of continuous transmission experiments from 18:00 JST on October 28, 2002 to 0:00 JST on December 31, 2006.
Table 2.2.1 Trouble list in the continuous transmissions from 18:00 JST on October 28, 2002 to 0:00 JST on December 31, 2006.

This is a blank page.

1. Introduction

1.1 preface

The difficulty of understanding the structures and physical states in the invisible interiors of the Earth has been a serious problem common to wide disciplines of science and technology. Typical examples are the prediction research works on the disastrous earthquakes and volcanic eruptions, the evaluation of long term stability of underground space for safe isolation of high level radioactive wastes, and also the exploration of underground resources such as oil, uranium and other metal ores.

One of the strong social demands has been the prediction of disastrous earthquakes, which may kill over 200,000 people at once as in the case of Sumatra earthquake of December 26, 2004. Therefore, seismologists have been working on geophysical exploration technology in addition to the extensive use in their research works without any success yet. Whereas the prediction of highly nonlinear phenomena such as earthquake occurrence is considered to theoretically be impossible, the practical prediction is supposed to be realized by appropriate monitoring of appropriate property of the target; the time-development of physical states at the expected focal region of the expected disastrous earthquakes. Recognizing the strong demand and importance of promoting the earthquake prediction research work, the Science and Technology Agency of Japan has launched the Earthquake Frontier Research Program in 1996 right after the Hyogoken-Nanbu earthquake on January 17, 1995, when over 6,400 citizens were lost in Kobe. Under this program, Tono Geoscience Center had started to develop a substantially new underground observation technology, called ACROSS. The idea of ACROSS has been born at Nagoya University and only a very small scale test experiment had just started in 1994. Consequently the major purpose of the development at Tono Geoscience Center had been placed only on the inland seismology for the earthquake prediction study, whereas ACROSS can be used for the reliable evaluation and monitoring of long term stability of the underground construction, and also exploration of the underground resources. The research and development group was organized under a name of 'ACROSS research team' led by Mineo Kumazawa of Nagoya University, and the study had lasted for 10 years till 2006, through the two phases of 5 year term.

This publication is intended to collect some of the basic works made mostly at and around Tono Mine test site in this research and development program at Tono Geoscience Center. Very recent works are not included, since urgent use of the developing technology (not mature enough yet, but appeared very promising) has been strongly demanded without appropriate supply of man power to use at the actual test sites. They are Horonobe for remote monitoring of the underground construction, and Morimachi (a new test site just between the Hamaoka Atomic Energy Power Plant and Tono Mine test site) for monitoring the focal region of coming disastrous Tokai earthquake in Shizuoka prefecture.

1.2 ACROSS as an active sounding tool for the underground space

Sounding is to obtain useful information by sending sound and hearing the echo. In the modern technology, it is usually made by transmitting elastic wave and/or electromagnetic wave or other agent and observing the response or returned waves. The structure of such sounding is regarded as a system analysis on a target; i.e. an analysis of linear dynamic system with an input as excitation and resulted output as response. Our developmental work of ACROSS (acronym of Accurately Controlled, Routinely Operated Signal System) is based on the consideration on how the system analysis of the underground can be made in a better way than previous approaches by organizing everything that appears essential for our purpose. Although the current level of theory and practice is still immature, we have been trying to trace the right way to go.

The continuous observation enables us to monitor the target. However, it is not self-evident how and to what we focus to reach the ultimate purpose of our concerns. Observation is made by waves, so that we have to study how our target looks like by waves. After the discussions on this matter, we review what we have to do in order to acquire the useful information on the underground space on the noisy ground surface. We noted that the most essential subject is the signal management and we call our technology by ACROSS. It means a 'Signal System', which is realized by 'Accurately Controlled' system that is to be 'Routinely Operated' to acquire time basically demanded to be robust against noise. The factors mentioned above are the necessary conditions but not sufficient ones yet. Additional requisite is the method of inverting the acquired data to what we really like to know. Consequently we have studied the wave theory in order to find out a better route to reach our target, although the current level is just at the beginning stage.

We shall shortly review only the basic framework of developmental study of ACROSS in this section. Some of the technical details together with prospect are reported by Kumazawa et al. [1]. At the end, we introduce how the developed ACROSS is being used, whereas the results have not yet come out visibly. However, an exciting finding is being made near the expected focal region of the coming Tokai earthquake. We are convincing that ACROSS would be recognized as one of the most important tools of studying the underground space within the next decade.

1.3 Interaction of materials to waves

Since we utilize waves for both input (excitation) and output (response) in our system analysis, the influences of the target materials and their spatial distribution to the wave propagation is the primary subjects to be considered. Our target medium is the heterogeneous structure consisting of a variety of different rocks, which are the heterogeneous polycrystalline composites consisting of a variety of mineral grains and possibly even a small amount of fluid.

Wave equation contains two independent medium parameters, density ρ and elastic constant c in elastic wave equation, and dielectric constant ε and magnetic permeability μ in electromagnetic wave (Maxwell's) equation. In both cases, the two parameters play their roles in wave propagation through two other parameters; wave impedance Z and wave slowness S as given by

$$S^2 = \sim(\rho/c)\ \sim(\mu\varepsilon) \tag{1.1.1}$$

$$Z^2 = \sim(c\rho)\ \sim(\mu/\varepsilon) \tag{1.1.2}$$

(The expressions as above are symbolic, since μ, ε and c are tensor.) These two are regarded as the primary observables in physics sense. Impedance is directly related to the refraction and transmission coefficients and scattering at the material boundary, so that it is useful in extracting the presence of sharp heterogeneity and its geometric information. The slowness (reciprocal of velocity; equivalent to refractive index) determines time delay of information propagation along the wave path constrained by Z and S. In this way, the use of waves for observation provides us with geometric structures with additional information on material parameters in a phenomenological sense.

As far as the sounding by using waves, we can utilize both elastic and electromagnetic waves almost in the same way in principle, whereas there are important differences both in method and target. The important difference lies on the difference in information carried by the observables in a sense of material sciences. The elastic slowness of the materials in the Earth's interiors has been studied considerably well and it can be used as a very good indicator of the material itself. Both Z and S in the rocks as polycrystalline aggregates are not constant but change with time due to the structure sensitivity, in which the macroscopic property evolves with time due to the small change of textures generated by the variation of tectonic stress and the resulted deformation. In particular, we note the presence of small amount of H_2O and its significant roles in controlling the kinetic properties of the materials even in the deep horizons of the Earth's interior. Water, we just call it by custom, is existent at the depth in many different forms with different functions:

(1) Hydrate minerals that are ductile, small Z and large S in comparison with the other anhydrous minerals. They are supposed to exist localized along the fault planes and are evolving in association with hydration and dehydration reactions.

(2) Supercritical fluid with hydrodynamic effects permeates through the texture as well as very strong catalytic agent with significant chemical activity, dissolving and making precipitation of everything depending on the change of physical conditions.

(3) Proton (hydrogen ion, H^+) in the crystalline lattice of mineral grains and interstitial fluid, which carries electric charge efficiently increases S and decreases Z, and significantly influences the propagation of electromagnetic wave. (Strictly speaking large mobility of proton contributes to electric conductivity σ, which is the main factor, $\sigma/i\omega$, of imaginary part of ε.)

The rheologic and kinetic properties represented by imaginary part of S and Z have the significant interaction with physical environments and the states of the materials themselves in a way of nonlinear feed back. In other words the simultaneous time-evolution of observables, the physical states and structure is supposed to take place, and this is what we expect to use for the monitoring the physical states in the Earth's interiors. For example, electromagnetic observation is more sensitive to the existence of 'water', whereas the elastic wave is more useful in extracting the information of the rheologic natures.

An important function demanded to sounding technology is the potential of observation by color or data acquisition as a function of frequency. There are two types of frequency dependence; one is the material dispersion originated from the structural sensitive nature of the material controlled by microscopic kinetic processes, and another is structure dispersion originated from resonance, when the spatial scales are in the same order of magnitude as wave length. Such dispersion provides us with the important clues to interpret the physical states together with structures, in particular. Observation by sweeping the frequency of transmission signal may be regarded as the sweeping survey of structure sensitivity with kinetic processes with different time scales and also of the geometric structures with different spatial scales. The background and examples of these subjects are discussed more in detail in later section in this publication.

The considerations as above lead to the necessary characteristics of spectroscopic observation to approach to our target. Our campaign towards the combined use and complimentary role of the elastic and electromagnetic waves in frequency domain goes as follows: Let us keep using both eyes (light as electromagnetic wave) and ears (sound as elastic wave; as bat utilize it to see) to look into the Earth's interiors by color to obtain better vision and thereby better understanding. The developmental works of ACROSS technology has been made along the concept of system analysis of our target as above.

1.4 Logical structure of the observation of linear dynamic system

Consideration on the logical structure of our observation system is essentially important to judge what is the most important and critical in developing the technology. Transmitting a certain controlled signal to the underground space as a target and we observe the response, thereby we try to deduce the information on the underground. This is exactly a typical way of system analysis as shown in Figure 1.1.1. A vector output Y is a result of a vector input X to the system with a property R (the second rank tensor) as represented by

$$Y(t,x) = \iint R(t,t',x,x')X(t',x')dt'dx' \tag{1.1.3}$$

or shortly by convolution in time and space domains

$$Y(t,x) = R(t,x) \otimes X(t,x) \tag{1.1.4}$$

and by multiplication in frequency and wave number domain

$$Y(\omega,\kappa) = R(\omega,\kappa)X(\omega,\kappa) \tag{1.1.5}$$

In our case Y is the wave field observed when an excitation X is given by transmission of wave signal. The $R(\omega,\kappa)$ is the 'frequency wavenumber response characteristics' as defined in (1.1.5): It includes all the information on the structure of the target system. When X(t,x) is a delta function, R(t,x) is identified with Green function denoted by G in time and space domain, and its Fourier transform $R(\omega,\kappa)$ is transfer function, which is often denoted by $H(\omega)$ by custom only in frequency domain.

Now we discuss the significance of the quantity, $R(\omega,\kappa)$, since it is the quantity assigned to the primary observable of ACROSS. The $R(\omega,*)$ is response function introduced theoretically for general case, so that we know conceptually everything about $R(\omega,*)$, but nothing in detail. In contrast, the observed data on $R(\omega,*)$ carry the empirical information on the signal transfer between a pair of known source to receiver within a limited condition. Therefore, notation $H(\omega)$ is used only for data of $R(\omega,*)$ and the closely related subject in ACROSS observation. Once an analytic expression of $R(\omega,\kappa)$ in terms of parameters describing the target, we shall have a better strategy and procedure for the forward and inverse problems in structural exploration, including the appropriate way of acquisition of $H(\omega)$ data.

In order to clarify the logical structure further, we restart from the wave equation.

$$D(\partial_t, \partial_x, p(x))\, Y(t,x) = X(t,x) \tag{1.1.6}$$

where ∂_t and ∂_x are the differentiation operator with respect to time and space, respectively, and p(x) is the material property (slowness S and wave impedance Z defined by (1.1.1) and (1.1.2)) as a function of space, x. The D is the wave equation operator and (1.1.6) is a statement of physics law in terms of a linear dynamic equation to give a wave field as an input and the resulted force or excitation as an output as follows,

$$X = DY \tag{1.1.7}$$

This equation may appear a little odd intuitively in common sense of causality; the excitation is a cause and the wave field is a result of excitation. However, an inverse expression of (1.1.5) is written by

$$X(\omega,\kappa) = R(\omega,\kappa)^{-1}Y(\omega,\kappa) \tag{1.1.8}$$

and it may suggest a presence of some route to obtain an expression of D as a function of ω and κ. Therefore, we have been trying to find out an inverse operator of D to give a wave field as an output (result) of the system excited by force;

$$Y(t,x) = D(\partial_t, \partial_x, p(x))^{-1} X(t,x). \tag{1.1.9}$$

Let an inverse of $R(\omega,\kappa)$ be denoted by $P(\omega,\kappa)$,

$$R(\omega,\kappa)P(\omega,\kappa) = 1$$

A trial of deriving of $P(\omega,\kappa)$ from $D(\partial_t,\partial_x,p(x))$ has also been made to make the theoretical framework and observational strategy of ACROSS perspective and consistent.

Once all of the procedures of observation and data analysis are formulated in the same and consistent framework of linear dynamic system, the strategy of active observation of underground space would evolve somehow towards much systematic way. The preliminary work that appears promising is also included in this publication.

1.5 Technology on the data acquisition under noisy condition

The essential points on the new underground observation technology are shortly reviewed together with its background. The practical difficulty of underground observation originates mostly from the low S/N in all the approaches having been employed so far. Then we need illumination to observe the invisible interiors of the Earth; natural source and controlled artificial source for both of elastic waves and electromagnetic waves. Natural sources such as earthquakes and geomagnetic variation are strong enough but neither well characterized in the necessary range of frequency nor abundant enough to enable us to obtain any satisfactory result. Strong sounding signals such as explosion lead to the environmental disturbance and also to reduce the reproducibility of the transmitted signal by fatigue destruction of the transmitter site. An idea of new methodology in ACROSS is the use of small amplitude sinusoidal signals continuously for longer period of time; the S/N is expected to increase in proportion to square root of the time period of data acquisition. We shall call this theoretical expectation '$T^{1/2}$ law' of data stacking for simplicity. The signal power should be spread in time domain; in other words, energy should not be localized in time domain but in frequency domain to realize the ideal system for sounding signal to satisfy $T^{1/2}$ law. Apparently the signal is to be designed as a set of spectral lines, or ideally a sequence of delta functions along

frequency axis. Since noise power is proportional to the band width along the frequency axis, spectral line with least width is most robust against noise. This is one of the most important basic requirements for data acquisition in noisy environment.

The noise may be defined by what we are not interested for the specific purpose even though it may have importance for the other purpose. Ironically we have to state, however, that noise is what we have to be interested most to build up the most robust system against noise according to our investigation. Actual noise we are facing practically in the observational works is neither stationary nor random in a sense of Gaussian distribution. For example, power line noise is almost coherent but amplitude and phase vary significantly with quasi-periodic nature such as traffic schedule, daily and weekly time scales. The noise originated from human activities is the most serious source of noise at highly populated places. Note that the simple $T^{1/2}$ law holds only when the noise is stationary random sequence. To face with such noise to raise quality of data, it is demanded to do the reasonable classification and modeling of all types of noise encountered in the observation.

Realization of such hardware system that satisfies the demands as above is the hard jobs to organize, since the system involves so many different units such as signal transmitters, sensors, control and recording systems and their subsystems supported by of so many different disciplines. Further technical level available currently was not high enough to fulfill the demand in some cases (accurate control of rotation of eccentric mass for elastic wave transmitter), whereas the latest one just meets our requirements in other cases (GPS clocks for accurate time keeping, and large memory to store within an accessible cost). Optimum designing of ACROSS signal within a limitation of hardware with momentum is a new discipline of signal management, and it can be useful for the measurement technology (frequency response analyzer) of linear dynamic system in other disciplines. A new efficient calibration technique of accelerometers developed by us may contribute to the seismometer technology. Designing and construction of stable antenna (which we call ground coupler) to transmit the stable elastic wave signal is one of the know-how acquired in this development works. We note that such a know-how is substantial in noise-robust signal system. Recognizing the importance of signal designing and noise management to optimize the data acquisition and data stacking for the relevant subject, we have devised successfully a systematized approach substantially better than any one existent before as noted in later sections.

1.6 Strategy and tactics of data acquisition and data analysis

Summarizing the whole technical requirements in data acquisition, we have adopted a set of $H(\omega,x,x')$ and $\sigma(\omega,x,x')$ as a unit of our primary observables. The $H(\omega,x,x')$ is the tensor transfer function between a signal source at x' and wave field at x during a certain period of time (e.g., $10^{2\sim4}$ sec), as given by a function of discrete frequency within a limited range. The $\sigma(\omega,x,x')$ is the

estimated reliability of $H(\omega,x,x')$ represented by standard deviation.

Suppose that we have obtained the transfer function $H(\omega,x,x')$ in frequency domain between the two sites, x and x'. If H is given in a very wide range of ω, say from 0 Hz to a Nyquist frequency f_N/Hz with an interval of Δf/Hz, for example, then the Fourier transform leads to the wave form on time axis up to Nyquist time $T_N = 1/\Delta f$. However, $\sigma(\omega,x,x')$ may not be small enough when we take wide frequency range. One of the practical strategies or policies of ACROSS is to place a prime importance on the quality of the data by reducing the unreliability of the transfer function. Then the data acquisition is made in the relatively narrow range. In other words, we like to devise a set of plural narrow windows in frequency domain to focus the characteristic part of the target. The systematic study of the optimized window design has not yet been developed yet, since it would be target-adaptive, in which the design is expected to be different from the specific purpose of the observation.

The optimum design as above depends on how the data acquired by the specified window could be analyzed and used. We have been developing a basic tool to relate the observed transfer function data within a specified narrow frequency range with the theoretical framework of wave theory. It is called 'Sompi Event Analysis' (SEA). Basically it enables us to give a good estimate of a sequence of arrival events from the transfer function data within a narrow frequency band at the observation site. This theory of SEA is also based on the linear dynamic system model of wave propagation; the traveling wave from an impulse source is written by

$$Y(t) = \Sigma_j \alpha_j/(t-\tau_j). \qquad (1.1.10)$$

This is based on the superposition of a $A\exp(i\omega t-i\kappa x)$ with a possible sets of a variety of κ (different medium), x (different length of wave path) and A (different amplitude). The SEA possesses also a very important function, by which dispersion (frequency dependence of slowness) is dealt well; the time delay of an impulse is analyzed to the delay time spectrum as a function of frequency.

1.7 Current state and prospects

After the developmental works of 10 years, we came to the level with which practical field test is compared with those of the different approaches having been developed towards the similar purpose by different research groups. The ACROSS has not sufficient time yet it is brought to be mature through the stationary utilization and innovation by many different groups of scientists and engineers. We had international workshop twice at Tono and many opportunities of academic exchange at the scientific meeting and visiting the scientists of Russia, United States and other countries [2,3]. We can confidently conclude that ACROSS, the latest comer, is the best one in the next generation as a matter of consequence. Note that we are free from the traditional thinking in this discipline. A short

review on the foreign technology follows:

First we examine the strategy of 'vibroseis®' (introduced earlier in 1958 in the USA), which has been used commonly most everywhere in the world. From our view point referring to the basic principle of data acquisition under noise, it does not satisfy the basic requirement that warrants the theoretically expected '$T^{1/2}$ law'. Russian workers have also been working since 1976 by using very large seismic transmitter equivalent to vibroseis with the same concept. The American and Russian workers and their followers use the chirp signal for elastic wave exploration, which appears similar to ACROSS in phenomenological sense. However, the vibroseis does not control the signal precisely and they use the correlation between the transmitted and the received signals by strongly asserting that it is the most robust against noise. This subject should be discussed some time and somewhere in near future. The Chinese government had undertaken the development of ACROSS, since 2001 in order to make a nation-wide network for the earthquake monitoring. The members of ACROSS Team have been working as technical adviser and also as trainer for young engineers and students.

The ACROSS is not only a specific technology for the underground space but it could be regarded as a methodology of measurement of any linear system. For example, the measurement of frequency response characteristics of audio-amplifier is most precisely made by the information management strategy of ACROSS. We have applied it to two subjects successfully; one is the secondary calibration of accelerometers, and another is the property measurement (complex dielectric permittivity) of rocks. The other important applications expected are the non-destructive health monitoring of any constructions coupled strongly with the Earth. The safety evaluation and detection of any deficit is made by measurement and analysis of vibration modes for buildings, bridges, tunnels and other structures. Typical example of our concern is the atomic power plant on the ground, which may be loose to amplify the vibration generated by seismic waves. A group at the Center for Computational Science and e-System (CCSE) of JAEA has been interested in the possibility of future application of ACROSS. Another example is remote monitoring of the underground reservoir for the safe isolation of high level radioactive wastes surrounded by bed rocks. The trial test has been started at Horonobe Underground Research Laboratory of JAEA since 2002 by utilizing the ray path analysis by seismic ACROSS combined with EM ACROSS. The similar but new different approach utilizing mode analysis is being considered at Tono Geoscience Center.

The most urgent and important subject is the start of actual test monitoring of the expected focal region of Tokai Earthquake as one of the national projects of earthquake prediction research works. The project of using ACROSS is managed by Meteorological Research Institute of Japan Meteorological Agency (JMA), which is responsible for the earthquake prediction itself for disaster reduction. In 2005, the new elastic wave transmitter was designed by us and installed at Morimachi, Shizuoka prefecture at the end of March, 2006. The monitoring observation after the tuning and test has started from September, 2006. Morimachi is situated just on a straight line between Tono, where our domestic test site is located and Hamaoka, where atomic energy power plant had been in

operation. In addition Morimachi is just above one of the possible initiation points of coming Tokai Earthquake fault plane. There are already some indications showing variation of the underground states beneath the western part of Shizuoka prefecture. Extension of the observation system both in quantity and quality is most demanded. A test experiment of EM ACROSS larger in scale in comparison with that of Tono has started at Shizuoka University campus from September, 2006. Recent seismological studies have suggested the simultaneous occurrence of Tokai Earthquake and Tonankai Earthquake, which may result in a really disastrous situation. There is a strong demand of developing ACROSS technology applicable on the sea surface and also on the ocean bottom and also of their use as soon as possible. The seismological use of the active monitoring by ACROSS technology and what we can deduce from that would be one of the hottest topics in the coming years.

In summary of this writing, we note that most of developmental works have been made by our research group at Tono Geoscience Center and that the ACROSS technology is going to spread to the rest of the world with the applications wider than that has been supposed at the start of developmental works. We thank our fortune for having been worked as originator of a new approach useful for wide discipline of science and technology.

References

[1] Kumazawa, M., T. Kunitomo, Y. Yokoyama, T. Nakajima, and K. Tsuruga, ACROSS: Theoretical and technical developments and prospect to future applications, *JNC Technical Review*, **9**, 115-129, 2000. (in Japanese)

[2] Earthquake Frontier Research Project, International workshop on "Frontiers in Monitoring Science & Technology for Earthquake Environments", Tono Geoscience Center JNC, Toki, Japan, 1998.

[3] Fujii, N., J. Kasahara, H. Higashihara, and K. Ogawa (Eds.), The Proceedings of the "1st International Workshop on Active Monitoring in the Solid Earth Geophysics (IWAM04)", Task Group for Active Monitoring, Mizunami, Japan, 2004.

Mineo KUMAZAWA, Takahiro KUNITOMO, and Takahiro NAKAJIMA
Tono Geoscientific Research Unit, JAEA

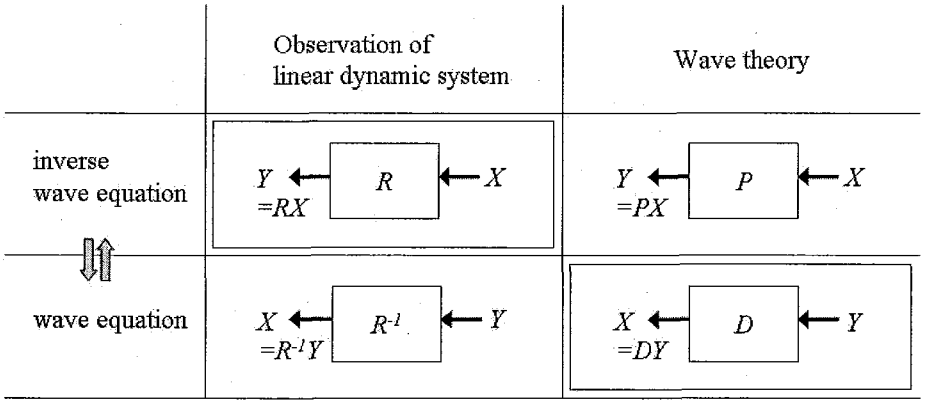

Figure 1.1.1 Relationship among the different representations of a linear system model of wave field Y generated by an excitation X. Both analytic and numerical transformations between Y=RX and X=DY are the subject of our concerns.

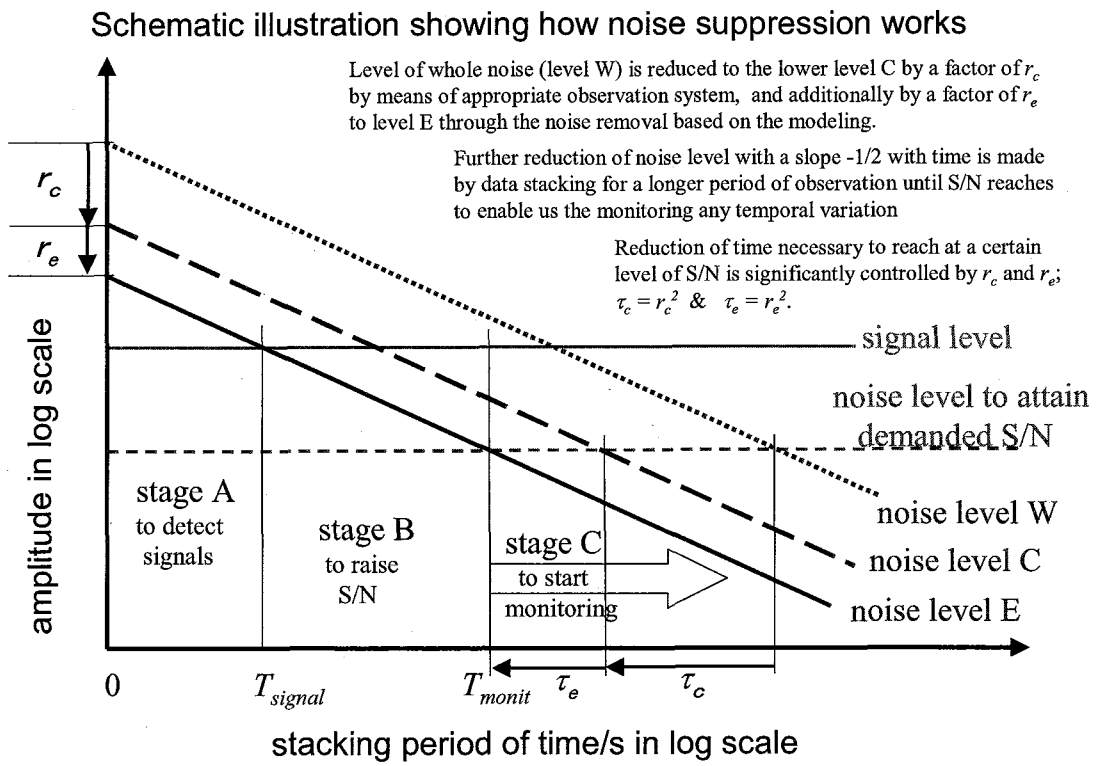

Figure 1.1.2 Noise processing to reach larger S/N by means of reasonable data stacking. Note that the reduction of noise level by 10% leads to the 20 % reduction of a time unit, T_{monit}, necessary to realize monitoring with a given reliability (S/N).

2. Seismic ACROSS

2.1 Overview of Seismic ACROSS and its development

2.1.1 Introduction

In order to investigate activities of the Earth's interior such as earthquakes and volcanic phenomena in detail, we need a device to monitor the underground status and detect its changes. Weather radars observe the status of rainfall and distribution of rainy areas from moment to moment over a wide region and forecast rainfall. If we have such a device to monitor how the underground status varies, prediction of earthquakes and volcanic activities will make remarkable progress. The development of ACROSS has been started for the purpose of realizing the subsurface monitoring system which actively radiates seismic or electromagnetic waves into the ground.

The following conditions are required for remote and active monitoring of slight variation in subsurface status, supposing phased development:

(1) There is a system that constantly transmits and receives seismic or electromagnetic waves carrying information about subsurface status, which enables us to survey deep underground from the surface or shallow underground.
(2) The behavior and the characteristics of both transmitting and receiving devices do not change, or they are correctable in required precision.
(3) The changes in behavior of surrounding rock around the transmitting and receiving points are small, or the changes are quantitatively describable.
(4) It is possible for us to know the propagation pass of the wave of which the change is detected, and to specify what changes in which region underground.

The first condition goes without saying unless we directly excavate. The second and third ones are necessary to indicate quantitatively that detected changes are not due to transmitting or receiving points but to the deeper region. Earth-scientific discussion about deep subsurface phenomena is possible only when all the conditions are satisfied. The subjects of the earth-scientific discussion referred here are in which region underground the detected change occurs, and what physicochemical phenomenon causes it. We have developed the seismic ACROSS system included the device to continuously transmit elastic wave into the ground and the device to receive it, so that the conditions (1) and (2) are almost achieved. The conditions (3) and (4) are the subjects we are struggling now through development of observation method and data analysis.

We outline the circumstances in development of the seismic ACROSS and the continuous transmission experiment being carried out at present, with the focus on the 20 tonf (ton-force) fixed transmitter we are mainly using.

2.1.2. History of development

(1) Development of transmitter

Seismic ACROSS (Accurately Controlled Routinely Operated Signal System) is a system for active monitoring of subsurface structure and status by transmitting and receiving elastic wave signals with the phase and amplitude controlled accurately. At the initial stage of development, 'SS' in ACROSS was 'Seismic Source' and only elastic wave was considered to be used. Takei & Kumazawa [1, 2] had their eyes on that a single-force source had the largest radiation efficiency to propagate for long distance, and began to examine development of ACROSS as a device generating elastic wave by single-force. A single-force source mentioned here means a source in which elastic wave is generated by acceleration of an inertial mass in the Earth's interior. The earnest development research of ACROSS, as the trinity of a transmitter, a receiver and an analysis method, had been started on the basis of the facts that a precisely controlled sinusoidal wave was the robustest against noise, stacking of narrow band signals provided measurement with large S/N (signal to noise ratio), and a prospect for travel time analysis from narrow band data looked bright [3, 4]. After that 'SS' altered to 'Signal System' because it had been recognized that the concept of ACROSS was applicable to electromagnetic wave and the most distinctive features of ACROSS were the signal carrying subsurface information and the treatment for it [5].

Constant active monitoring of subsurface status requires a nondestructive transmitter with stable transmitting condition to be operated continuously for a long term. The method in which an eccentric mass rotated by a servomotor was selected as such a transmitter [6]. The servomotor at the present time has ability to rotate precisely by digital phase control and reliability for long-term operation.

The first transmitter was produced at Nagoya University. This trial transmitter is a small machine whose eccentric moment was about 0.5 kgm (~1.2 tonf at 25 Hz). It laid the foundation for development of standard transmitters and succeeding research on ACROSS through promoting the recognition of several problems on the transmitter such as hunting condition and cooling of the bearings [7], and ones on measurement such as instability of seismometers [8], though the control and the measurement was very rough. The first experiment on ACROSS measurement using the small trial transmitter was carried out in Nagoya University campus. A transfer function was obtained by single frequency measurements for plural sequential frequencies, the wave

arrivals corresponding to the surface wave velocity were detected [9, 10]. The frequency modulation (FM) method to generate signals of plural frequencies simultaneously [11] and the synchronization of transmission and reception by GPS clock [12] were proposed about that time. In addition, the numerical experiment for optimization of FM signals to suppress the frequency dependency of the amplitude spectrum and limit the frequency range had started, and preliminary experiment for FM transmission by the trial transmitter succeeded [13].

In 1995, they began to design 20 tonf class fixed transmitter and 2 tonf class movable one. The former was funded by the Earthquake Frontier Research Project of PNC (present JAEA) and the Scientific Drilling Program of the Nojima Fault (Kyoto University, Nagoya University etc., [14]) founded after the Kobe earthquake, and the latter by NEDO [15, 16, 17]. The fixed transmitters had been completed in the first half of 1996 and installed at Awaji Island and the Tono Mine, then trial operation started. The movable transmitter had been ready in the latter half of 1996 and were examined the operation in Nagoya University campus.

The trial transmission and reception under GPS synchronization for single frequency succeeded at the Tono Mine in August 1996, and examined how far the transmitted signal reached [18]. The procedure for phase measurement and mass-position control was established about the same term [19]. After that we detected the single-frequency signal of 25 Hz (10 tonf) at Kamitakara station of the university network 100 km apart from the transmission site, stacked for about 1 week [20]. The first observation by seismic array was carried out at Yamagawa geothermal power plant (Yamagawa, Kagoshima), by using the movable transmitter in March 1997. Measurement was made by single-frequency signals within a wide frequency range, and body wave arrivals were detected for the first time through array analysis [21].

We had established the first product of the pulse generator for GPS-synchronized FM control which based on the distinct concept from the preliminary work in March 1997 [22]. Taking this opportunity, a full-scale experiment for FM transmission was started. By transmission from the Tono Mine, several body wave arrivals were identified through seismic array observation; the direct, refracted and reflected wave for both P and S waves [23, 24]. Other various results have been published such as successful long-term continuous operation at Awaji Island and detection of travel time variation in direct S wave associated with the Western Tottori Earthquake on October 6, 2000 etc. [25].

Thereafter many basic technologies which lead the present have been established; raising the accuracy of the pulse generator for GPS-synchronized FM control [26], development of control system to switch the rotation direction automatically and periodically [27], optimization of FM signal [28] and so on. In this context, we are

performing a continuous transmission experiment at the Tono Mine, aiming to realize constant active monitoring of Earth's crust since October, 2002 with the cooperation of Meteorological Research Institute, JMA [29]. See below for details.

Thus we outline the history of development focusing on the 20 tonf class fixed transmitter.

(2) Development of observation system

The observation system has been developed in parallel with the development of transmitters. We and our colleagues have developed various kinds of the time segment stacking recorder, which performs real-time stacking in synchronization to GPS, in order to select for various observation conditions such as temporal observation, borehole observation, array observation and so on [30, 31]. We have also made efforts to select the seismometers for ACROSS and develop the calibration method. For these receiving devices, the sampling clock and the characteristics of amplifiers, filters and seismometers are adjusted and selected not to vary with temperature as well as possible, and the situation to install them is also cared. The seismometers are sensitive to temperature variation so that we basically lay them underground about 2 m in depth; in addition, it has a purpose to avoid very weak and heterogeneous part near the ground surface. Correct calibration of seismometers is necessary for us to compare properly the amplitudes and phases observed at different sites or different sensors. See other reports for details. The time segment stacking recorder is partly introduced in [31] and the case studies [32, 33, 34, 35, 36]. Tsuruga *et al.* [37] present a calibration method of seismometers.

2.1.3 Active monitoring experiment in Chubu region

(1) Observation

Hi-net (High-sensitivity seismograph network in Japan) produced by NIED (National Research Institute for Earth Science and Disaster Prevention) acquires sequential data with the sampling synchronized to GPS, and the data are open to public. Development of such seismic stations to the amount of about 700 points in Japan, which once we thought to be our future mission, provides us an early-coming preparation for full-scale transmission experiment.

Figure 2.1.1 illustrates the observation situation of the experiment for constant active monitoring of the crust by means of seismic ACROSS transmitters at the Tono Mine. Figure 2.1.1(a) shows the station distribution around the transmission site. The transmitters called FIT (Fixed Illumination Tool) are installed at the Tono Mine (Tono

Geoscience Center, JAEA, Toki, Gifu). In the neighboring underground gallery, we have an L-shaped seismic array with three-component seismometers settled at eight points and two borehole seismometers. The seismic array in the gallery was pulled out in April 2005 with termination of geoscientific research at Tono Mine. The observation result of this array is presented by Kunitomo & Kumazawa [32]. We also have a dense array of three-component seismometers distributed at 6×6 grids with a spacing of 5 m in Shobasama Site (JAEA, Mizunami, Gifu) 900m apart from the transmission site [33, 38]. In addition, observation is made by a cross-shaped array composed of 15 three-component seismometers with 8 m spacing [34] in a crustal-movement observation gallery of Nagoya University (Mizunami, Gifu).

Figure 2.1.1(b) shows the distribution of existing seismic stations in Chubu region. The circles indicate the distance from the transmission site marked by a star, where the outermost circle is the approximate limit the transmitted signal reaches. Nagao *et al.* [39] and [40] report on the detection of ACROSS signal and acquisition of transfer functions by using the data observed at Hi-net and JMA stations.

(2) Seismic ACROSS transmission site at the Tono Mine

Figure 2.1.2 is a photograph of FIT installed at the Tono Mine. The black part noted 'FIT No.1' is a servomotor, and the body containing an eccentric mass is inlaid into a concrete base we call 'ground coupler' and fixed by wedges. The ground coupler is a hard concrete base with a steel frame inside, and purposes to transmit generated force through large contact area and lower the stress level to the ground preventing from fatigue failure (Figure 2.1.3).

FIT at the Tono Mine generates force by rotating an eccentric mass. Kunitomo & Kumazawa [31] give a detailed explanation of a control formula successfully utilizing the characteristic of such a transmitter. Three FIT transmitters installed in this site have different eccentric moment from each other, and are supposed to operate in different frequency ranges (Table 2.1.1, FIT No.1: ~25 Hz, FIT No.2: 35~50 Hz, FIT No.3: 25~35 Hz).

FIT No.1 and No.3 have their axis of rotation in the vertical direction and vibrate the ground in the horizontal direction, whereas FIT No.2 has the horizontal axis of rotation and vibrate the ground in vertical and NW-SE directions One of the purposes of the present experiment is to investigate the ability of monitoring deep underground using S wave which is sensitive to variation of material property, so that we mainly use FIT No.1 that has a vertical axis and generates the largest force in low frequencies. We perform the FM transmission with the rotation direction switched every one hour, leading to acquirement of transfer functions in frequency domain which correspond to

the linear vibration in two perpendicular directions: radial and transverse ones for a station in any direction [31,32].

(3) Outline of the continuous transmission

In the end of 2002, preparation of observation system and establishment of control software had been in prospect, and then we started a full-scale continuous transmission from the Tono Mine (Table 2.1.2). The continuous transmission experiment is divided into five terms (The 1st to the 5th experiments) with different properties such as the source signal spectrum and the frequency range. The 5th transmission lasts up to the present (April, 2004). We explain the content and the result of each experiment below.

1) The 1st transmission experiment

Transmission using a narrow band FM signal (FIT No.1: 18.02-19.02 Hz) and a single frequency signal (FIT No.3: 25 Hz) was carried out to examine how far the signal was detectable. Another purpose was to inspect the existing stations for the problems. Stacking data for 11 days enabled signal detection at the stations over 100 km apart from the transmission site, e.g. Hi-net Fujimi station at 115 km [29, 39]. It was revealed that many existing stations had their problems such as contamination of electrical noise at integer frequencies [41]. Thereafter we decided to use FM signals without any integer frequency components for transmission intended at Hi-net or JMA stations. The rotation of the motor is only in normal direction in the 1st transmission.

2) The 2nd transmission experiment

FM signals of relatively wide band were transmitted for the main purpose of identifying the kind of elastic waves observed near the transmission site. It was difficult to detect signals far from the source as the amplitude of source spectrum was small. FIT No.1 and No.2 were simultaneously operated without interference even in overlapped frequency band, because we took the different frequency series where transmitted signals appear. The results of observation at the underground seismic array in the Tono Mine [32] have been reported. We controlled the rotation directions switching every one hour, so that the transfer function for linear vibration is able to be discussed.

3) The 3rd transmission experiment

This was a preliminary experiment for optimization of FM signals. Until the 3rd transmission we had been able to suppress variety in spectral amplitude of a

transmitted signal and limit the frequency band. However the design of source spectrum with constant amplitude had not been achieved, and signals in low frequencies had smaller amplitudes. As both of FIT No.1 and FIT No.3 were in operation during the first month, Saiga *et al.* [34] analyzed the transfer functions measured by seismic array in sources together to separate waves into Mizunami Crustal Movement Observation Tunnel for both refracted P, refracted S and so on, leading to discussion of their temporal variation.

4) The 4th transmission experiment

In this experiment, we used the transmission signal designed by the optimization method we had developed during the 3rd transmission [28]. Its amplitude spectrum was almost constant within the frequency range, which was strongly restricted [31].This experiment resulted in completion of the design for FM signal, and it shifted into long-term continuous transmission. For this experiment many results have been reported; detection of clear temporal variation in multiple reflection of S wave inside the Neogene Mizunami Group by Kunitomo & Kumazawa [32], estimation of arrival direction and temporal variation in travel times using seismic array observation by Tsuruga *et al.* [33] and Hasada *et al.* [38], detection of seismic arrival at far stations by [40] and so on.

5) The 5th transmission experiment

The modulation period of FM operation of the 1st to 4th experiments was 20 s. However it became clear that the signal transmitted in the 4th experiment was detectable even at the station over 50 km apart from the source [40], therefore we selected 50 s as the modulation period for the 5th transmission in order to observe later phases with travel times over 20 s. And furthermore, we extended the lower limit of frequency range to investigate transfer functions for low frequencies.

2.1.4 Concluding remarks

About ten years have passed since development of the seismic ACROSS was started. Meanwhile, various attempts have been made by many people, and the sober basic developments have proceeded. We have introduced the history of development of seismic ACROSS focusing on the trail to the continuous transmission experiments at the seismic ACROSS transmission site in the Tono Mine. Although we would like to include all related studies and persons, it is impossible to our regret. We listed as many reference documents as possible instead. Most of the references are abstracts of presentation, which is a side of ACROSS research.

Toward the constant active monitoring of the crustal status in Japan Islands, as a dream we had at the beginning, we are just making the first step by starting the continuous transmission experiments that follow the development of instruments. Gathering the dreams and zeal of new people, the development research is taking a new turn.

References

[1] Y. Takei and M. Kumazawa, Why have the single force and torque been excluded from seismic source models? *Geophys. J. Int.*, 118,20-30,1994.

[2] Y. Takei and M. Kumazawa, Phenomenological representation and kinematics of general seismic sources including the seismic vector modes. *Geophys. J. Int.*,121,641-662,1995.

[3] M. Kumazwa and Y. Takei, Active method of monitoring underground structures by means of accurately controlled rotary seismic sources (ACROSS) 1.Purpose and principle, *Abstracts of fall meeting of the Seismological Society of Japan*,158,1994a (in Japanese).

[4] M. Kumazwa and Y. Takei, Active method of monitoring underground structures by means of accurately controlled rotary seismic sources (ACROSS) 3.Event detection from a small number of Fourier components observed by ACROSS system, *Abstracts of fall meeting of the Seismological Society of Japan*,160,1994b (in Japanese).

[5] K. Ogawa and M. Kumazawa, Towards the continuous remote sensing of H_2O, tectonic stress and physical states in the Earth's crust by means of acoustic and electromagnetic ACROSS, *Abstracts of fall meeting of the Seismological Society of Japan*,151, 1996 (in Japanese).

[6] Y. Takei, M. Kumazawa, K. Suzuki, Active method of monitoring underground structures by means of accurately controlled rotary seismic sources (ACROSS) 2. Designing and specification of the ACROSS, *Abstracts of fall meeting of the Seismological Society of Japan*,159,1994 (in Japanese).

[7] K. Suzuki, S. Ishikawa, M. Kumazawa, Y. Takei, Y. Hase and Y. Koganei, Designing and testing of a small prototype ACROSS & the desinging polycy decision for the routine machines, *Abstracts of fall meeting of the Seismological Society of Japan*,8, 1995 (in Japanese).

[8] M. Kumazawa, M. Nakano, M. Nakatani, K. Miyagawa, K. Yamaoka, H. Komura, A. Seki, T. Koshirai and M. Araya, Malfunction of existing seismometers and a proposal of developing a new type of reliable accelerometry system for reliable acquisition of across signal, *Abstracts of Japan Earth and Planetary Science Joint Meeting*,183,1997 (in Japanese).

[9] Y. Takei, M. Kumazawa, H. Kumagai, Y. Hasada, K. Yamaoka, S. Tsukada, M. Nakano, N. Ikeda, S. Inoue and K. Miyakawa, ACROSS Does Work 3. Transfer function as a frequency sequence and cepstrum analysis, *Abstracts of fall meeting of the Seismological Society of Japan*,7,1995 (in Japanese).

[10] Y. Hasada, M. Kumazawa, H. Kumagai, Y. Takei, ACROSS does work 4. Determination of Travel Times by Cepstrum Analysis, *Abstracts of fall meeting of the Seismological Society of Japan*,152, 1995 (in Japanese).

[11] M. Kumazawa, S. Watanabe and K. Yamaoka, Frequency Modulation of ACROSS for Simultaneous Excitation of a Set of Equally Spaced Frequencies, *Abstracts of fall meeting of the Seismological Society of Japan*,9,1995 (in Japanese).

[12] K. Yamaoka, Y. Hasada, M. Nakano, M. Kumazawa, H. Maruo, H. Oshima, Control system of Frequency Modulated ACROSS to be linked with TS Stacking recorders, *Abstracts of fall meeting of the Seismological Society of Japan*,9,1995 (in Japanese).

[13] N. Ikeda, K. Yamaoka, M. Kumazawa, S. Inoue and S. Watanabe, Proof experiment and optimization of FM-ACROSS, *Abstracts of Japan Earth and Planetary Science Joint Meeting*,177, 1997a (in Japanese).

[14] M. Ando, K. Shimazaki and K. Takemura, the Scientific Drilling Program of the Nojima Fault, Japan, *Chikyu Monthly*,21, 5-12,1998 (in Japanese).

[15] M. Kumazawa, T. Kunitomo, Y. Yokoyama, T. Nakajima and K. Tsuruga, ACROSS: Theoretical and Technical Developments and Prospect to Future Applications, *JNC technical review*,9,115-129, 2000 (in Japanese with English abst.).

[16] N. Fujii, K. Yamaoka, T. Ooida, M. Yamada, M. Kumazawa, M. Ando and K. Nishigami, ACROSS Project in Awaji, *Abstracts of fall meeting of the Seismological Society of Japan*,10,1995 (in Japanese).

[17] K. Ogawa, M. Kumazawa, K. Ishihara, M. Nakatani, T. Kunitomo, N. Fujii, K. Yamaoka, H. Kumagai, Y. Takei, Y. Hasada, K. Miyakawa, N. Ikeda and K. Suzuki, HIT: A Mobil ACROSS, *Abstracts of Japan Earth and Planetary Science Joint Meeting*,181,1997 (in Japanese).

[18] K. Yamaoka, T. Kunitomo, T. Hanaki, K. Ishihara, N. Ikeda, Y. Hasada, K. Miyakawa, M. Nakano and M. Kumazawa, Experiment on synchronization between ACROSS and TS-Stacker refering to GPS time, *Abstracts of fall meeting of the Seismological Society of Japan*,151,1996 (in Japanese).

[19] T. Kunitomo, K. Ishihara, N. Ikeda, K. Yamaoka, M. Kumazawa and K. Ogawa, Frequency stability of the rotary-type ACROSS, *Abstracts of fall meeting of the Seismological Society of Japan*,152,1996 (in Japanese).

[20] K. Yamaoka and R. Ikuta, Feasibility of Reflection Monitoring for Plate Coupling using ACROSS System, *In the Proceedings of "1st International Workshop on Active Monitoring in the Solid Earth Geophysics (IWAM04)", Task Group for Active Monitoring, Mizunami, Japan*, 2004.

[21] N. Ikeda, K. Ishihara, M. Nakatani, K. Miyakawa, K. Ogawa, K. Yamaoka, T. Kunitomo and Y. Hasada, Array observation using ACROSS/HIT and its analysis, *Abstracts of fall meeting of the Seismological Society of Japan*,70,1997b (in Japanese).

[22] T. Kunitomo, M. Kumazawa, K. Yamaoka, M. Aoki and K. Ishihara, Accurate Frequency-Modulation Control of the Rotary-type ACROSS, *Abstracts of Japan Earth and Planetary Science Joint Meeting*,182,1997 (in Japanese).

[23] N. Ikeda, K. Yamaoka, T. Kunitomo, M. Hirai, K. Ogawa, K. Miyakawa, K. Kobayashi, M. Kumazawa, Array Experiment and Analysis of ACROSS, *Abstracts of Japan Earth and Planetary Science Joint Meeting*,24,1998 (in Japanese).

[24] A. Saiga, K. Yamaoka, T. Kunitomo, R. Ikuta, K. Miyakawa, K. Moriguchi, An experiment receivinc ACROSS signal with a seismic array, *Abstracts of Japan Earth and Planetary Science Joint Meeting (CD-ROM)*,Su-P002,2001.

[25] R. Ikuta, K. Yamaoka, K. Miyakawa, T. Kunitomo, M. Kumazawa, Continuous monitoring of propagation velocity of seismic wave using ACROSS, *Geophys. Res. Lett.*, 29, 10.1029/2001 GL013974, 2002.

[26] T. Kunitomo and M. Kumazawa, New Control System of the Rotary-type ACROSS Seismic Source, *Abstracts of fall meeting of the Seismological Society of Japan*,168,2001 (in Japanese).

[27] T. Kunitomo and M. Kumazawa, New Control Method of the Rotary-type ACROSS Transmitter, *Abstracts of fall meeting of the Seismological Society of Japan*,P076,2002 (in Japanese).

[28] T. Kunitomo and M. Kumazawa, Optimum FM signal for monitoring the underground states by means of the seismic ACROSS, *XXIII General Assembly of the International Union of Geodesy and Geophysics, Sapporo, Japan, IUGG2003 Abstracts*, A.145,June 30 - July 11,2003.

[29] H. Ueno, Y. Yoshida, H. Matsuoka, Y. Ishikawa, T. Kunitomo and M. Kumazawa, The observation and analysis of ACROSS signals by seismic networks (Part I) The detection of seismic signals by JMA and Hi-net, *Abstracts of Japan Earth and Planetary Science Joint Meeting (CD-ROM)*,S050-P003,2003.

[30] K. Yamaoka, K. Kobayashi, T. Kunitomo, M. Kumazawa, H. Ando and M. Iwasaki, TS-Stacker on the data logger DATAMARK LS8000, *Abstracts of fall meeting of the Seismological Society of Japan*,156,1997 (in Japanese).

[31] T. Kunitomo and M. Kumazawa, Active Monitoring of the Earth's Structure by the Seismic ACROSS - Transmitting and Receiving Technologies of the Seismic ACROSS -, *In the Proceedings of "1st International Workshop on Active*

Monitoring in the Solid Earth Geophysics (IWAM04)", Task Group for Active Monitoring, Mizunami, Japan, 2004a.

[32] T. Kunitomo and M. Kumazawa, Active Monitoring of the Earth's Structure by the Seismic ACROSS- Field Examples at the Tono Mine ACROSS Experimental Site -, *In the Proceedings of "1st International Workshop on Active Monitoring in the Solid Earth Geophysics (IWAM04)", Task Group for Active Monitoring, Mizunami, Japan,*2004b.

[33] K. Tsuruga, T. Kunitomo, Y. Hasada, M. Kumazawa, J. Kasahara and N. Shigeta, A dense seismic array for acquisition of high quality data in the ACROSS observation, *In the Proceedings of "1st International Workshop on Active Monitoring in the Solid Earth Geophysics (IWAM04)", Task Group for Active Monitoring, Mizunami, Japan*, 2004a.

[34] A. Saiga, K. Yamaoka, T. Kunitomo, T. Watanabe, Continuous observation of travel time variation of seismic waves using the ACROSS and the seismic array at 2.4km distance, *Chikyu Monthly, Special issue "Active Monitoring"*, 2004.

[35] T. Nakajima, T. Kunitomo, H. Nagao, M. Kumazawa and N. Shigeta, Long-Term Operation of the EM-ACROSS and Derived Transfer Function in the Diffusion Field Region, *In the Proceedings of "1st International Workshop on Active Monitoring in the Solid Earth Geophysics (IWAM04)", Task Group for Active Monitoring, Mizunami, Japan*, 2004.

[36] H. Nagao, T. Nakajima, Y. Hasada, M. Kumazawa, N. Shigeta and T. Kunitomo, Detection of a Reflected Wave by Application of the Sompi Event Analysis Method to EM-ACROSS Transfer Functions, *In the Proceedings of "1st International Workshop on Active Monitoring in the Solid Earth Geophysics (IWAM04)", Task Group for Active Monitoring, Mizunami, Japan*, 2004.

[37] K. Tsuruga, M. Kumazawa, T. Kunitomo and N. Shigeta, Seismometers for ACROSS by ACROSS, *Chikyu Monthly, Special issue "Active Monitoring"*, 2004b.

[38] Y. Hasada, M. Kumazawa, K. Tsuruga and T. Kunitomo, ravel time estimation from the data observed by ACROSS, *In the Proceedings of "1st International Workshop on Active Monitoring in the Solid Earth Geophysics (IWAM04)", Task Group for Active Monitoring, Mizunami, Japan*, 2004.

[39] H. Nagao, T. Nakajima, M. Kumazawa and T. Kunitomo, Optimum weighted stacking method for acquisition of the ACROSS transfer functions having the maximum signal-to-noise ratio, *In the Proceedings of "1st International Workshop on Active Monitoring in the Solid Earth Geophysics (IWAM04)", Task Group for Active Monitoring, Mizunami, Japan*, 2004b.

[40] Y. Yoshida, H. Ueno, Y. Ishikawa, T. Kunitomo and M. Kumazawa, The observation and analysis of ACROSS signals by seismic networks – Determination of the transfer function -, *In the Proceedings of "1st International Workshop on Active Monitoring in the Solid Earth Geophysics (IWAM04)", Task Group for Active Monitoring, Mizunami, Japan*, 2004.

[41] K. Yamaoka, T. Kunitomo, M. Kumazawa, Are the conventional telemetry seismic networks suitable for receiving ACROSS signal?, *Abstracts of Japan Earth and Planetary Science Joint Meeting (CD-ROM)*,S048-005,2003.

Takahiro KUNITOMO and Mineo KUMAZAWA
Tono Geoscientific Research Unit, JAEA

Table 2.1.1 Specifications of the seismic ACROSS transmitters at the Tono Mine. No.2 machine was moved to Horonobe Underground Research Center in October 2005.

No.	Eccentric Moment	Max. Frequency	Max. Force
1	8.0 kgm	25 Hz	2.0×10^5 N
2	1.6 kgm	50 Hz	1.6×10^5 N
3	3.9 kgm	35 Hz	1.9×10^5 N

Table 2.1.2 Outline of continuous transmission experiments from 18:00 JST on October 28, 2002 to 0:00 JST on December 31, 2006..

No.	Term	Length	FIT No.	Frequency Band (Hz)	Carrier Frequency (Hz)	FM Period (s)	Switch Rot. Direction
1	2002/10/28 18:00:00～ 2002/11/08 18:00:00	11 days	1	18.02-19.02	18.52	20	Normal
			3	25.00 (single frequency)			Normal
2	2002/11/19 18:00:00～ 2002/12/02 18:00:00	13 days	1	15.02-20.02	15.02	20	Every one hour
			2	20.00-40.00	30.00	20	Every one hour
3	2002/12/29 18:00:00～ 2003/01/28 11:00:00	30 days 17 hours	1	15.02-20.02	17.52	20	Every one hour
			3	23.03-28.03	25.53	20	Every one hour
	2003/01/28 11:00:00～ 2003/04/10 13:00:00	72 days 2 hours	1	15.02-20.02	17.52	20	Every one hour
4	2003/04/15 17:00:00～ 2004/01/28 18:00:00	288 days 1 hours	1	15.47-20.57	17.52	20	Every one hour
5	2004/02/20 19:00:00～ ongoing	1044 days+	1	10.25-19.45	13.01	50	Every one hour

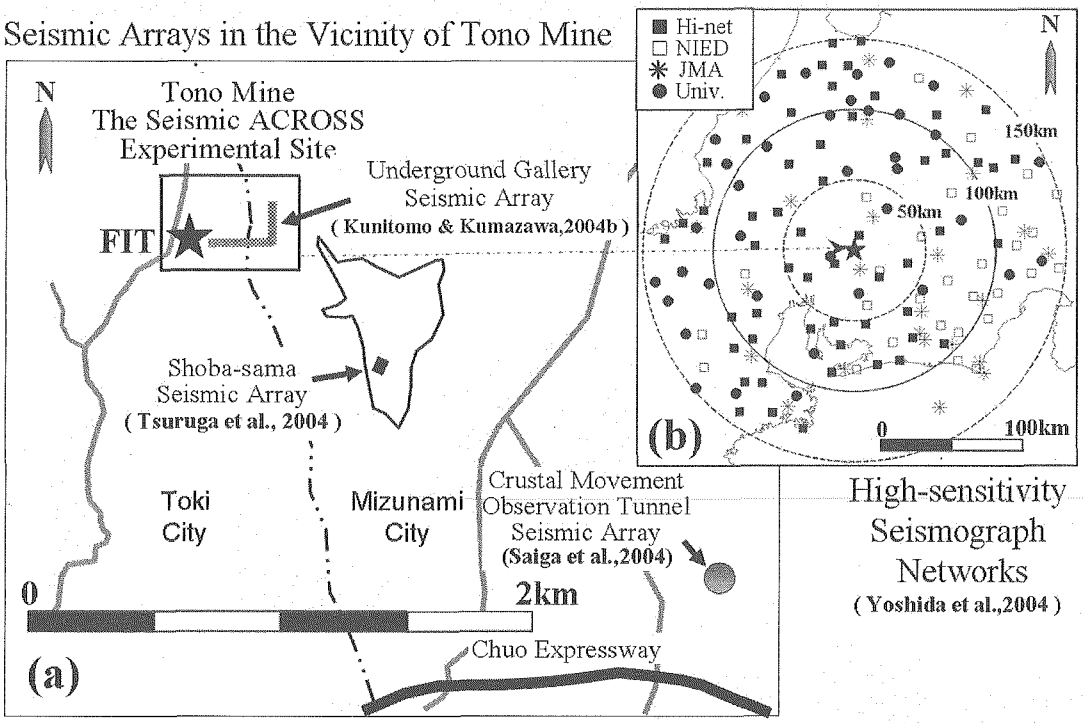

Figure 2.1.1 Observation site distribution around the transmission site. (a) Seismic arrays around the seismic ACROSS transmission site at the Tono Mine. (b) High-sensitivity Seismograph Networks in central Japan (Chubu region).

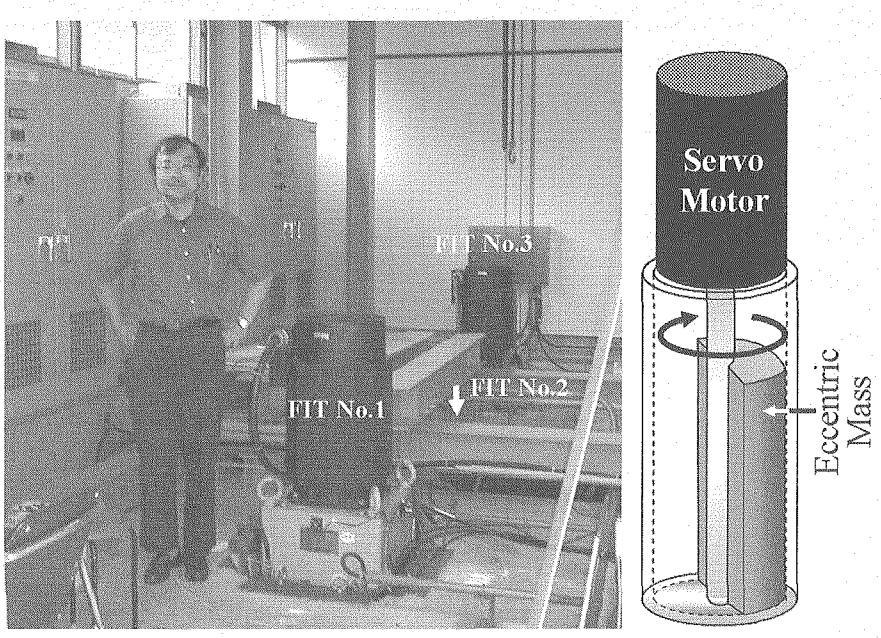

Figure 2.1.2 Photograph and schematic of the seismic ACROSS transmitters at the Tono Mine.

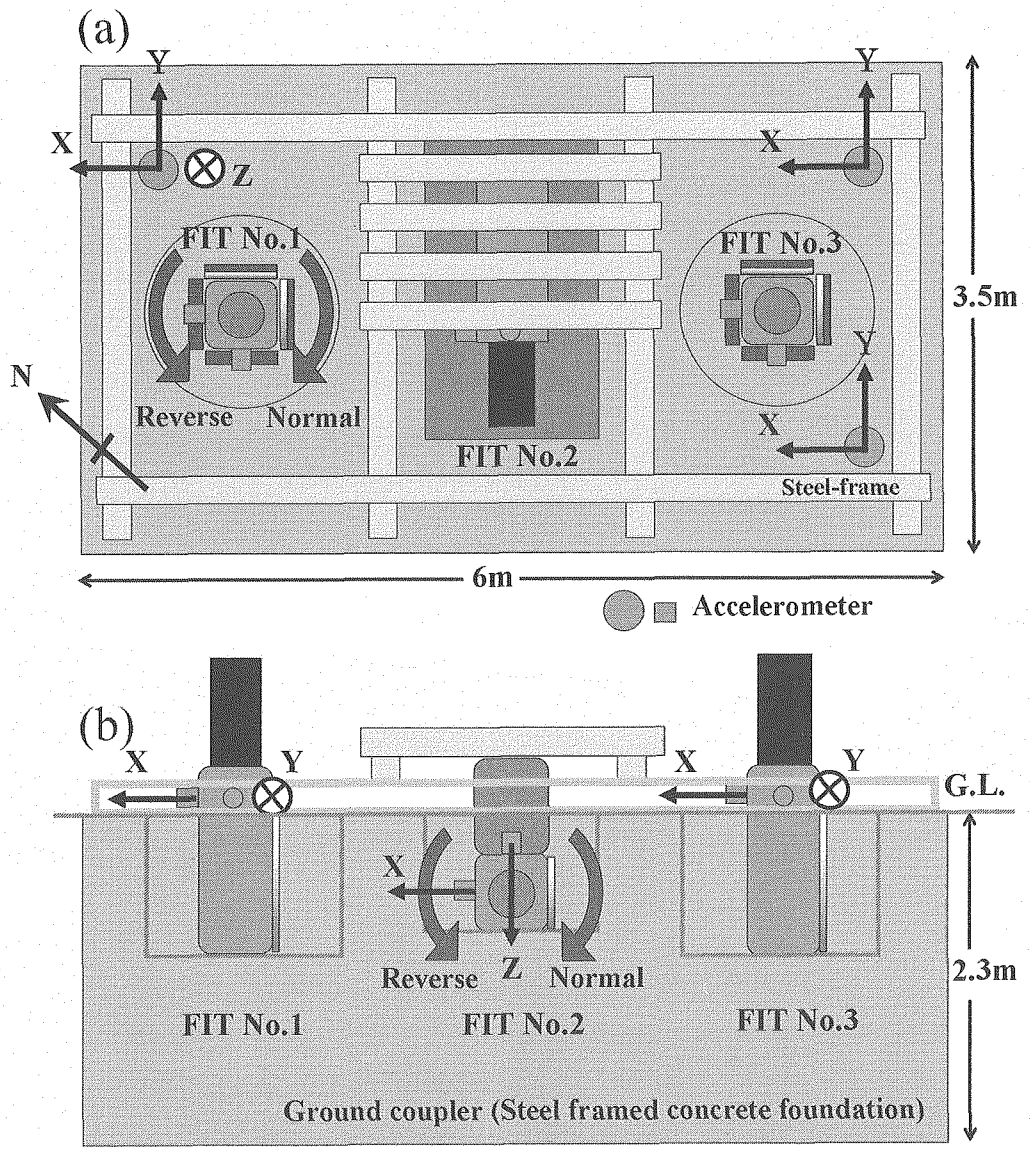

Figure 2.1.3 Layout of the seismic ACROSS transmission site at the Tono Mine. (a) top view (b) side view. FIT No.2 was moved to Horonobe Underground Research Center in October 2005.

2.2 Transmitting and receiving technologies of the Seismic ACROSS

2.2.1 Introduction

The ACROSS (Accurately Controlled Routinely Operated Signal System) is a technology to detect possible subtle changes of the physical state of the Earth's structure using precise and continuous signal transmitter-receiver systems. The ACROSS research group in the Tono Geoscience Center has made efforts to develop key technologies for this system in viewpoint of the seismological and electromagnetic application [1]. In the seismic ACROSS, there are several important research targets: external phase control mechanism for the source, long durational operation, use of rotational seismic source by a servo-motor and timing control system by GPS synchronization. In addition to the above, we also made efforts to develop a seismometer calibration method, the receiving system for signals transmitted by ACROSS, and theoretical studies for analyzing ACROSS signals. In this article, we report technologies of transmission and recording and controlling of seismic source.

The current system is 20 tonf seismic source developed in 1996. The magnitude of force created by this system depends on the rotational frequency. Although the system has relatively small force in low frequency such as 1-10 Hz used in the Earth's structural studies due to the above relation, the current ACROSS system with approximately 10-35 Hz band has advantages in precise GPS timing synchronization, the design of FM transmission, and periodical change of rotational direction. These advantages are important factors in long duration stable transmission of signals and obtaining high S/N by the precise data stacking.

2.2.2 Transmission technologies

(1) Features of the current seismic signal transmitter

The current ACROSS system placed in the Tono Mine, Toki city, Japan is shown in Figure 2.2.1. This system can create seismic signals by rotation of an eccentric mass controlled by a servo-motor. The centrifugal force generated by rotation of mass gives vibration to the ground. The vibration force is proportional to the square of rotational angular frequency. The force F is given by the following equation,

$$F(\omega) = MR\omega^2 \qquad (2.2.1)$$

where M is eccentric mass, R is radius of rotation, and ω is angular frequency. MR in equation (2.2.1) is also called eccentric moment or first moment. Due to this relation,

the force in low frequency is smaller than that in the high frequency. If we can control the magnitude of the eccentric moment, we can adjust the frequency dependence of F. The current ACROSS has no function to control the magnitude of the eccentric moment [2].

The single unit has one rotational mass and rotates the direction of force with time. The data using a single unit seems not easy to process by rotation of the force direction. In order to overcome this complexity, the combination of two oppositely rotational units has been used. The combination of two units is called linear vibration unit. This method has been adopted for vibrators targeting buildings and structure tests. In the past ACROSS research, this liner unit was also developed [3].

However, we have adopted to use the single unit rather than linear unit because of it simplicity of control, relatively low costs and easiness to develop. The linear unit can be easily prepared if we combine plural units at the same time. In this article, we describe the single unit, which has been used by the seismic ACROSS.

(2) FM transmission with GPS synchronization

In order to obtain the transfer function or the Green function between source and receiver, it is necessary to obtain the source signature. The simplest way to send synchronized signal to many stations, use of the common timing clock can be the best. Recently we can buy a GPS clock by reasonable costs. The GPS system uses atomic oscillators. The FM transmission in the ACROSS uses the GPS synchronization technique. The details are given in later section.

In the current seismic ACROSS transmitter, the phase-control method, in which the rotation of the servo-motor is controlled by supply of external pulses (Yamaoka *et al.*, 1995[4]) is used. One pulse makes 1/2000 of one rotation. The angle of rotation is measured by a rotary encoder, whose precision is 1/8000 (7.9×10^{-4} radian). Control pulses are generated by a pulse generator with the precise DDS (Direct Digital Synthesizer) synchronized with 10MHz signal supplied by GPS clock. By the expression of linear drift of phase of the transmitter used by the pulse generator, this rotational precision equals to 7.9×10^{-4} radian during 8.9 years. The FM transmission can be achieved by continuous change of frequency of control pulses with order of milliseconds holding phase continuity. The timing of frequency change is also based on 10MHz signal supplied by GPS clock.

The phase angle of the eccentric mass is measured by Z-phase, which is the 0-base of the rotary encoder. The synchronization of the true North and the rotational direction is achieved by fine control of rotation frequency.

Figure 2.2.2 shows the results of measurement of phase angle variation with time when the source is operated by 25 Hz monotonic frequency. In the ideal case, the

direction of mass should head to the same direction every second, and the data show slight change with time due to the perturbation of the motor rotation. We may recognize $1 - 2 \times 10^{-5}$ radian variation of phase in good correlation to the temperature variation. The variation seen in phase angles has diurnal variation, which may be caused by the electrical response change due to temperature change. The electronics circuit of the measurement and servo-control systems may be affected by temperature change. The random component in the perturbation of the phase angle may increase the noise level, but it may be not large. The phase variation of 10^{-5} radian with 25 Hz corresponds to 6.4×10^{-8} second (64 ns). The drift of phase shift may cause degradation of stacking, which affects the precision of transfer function. For 25 Hz transmission frequency, the error on the frequency is 3.56×10^{-13} Hz in calculated value. If we allow the drift of phase is nearly equal to the error of rotary encoder (7.9×10^{-4} radian), the seismic ACROSS source can be operated during 11 year without adjustment. In real operation, the life of bearings and electrical power failure may be shorter or more frequent occurrence than 11 years.

(3) FM transmission and optimization of transmission signal

P, S and surface waves are generated by applying force to the ground. In general, the Earth's crust is heterogeneous and an observed record at far distance may comprise several different phases such as P, S, reflected waves and surface waves. Identification of each phase requires transmission of plural frequencies considering modes of seismic waves and heterogeneities.

For the necessity of plural frequencies, the change of frequency can be done by transmission of a particular frequency with some time frame and gather of each session data for the particular frequency. However, it may not apply to the case of rapid change of physical state through the media. Alternative way is the FM method, which uses transmission of plural frequencies with a short time window, and we have used this FM transmission [5].

In the FM method, the acceleration and the deceleration of motor should be repeated by the precise period, say T, and the frequency sweep from f1 to f2. This is called FM (or chirp) signal transmission. This FM transmission generates a series of line spectrum from f1 to f2 with $1/T=\Delta f$ separation (e.g., [6]). By selection of sweep band and the carrier frequency, arbitrary series of line spectrum can be obtained. Even two different series of lines spectrum can be transmitted with less interference each other. We have examined the optimum method for the FM sweep [7]. In this study, two criterions are considered to evaluate the precision of transmission: the leakage of the source power to the outside of the transmission frequency band and the unity amplitude of spectrum over the band. Figure 2.2.3 shows one example of frequency sweep design

(4^{th} transmission, [2]). In comparison, a saw shape transmission used in the early development stage is shown. The comparison of two indicates small leakage of the source power to the outside of the transmission frequency band for the sweep method used in the recent. In the recent one can get nearly unity amplitude over the frequency band and small leakage outside of the band.

(4) Transfer function by linear vibration

The vibrations heading toward the receiver and oscillate in vertical and horizontal direction correspond to SV wave and P wave, respectively. The vibration perpendicular to SV and P oscillation corresponds to SH wave. The linear vibration is obtained by addition and subtraction of two opposite rotational records generated by a single unit. Figure 2.2.4 shows switch of rotation with a time schedule. Figure 2.2.5 shows particle motion records observed by X and Y accelerometers, which are perpendicular each other, put on the ACROSS unit using the transmission from 17:00 JST on April 15, 2003 to 17:00 JST on April 19, 2003 [2]. The transmission signal is shown in Figure 2.2.3. The stacking of each 100 seconds with normal and reverse rotation was applied. The heading of eccentric mass was true N at start time of every 100 seconds. The vibration to N-S and the E-W vibration were obtained by addition and subtraction of normal and reverse vibrations, respectively. Seeing the results shown in Figure 2.2.5, the synthetic vibrations give nice linear vibrations.

(5) Continuous transmission

The next difficulty on the transmission of seismic waves is continuous operation for a long period. We succeeded to transmit seismic signals for one and half year nearly continuous operation since the year's end of 2002 [2]. There are no serious problems during this period. Table 2.2.1 lists the troubles during this long operation. Most of troubles were caused by switching of rotational directions due to miss-control by the PC. The rotation for normal direction has no experience of troubles. Another trouble was caused by the 49.7 days problem in the Window 98 PC operating system. This caused hang-up the PC when PC was operated more than 49.7 days. This problem was solved by the replacement of the windows OS.

2.2.3 Receiving technologies

(1) Data sampling synchronized with GPS clock

In order to use accurate seismic source signals, it is necessary to get GPS synchronized clock for seismometers, too [4]. A/D converters and internal clock of seismometers can be synchronized to GPS clock within 1 micro second.

The miss adjustment of clock may cause broadening of spectrum. We assume 1 kHz sampling, and 100 seconds for the window length. By Fourier transform of receiving data, a series of line spectrum from 0 to 500 Hz with 0.01 Hz spacing is obtained. We call this observation channel. The observation channel may include ground noise and electrical noise. We assume the transmission of sweep signal from 13 to 23 Hz with 20 seconds repetition period. This generates the series of line spectrum from 13 to 23 Hz with 0.05 Hz spacing. This is called signal channel. Other spectral peaks than signal channel are called noise channel. The signal channel gives intensity of signal, and the noise channel has information of noise level near the source signals. Figure 2.2.6 shows the observed spectrum of horizontal records near the receiver during the 4^{th} transmission. In this case, every 100 seconds stacking and 90 hours operation are used. S/N for the frequency range from 15.47 to 20.57 Hz is ~10^5. The results show a series of line spectrum suggesting nice control of transmission. In the spectral space between adjacent line spectra, another series of spectrum transmitted by another sweep can be inserted by shit of the carrier frequency. This method enable us multiple transmission [6].

(2) Time segment stacking

When we want to obtain very precise transfer function or carry out small signal observation at long distance, it may be difficult to use long data, which may cause problem on memory size in the compute for a processing. In this purpose, time segment stacking method was made [8]. Stacking using the segments with duration T with the same beginning can extract signals with n/T signals. This corresponds to the comb filter. We and our colleagues developed a recorder which has this time segment staking called TSS (Time Segment Stacking) recorder. The records shown in Figure 2.2.6 was obtained by this TSS recorder, which equips 16 bit A/D and GPS synchronization facility. There are three different kind of TSS recorder: LS-8000SH [9], ECD-1200 and MD8464 [10].

2.2.4 Summary

We described the transmitting and receiving technologies of the seismic ACROSS. The highlights of the system are very precise controls in frequency, phase and amplitude obtained by GPS synchronization technique. In addition to the precise control, the combination of normal and reverse rotations can generate synthetic records equivalent to the linear directional vibrations. The swept FM (chirp) signals from f1 to f2 with T second duration generate a series of line spectrum from f1 Hz to f2 Hz with 1/T Hz separation. This system enables us to observe subtle change of physical and chemical states in the Earth's interior. One example is velocity change in the interior

and another example is change of reflectivity at the surface of subducting slab [11].

Reference

[1] M. Kumazawa, T. Kunitomo, Y. Yokoyama, T. Nakajima and K. Tsuruga, ACROSS: Theoretical and Technical Developments and Prospect to Future Applications, *JNC technical review*, 9, 115-129, 2000 (in Japanese with English abst.).

[2] T. Kunitomo and M. Kumazawa, Active Monitoring of the Earth's Structure by the Seismic ACROSS - Development of the Seismic ACROSS and Continuous Transmission at Tono Mine ACROSS Station -, *In the Proceedings of "1st International Workshop on Active Monitoring in the Solid Earth Geophysics (IWAM04)", Task Group for Active Monitoring, Mizunami, Japan*, 2004a.

[3] K. Ogawa, M. Kumazawa, K. Ishihara, M. Nakatani, T. Kunitomo, N. Fujii, K. Yamaoka, H. Kumagai, Y. Takei, Y. Hasada, K. Miyakawa, N. Ikeda and K. Suzuki, HIT: A Mobil ACROSS, *Abstracts of Japan Earth and Planetary Science Joint Meeting*, 181, 1997 (in Japanese).

[4] K. Yamaoka, Y. Hasada, M. Nakano, M. Kumazawa, H. Maruo, H. Oshima, Control system of Frequency Modulated ACROSS to be linked with TS Stacking recorders, *Abstracts of fall meeting of the Seismological Society of Japan*, 9, 1995 (in Japanese).

[5] M. Kumazawa, S. Watanabe and K. Yamaoka, Frequency Modulation of ACROSS for Simultaneous Excitation of a Set of Equally Spaced Frequencies, *Abstracts of fall meeting of the Seismological Society of Japan*, 9, 1995a (in Japanese).

[6] T. Kunitomo, K. Yamaoka, M. Kumazawa, S. Inoue, N. Ikeda, K. Miyakawa and S. Watanabe, Frequency Modulation Technology of ACROSS (Accurately Controlled Routinely Operated Signal System), *Proceedings of SEGJ 101th Annual Fall Meeting*, 79-83, 1999 (in Japanese).

[7] T. Kunitomo T. and M. Kumazawa, Optimum FM signal for monitoring the underground states by means of the seismic ACROSS, *XXIII General Assembly of the International Union of Geodesy and Geophysics, Sapporo, Japan, IUGG2003 Abstracts*, A.145,June 30 - July 11,2003.

[8] M. Kumazawa, K. Yamaoka, Y. Takei, H. Oshima and H. Tateishi, TS stacker as a narrow band multichannel device to record Fourier components of transfer function between a source and a receiver, *Abstracts of Japan Earth and Planetary Science Joint Meeting*, 373, 1995b (in Japanese).

[9] K. Yamaoka, K. Kobayashi, T. Kunitomo, M. Kumazawa, H. Ando and M. Iwasaki, TS-Stacker on the data logger DATAMARK LS8000, *Abstracts of fall meeting of the Seismological Society of Japan*, 156, 1997 (in Japanese).

[10] T. Kunitomo and M. Kumazawa, Active Monitoring of the Earth's Structure by the Seismic ACROSS- Field Examples at the Tono Mine ACROSS Experimental Site -,

In the Proceedings of "1st International Workshop on Active Monitoring in the Solid Earth Geophysics (IWAM04)", Task Group for Active Monitoring, Mizunami, Japan, 2004b.

[11] J. Kasahara, K. Tsuruga, Y. Hasada, K.Yamaoka, N. Fujii, Y. Yoshida, T. Kunitomo and M. Kumazawa, A proposal of imaging of the plate boundary using the active monitoring method, *In the Proceedings of "1st International Workshop on Active Monitoring in the Solid Earth Geophysics (IWAM04)", Task Group for Active Monitoring, Mizunami, Japan*, 2004.

Takahiro KUNITOMO and Mineo KUMAZAWA
Tono Geoscientific Research Unit, JAEA

Table 2.2.1 Trouble list in the continuous transmissions from 18:00 JST on October 28, 2002 to 24:00 JST on December 31, 2006.

Event	Cause	Time	Solution
Power failure	Thunderbolt and Power failure	13	Restart by the remote operation used LAN
Automatic stop	Human error	3	Adjustment of the threshold level or restart
GPS clock failure	Failure of the power module of GPS clock	1	(8th year from the date of purchase) Repair
leap second	Phase shift by inserting a leap second	1	Phase adjustment
PC trouble	Trouble of the internal clock	4	Update of the control software during 3rd transmission
	OS bug (Windows 98)	5	Windows update (Windows 98) during 5rd transmission Windows replace (Windows98→Windows2000)
	PC hung-up	2	Update of the control software on Windows2000

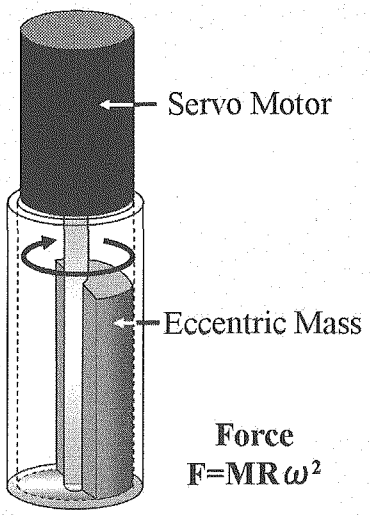

Figure 2.2.1 Schematic of the current seismic ACROSS transmitter.

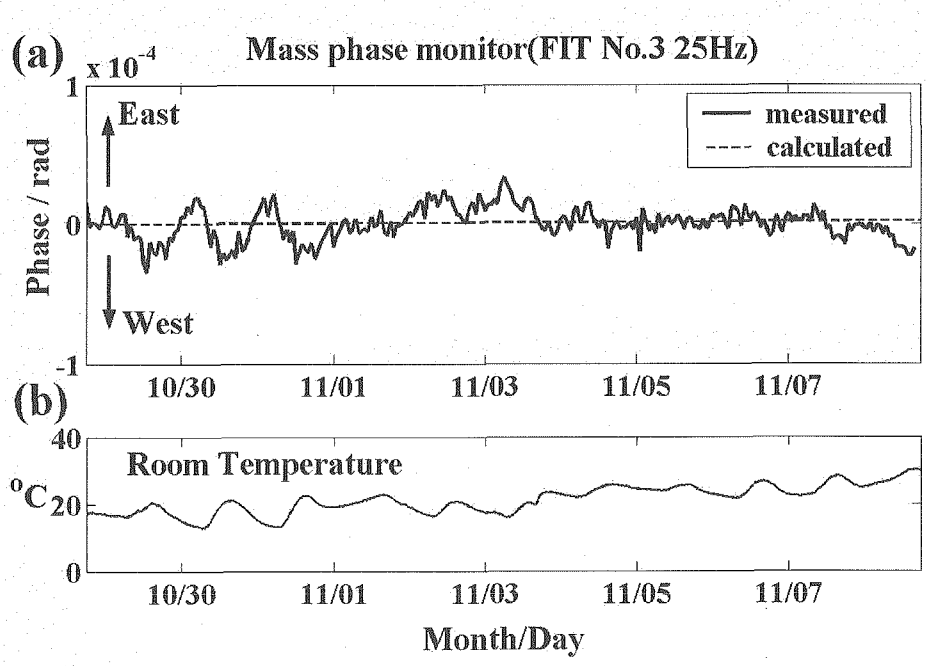

Figure 2.2.2 (a) Phase angle variation with time of the eccentric mass at 25Hz rotation. Average per hour of phase data measured every second. (b) Room temperature in the transmission site.

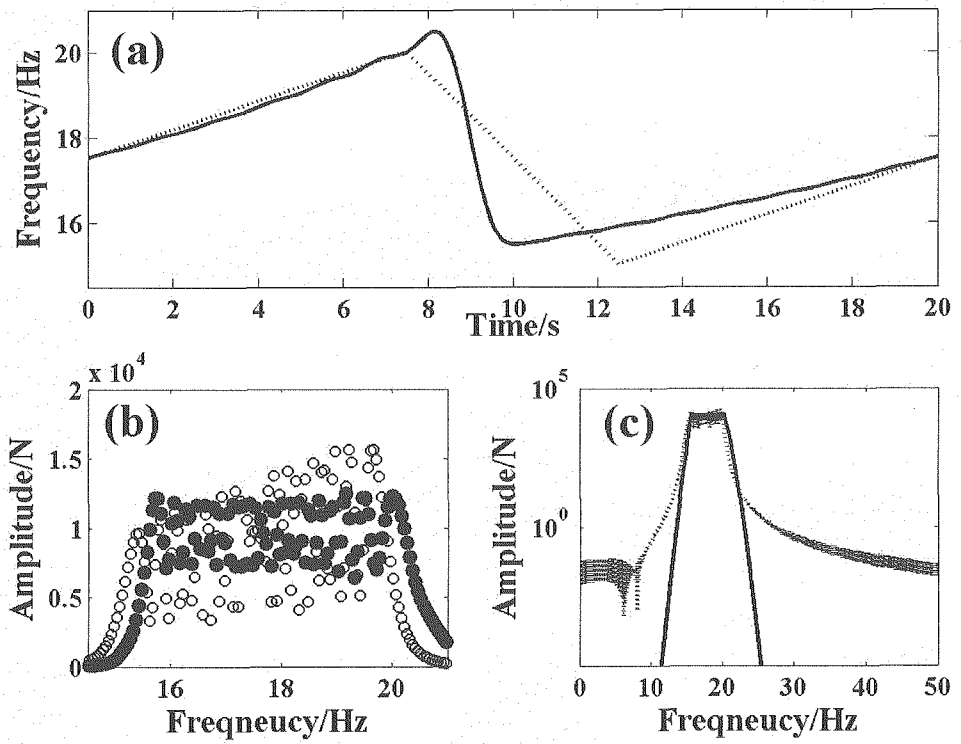

Figure 2.2.3 (a) Comparison of FM signal waves whose carrier frequency and sweep period are the same as 17.52Hz, 20 seconds, respectively. Solid line:4th transmission. Dotted line: early transmission (linear sweep). (b) Flatness of force source amplitude spectrum. solid circle:4th transmission. Dots line: early transmission. (c) Leakage of the source power to the outside transmission frequency band. Solid line:4th transmission. Dotted line: early transmission.

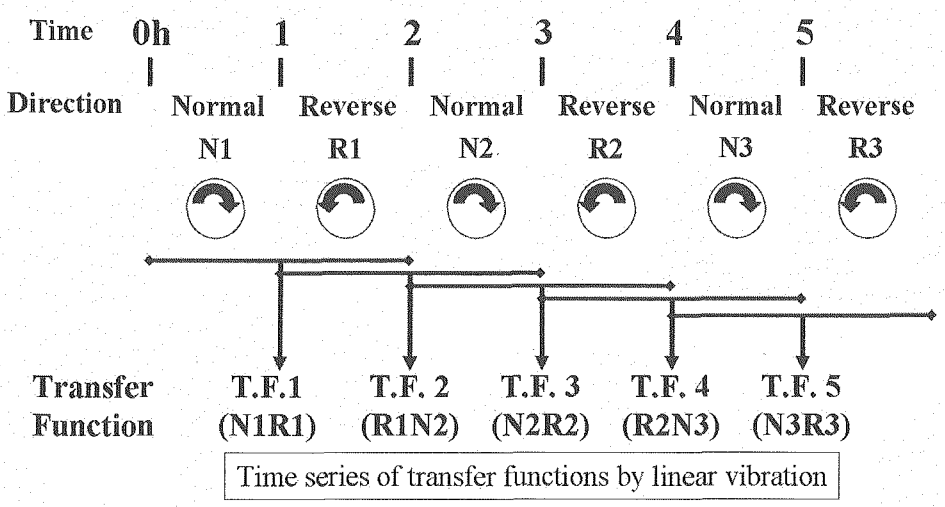

Figure 2.2.4 Continuous switch of rotational direction to obtain time series of transfer function by linear vibration with the single unit ACORSS transmitter.

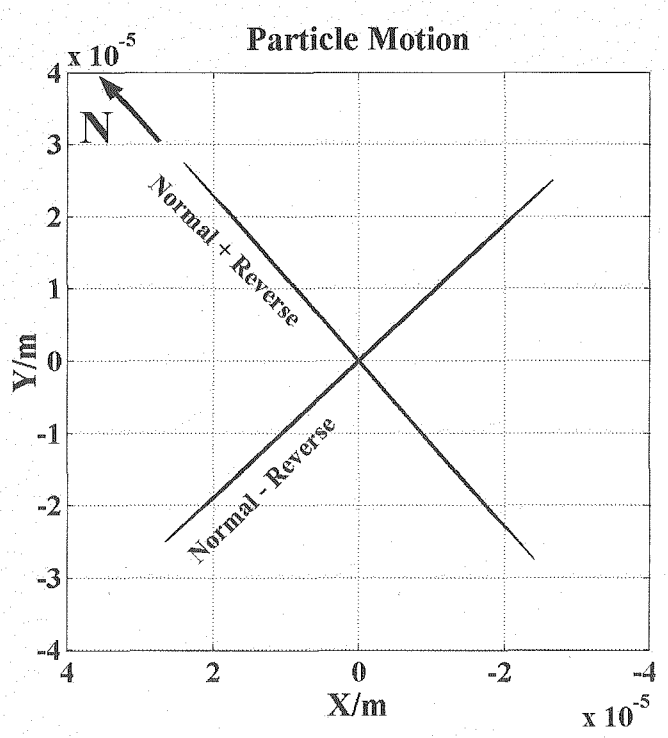

Figure 2.2.5 Particle motions of composite record sections of normal and reverse rotation of the seismic ACROSS transmitter.

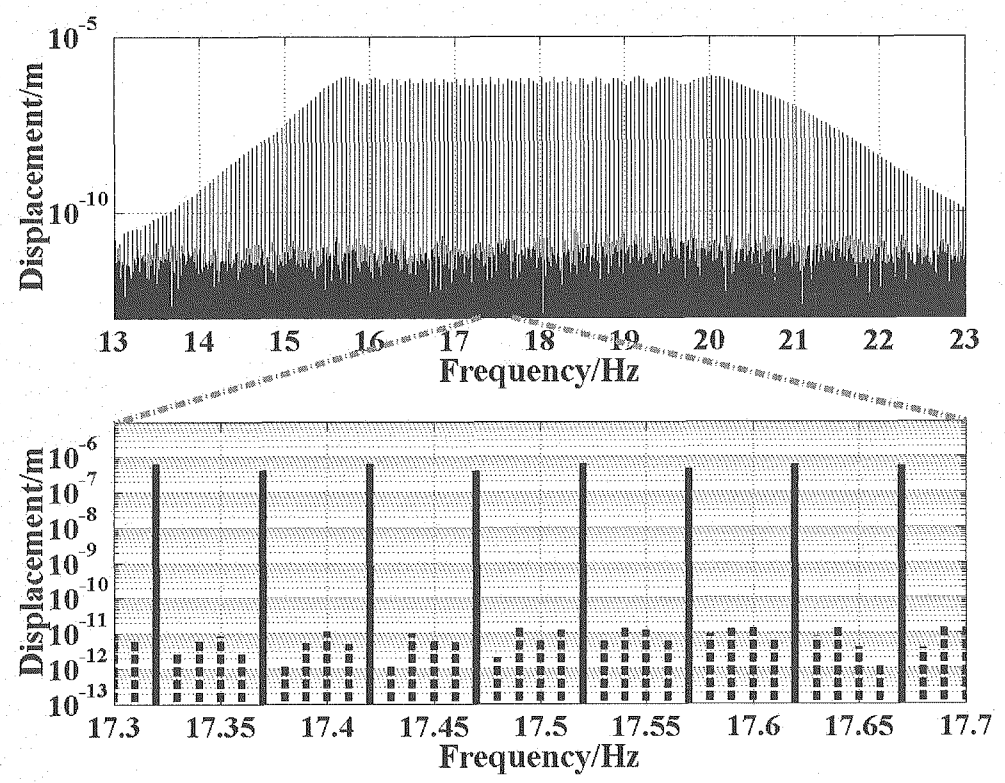

Figure 2.2.6 Observed amplitude spectrum in displacement during 4th transmission. Solid lines: signal channels. Broken lines: noise channels.

2.3 Field examples by Seismic ACROSS at the Tono Mine experimental site

2.3.1 Introduction

In order to monitor the subtle change occurring in the Earth's crust, we have continuously transmitted precisely controlled FM seismic signals from the seismic ACROSS (Accurately Controlled Routinely Operated Signal System) transmission site located at the Tono Mine, Toki, Japan during one and half year since the end of 2002. The above signals have been monitored by the Hi-net seismic observation network of the NEID and the JMA seismic network [1, 2] and nearby seismic arrays [3, 4]. In this report, we describe the results obtained by the seismic array in the gallery of the Tono Mine, which is located at the depth of about 120 m below the surface. The seismometers are placed from 140m to 360m distance from the source. The objectives of this observation are to monitor the source signature in order to obtain the transfer function and know temporal variation of seismic wave signatures between the source and receivers if exist.

In this report, we show some observed characteristics of source signatures and the effects of rain and diurnal variation on the S phase and the coda parts by this continuous transmission. Using these results, we discuss the temporal stability of the seismic ACROSS in viewpoint of the shallow seismic structure change due to rainfalls.

2.3.2 Radiated signals

The outline of the seismic ACROSS is given in the Kunitomo & Kumazawa [5]. In this report, we describe the identification of observed phases and the temporal change of these phases observed by the 2nd and the 4th transmissions.

(1) The outline of transmissions

The 2nd transmission was carried out from 18:00 JST on November 19, 2002 to 18:00 JST on December 2, 2002. The transmission was the broadband FM signal in the seismic ACROSS. The frequency bands was 10.02-20.02 Hz. Using the records of this broadband transmission signals, the identification of phases can be done by the time domain seismic records obtained by the inverse Fourier transform of the estimated transfer function because each phase has the distinct travel time. During this transmission, we used two ACROSS units simultaneously. The S-wave analysis was carried out only by the record obtained by the horizontal vibration using the FIT– No.1 unit.

The 4th transmission was carried out from 17:00 JST on April 15, 2003 to 17:00 JST

on January 28, 2004. The transmission band using the FIT No.1 unit was 15.47-20.57 Hz. As this transmission band is narrower than that of the 2nd transmission, the seismic energy may be concentrated in a narrow frequency band enabling to detect signals at further distance than by the 2nd case.

The modulation periods for both transmissions were 20 seconds and produced a series of line spectrum with 0.05 Hz separation in the spectral domain. The rotational direction was reversed every one hour. Using opposite rotation records, we can produce the seismic records, one heading to the source and the other perpendicular to the radial direction [6].

(2) The transmission spectra

The transfer function is defined by the division of receiving signal of the displacement at the receiver by the source spectrum of the applying force. The applying force $F(\omega)$ is given by equation 2.2.1.

The eccentric moment is MR and constant, and it can be estimated. Using MR and the revolution number, we can obtain the applying force $F(\omega)$. If we know the instantaneous angular frequency ω, we can obtain the force $F(\omega)$, as a function of time. Although we can know the ideal estimation value of the applying force when we use the FM transmission method, the real value has some errors due to the delay of rotation of motor against to the controlled signals. To correct the rotational delay, we use the output time-series signals of the rotary encoder synchronized with a GPS clock. The difference between the designed rotation and measured values are estimated as order of one percent.

Figure 2.3.1 shows an example of transmission force spectrum $F(\omega)$ during the 4th transmission. The phase angle of the rotation was measured by the rotational encoder counter. The sampling frequency is 1kHz with synchronized with a GPS clock. To improve the S/N, the stacking of observed waveforms during 100 seconds was applied. The time series of the rotational phase measurements was transformed to the spectral domain using the FFT, and the transfer function can be obtained by the applying force and the observed displacement.

(3) Procedure of the reverse rotation

In this section, we explain the procedure to get reverse rotation. The time schedule table is needed to observe the source signatures. During the 2nd and 4th transmissions, the rotational direction was switched every one hour to prepare for the reverse rotation. This transient period comprises deceleration, switching, and acceleration terns as shown in Figure 2.3.2. This transient period is not used for the analysis. We used 100 seconds time frame assuming the shorter travel time than 100 seconds in case of the

current interests. Figure 2.3.2 shows the time frame for the 100 seconds transmission.

The prelude is the period to avoid the overlapping of FM signal and transmission during the transient period. Excluding the 200 seconds including the transient period and the prelude, the rest of 3400 seconds during every one hour time frame should give the pure transmission signal without effects of switching of the rotational direction.

2.3.3 Observation

Figure 2.3.3 shows the locations of the Tono Mine transmission site (35°23'15.4"N, 137°12'55.0"E, 265 m in altitude) and the seismic array in the gallery of the Tono Mine (125 m below the surface), where is near the transmission site. The seismic array comprises 8 borehole seismometers.

The borehole seismometers are accelerometers made by Akashi Co., Ltd (model JEP-7B3). This was selected in viewpoint of better characteristics in linearity, self-noise in transmission frequency band (5-50Hz), and absolute calibration by the manufacturer [7, 8].

The seismometers are buried in 2m deep near the geological boundary between the Toki granite layer and the tertiary Mizunami Group to minimize the temperature effect and make good contact to the hard rock. The seismometers are placed in NS, EW and UD. The temperature change in the hole of sesmometers during the day was within 0.1 °C.

The outputs from the seismometers were record by a PC base recorder with a time accumulated mode (time segment stacking mode). This recorder has 16-bit A/D converters. The timing accuracy of the A/D sampling is approximately 40 ns by use of the GPS clock synchronization. The GPS antenna signal is sent to the recorder with a 400m long optical fiber.

The sampling frequency of the 2nd and the 4th transmissions are 1 kHz, and the real-time stacking was done in time domain, which stacking interval (time segment) is 100 seconds. To minimize the effect of contamination of unfavorable large signals such as natural earthquake and/or blasting, the larger signals higher than the threshold are excluded from the stacking process. Each one hour stacking data was stored as one data file in the PC hard-disk.

2.3.4 Analysis

(1) 2nd transmission

The 2nd transmission is done in the frequency band between 10.02 and 20.02 Hz, and it enables us to separate the travel times of different phases. The steps of the

analysis are:

1) Stacking of 48 files of one hour stacking data for each normal and reverse rotation.
2) FFT to obtain frequency domain records.
3) Applying compensation of seismometer, amplifier and filter characteristics to the records.
4) Obtaining the transfer function by the division of the received spectrum by the source spectrum.
5) Making radial and transverse component by addition and subtraction of the normal and reverse rotation records, modifying phase of recorded signals depending on the azimuth of receiver viewed from the source.
6) Making radial, transverse and vertical components by coordinate rotation of NS, EW and UD component shown in Figure 2.3.4.
7) Obtaining line spectra in 8.02-25.02Hz every 0.05Hz separation. And converting into time domain records by the inverse Fourier transform [6].

In order to avoid the side-robe effect due to the large amplitude phases, we applied the Hanning window before the inverse Fourier transform.

(2) 4th transmission

The frequency band of the 4th transmission is between 15.47Hz- 20.57Hz. The data from 0:00 on September 18, 2003 to 0:00 on October 12, 2003 were used for the analysis. The stacking was made by every one hour. The processing is the same as one in the 2nd transmission. Total data length is 576 hours.

2.3.5 Results

(1) Results obtained by the 2nd transmission

Figure 2.3.5 shows the record section of whole components with distance from the source. The transverse vibration and the radial vibration generated large amplitude arrivals in t-component records (tT) and v-component records (vR), respectively. The t-component and r-component, however, show arrivals with some amplitude heights by the radial and the transverse vibration, respectively. These phenomena may be caused by heterogeneous structure near the source.

Figure 2.3.6 shows part of record sections shown in Figure 2.3.5 in order to indicate the propagation of P and S waves. The phase seen in tT component is considered as the direct SH wave and one seen in vR component is as the direct SV wave. The solid circles are position of the maximum amplitudes. The apparent velocities for tT and vR are 1,250m/s and 1,080 m/s, respectively. The difference between two is considered due to the seismic anisotropy. There are some arrivals after the SV and SH phases. We think

these arrivals are multiple reflected phase generated within the tertiary Mizunami Group shown in Figure 2.3.7. The velocity structure near this seismic array was obtained by several surveys and there is no evident reflector in the Toki granitic layer, which is covered by the Mizunami Group. Considering this, the later arrivals are estimated as reflections in the tertiary layer.

(2) Results obtained by the 4th transmission

Figure 2.3.8 shows one hour records overlapping of 576 traces for the five seismometers. Due to the narrow frequency band transmission, some broadening is identified in comparison to the 2nd transmission case. The envelope of the wave packets seen around 0-0.4 second corresponds to the S wave arrival. It is seen that the temporal change of this phase is extremely small. The later arrivals seen around 0.3-0.4 second have thickening of wiggles suggesting temporal change. In order to see the temporal variation of waveforms, we made the seismic records of travel time vs. period (Figure 2.3.9a). Figure 2.3.9b shows the rainfall during the observation period. As seen in these figures, the arrivals around 0.3-0.8 seconds show clear temporal change. The large change occurred in September 21 and September 24-25. The comparison of large changes in later arrivals and rainfalls suggests that these large changes of the later arrivals are caused by the rainfall. The detailed comparison of temporal change and the rainfalls gives: 1) large change appearance during the rainfall, 2) small rainfall effect on direct S arrivals, but large for later arrivals, 3) quick response of rainfall suggesting contribution of very shallow depth, and 4) longer recover such as several weeks.

We examined the temporal change of the direct S arrivals using the 4th transmission. The arrival difference is computed by the phase and the gradient of cross-spectrums with the one hour record at 0:00 on September 18, 2003. Figure 2.3.10 show the temporal change of delay times of four vR and tT seismometer records with ones of the coupling base between the source and the ground. The results indicate larger temporal change for further seismic stations with magnitude of 0.2-0.4 ms. The SV component shows diurnal change and some effect of rainfall, but SH wave shows no diurnal change and less temporal change. The seismometer on the coupling base shows extremely small change, less than 0.1 ms.

2.3.6 Summary and discussions

We carried out long continuous operations of the seismic ACROSS. The 2nd operation was from 18:00 on November 19, 2002 to 18:00 on December 2, 2002. The 4th transmission was carried out from 17:00 on April 15, 2003 to 17:00 on January 28, 2004.

The frequency bands of the 2nd and 4th were 10.02-20.02 Hz and 15.47-20.57Hz, respectively. The small seismic array beneath the source was used for the estimation of the source signatures and temporal change of the transfer functions. It is proved that the seismic ACROSS is extremely stable for long and continuous operations which are one of mandates for long time monitor to investigate the temporal change in the Earth's interior. To obtain the better S/N, one hour time domain stack was applied.

Using the observed transfer functions, it is found that the SH and the SV waves have large seismic wave anisotropy. Using 4th transmission, it is also found that there are some temporal changes on the later arrivals, which may correspond to the reflection between the bottom of tertiary Mizunami Group, or the top of granitic layer and the ground surface (multiple reflection). The magnitude of temporal change on the SH and the SV waves are small. The temporal change has good correlation to the rainfalls. This can be explained that the ground surface layer may change the elastic properties due to rainfall affecting to the reflection coefficients. On the other hand, the direct S phase may travel through the deeper part of the Mizunami formation and may be less affected by rainfalls due to the differenced of ray paths. The quick response of temporal change supports the effect of water for the shallow part. The longer recovery period can be explained by the time constant of the formation due to low permeability of the clay contents.

References

[1] Y. Yoshida, H. Ueno, Y. Ishikawa, T. Kunitomo and M. Kumazawa, The observation and analysis of ACROSS signals by seismic networks – Determination of the transfer function -, *In the Proceedings of "1st International Workshop on Active Monitoring in the Solid Earth Geophysics (IWAM04)", Task Group for Active Monitoring, Mizunami, Japa*n, 2004.

[2] H. Nagao, T. Nakajima, M. Kumazawa and T. Kunitomo, Optimum weighted stacking method for acquisition of the ACROSS transfer functions having the maximum signal-to-noise ratio, *In the Proceedings of "1st International Workshop on Active Monitoring in the Solid Earth Geophysics (IWAM04)", Task Group for Active Monitoring, Mizunami, Japan*, 2004.

[3] K. Tsuruga, T. Kunitomo, Y. Hasada, M. Kumazawa, J. Kasahara and N. Shigeta, A dense seismic array for acquisition of high quality data in the ACROSS observation, *In the Proceedings of "1st International Workshop on Active Monitoring in the Solid Earth Geophysics (IWAM04)", Task Group for Active Monitoring, Mizunami, Japan*, 2004.

[4] A. Saiga, K. Yamaoka, T. Kunitomo, T. Watanabe, Continuous observation of travel time variation of seismic waves using the ACROSS and the seismic array at 2.4km distance, *Chikyu Monthly, Special issue "Active Monitoring"*, 2004.

[5] T. Kunitomo and M. Kumazawa, Active Monitoring of the Earth's Structure by the Seismic ACROSS -Development of the Seismic ACROSS and Continuous Transmission at Tono Mine ACROSS Station-,*In the Proceedings of "1st International Workshop on Active Monitoring in the Solid Earth Geophysics (WAM04)", Task Group for Active Monitoring, Mizunami, Japan*, 2004a.

[6] T. Kunitomo and M. Kumazawa, Active Monitoring of the Earth's Structure by the Seismic ACROSS -Transmitting and Receiving Technologies of the Seismic ACROSS-, *In the Proceedings of "1st International Workshop on Active Monitoring in the Solid Earth Geophysics (IWAM04)", Task Group for Active Monitoring, Mizunami, Japan*, 2004b.

[7] T. Kunitomo, M. Kumazawa and M. Hirai, A Seismometer for Reliable Acquisition of ACROSS Signal, *Abstracts of fall meeting of the Seismological Society of Japan*, 170, 1998(in Japanese).

[8] T. Kunitomo and M. Kumazawa, Tono seismic array observation system for ACROSS, *Abstracts of Japan Earth and Planetary Science Joint Meeting(CD-ROM)*, Ai-P005, 2000.

Takahiro KUNITOMO and Mineo KUMAZAWA
Tono Geoscientific Research Unit, JAEA

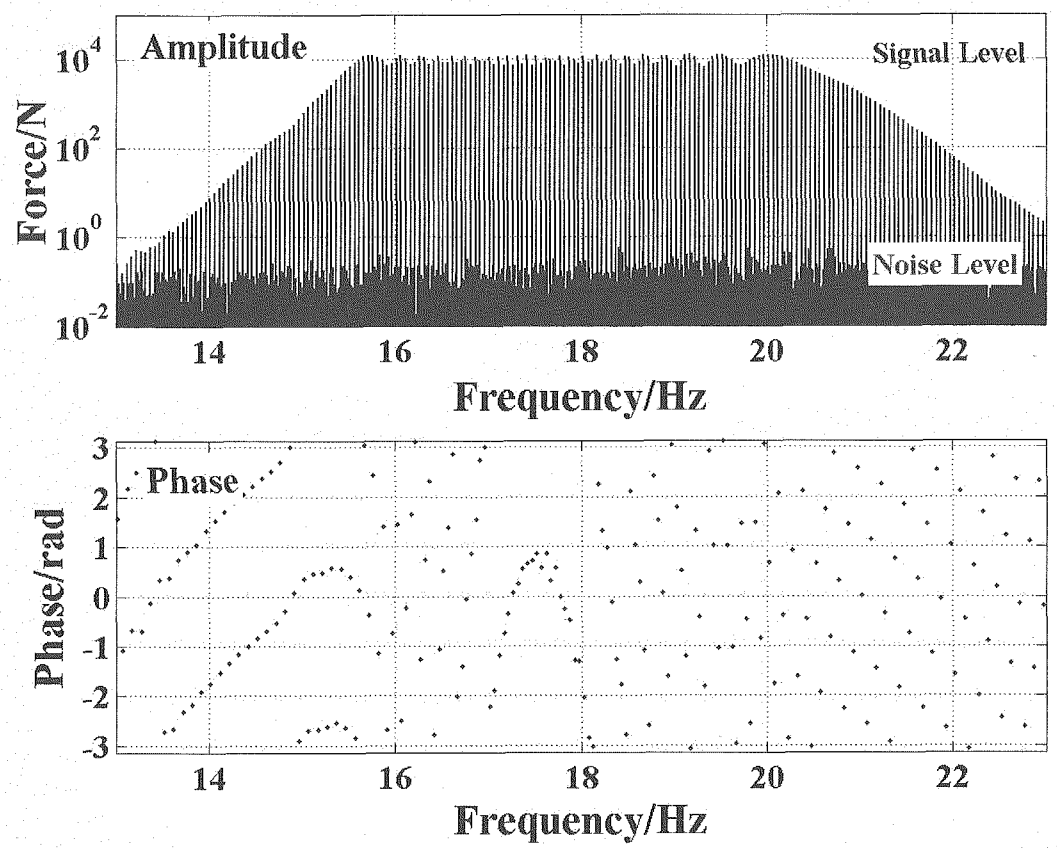

Figure 2.3.1 An example of transmission force spectrum during the 4th transmission.

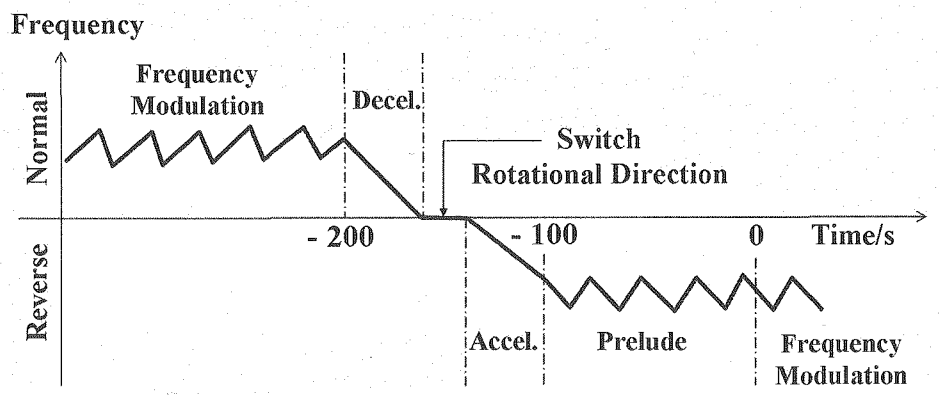

Figure 2.3.2 Procedure to switch the rotational direction.

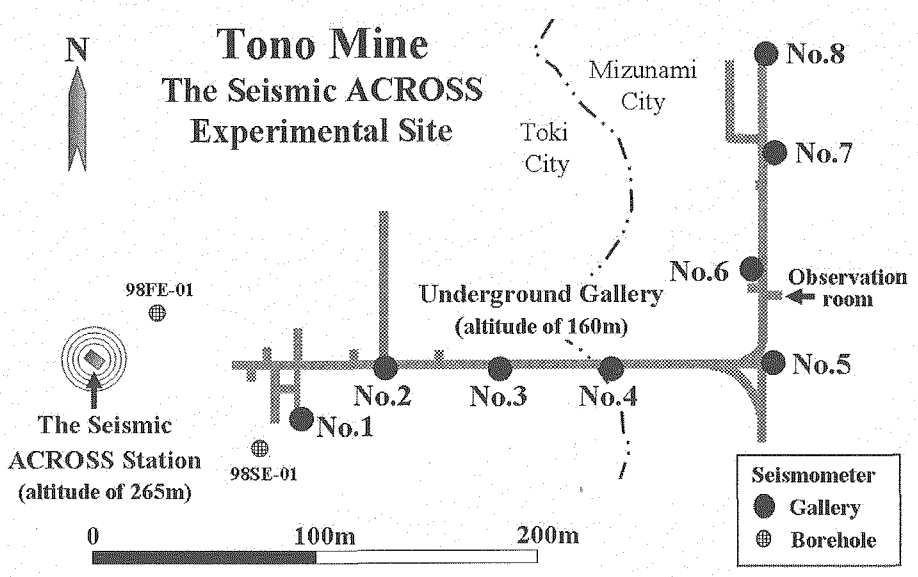

Figure 2.3.3 Location map of the facilities in the Tono Mine ACROSS experimental site.

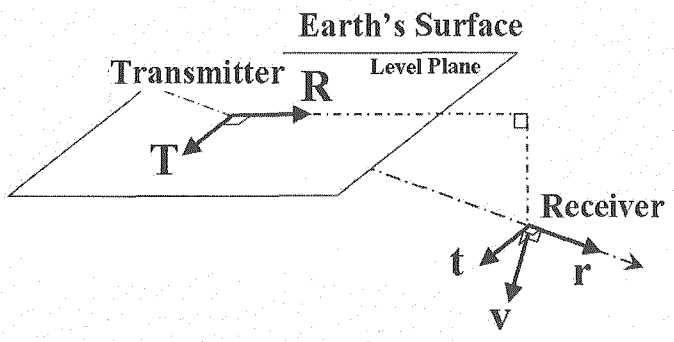

Figure 2.3.4 Definitions of vibration components at transmission site and at observation site, respectively. R (Radial), T (Transverse), r (radial), t (transverse), v (vertical).

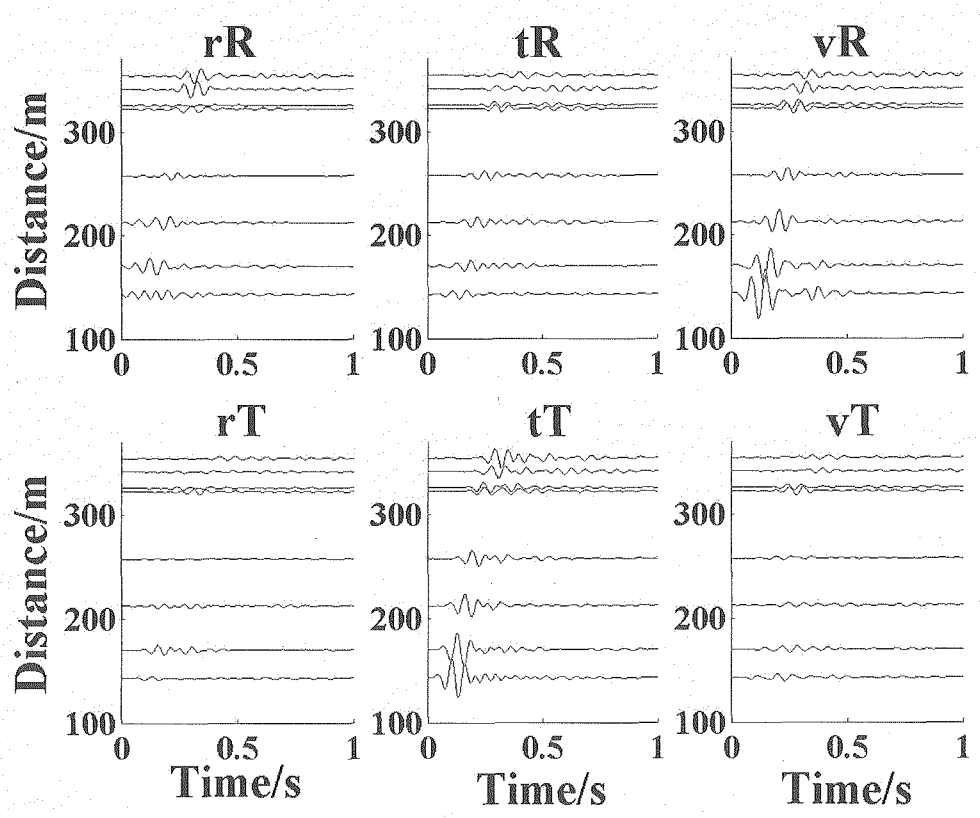

Figure 2.3.5 Record sections of whole components during the 2nd transmission.

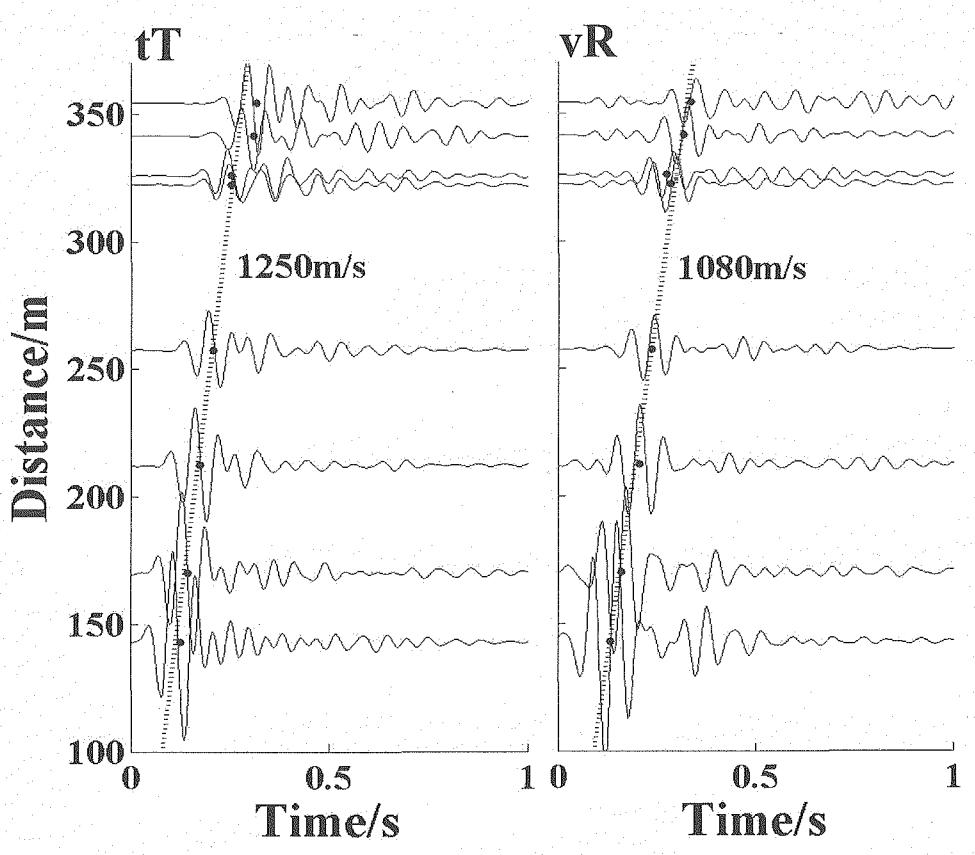

Figure 2.3.6 Record sections of tT and vR components during the 2nd transmission. Dots are arrival times of direct S waves estimated from peak of envelope.

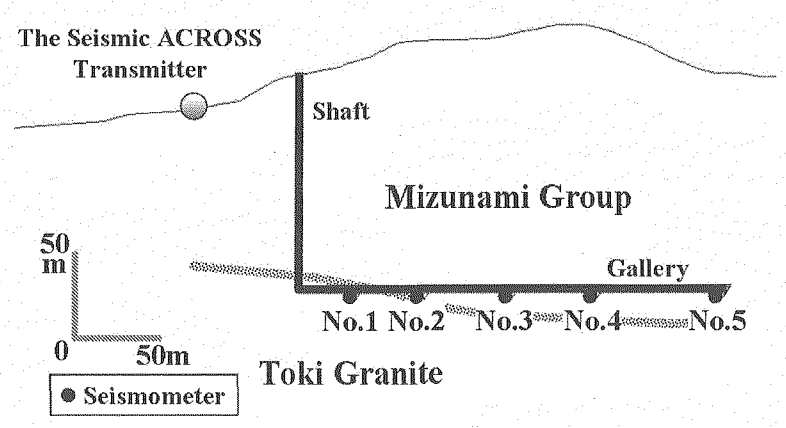

Figure 2.3.7 Schematic view of geological cross section at the Tono Mine ACROSS experimental site

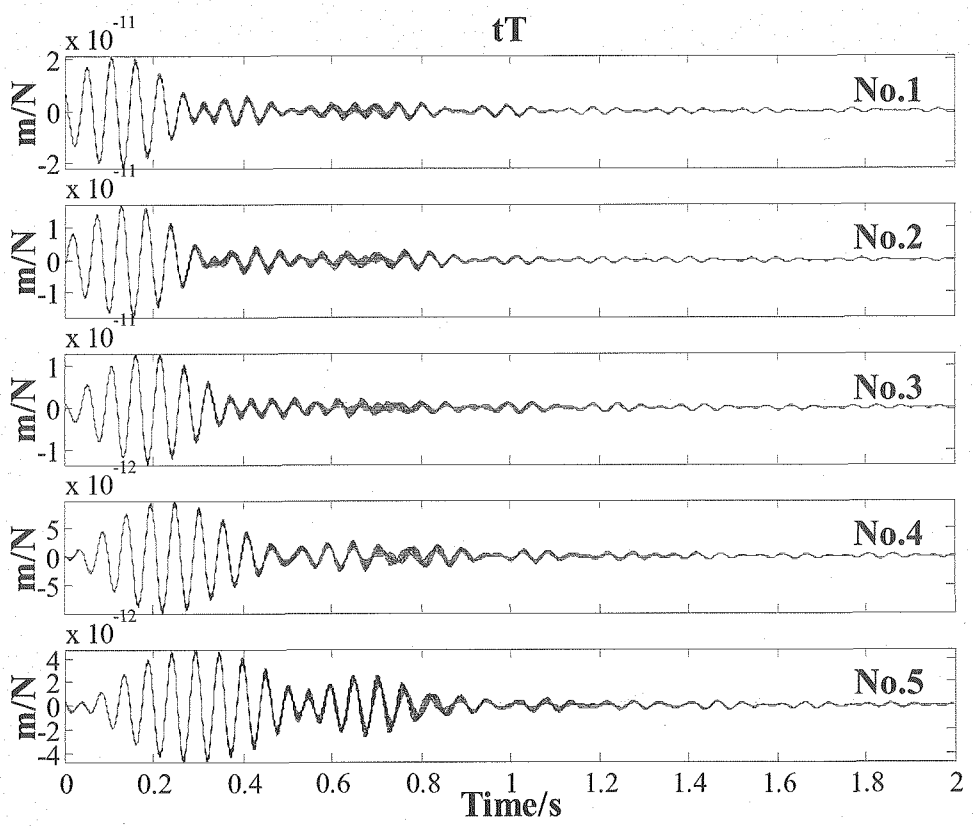

Figure 2.3.8 Record sections overlapping of 576 traces (576 hours) during the 4th transmission.

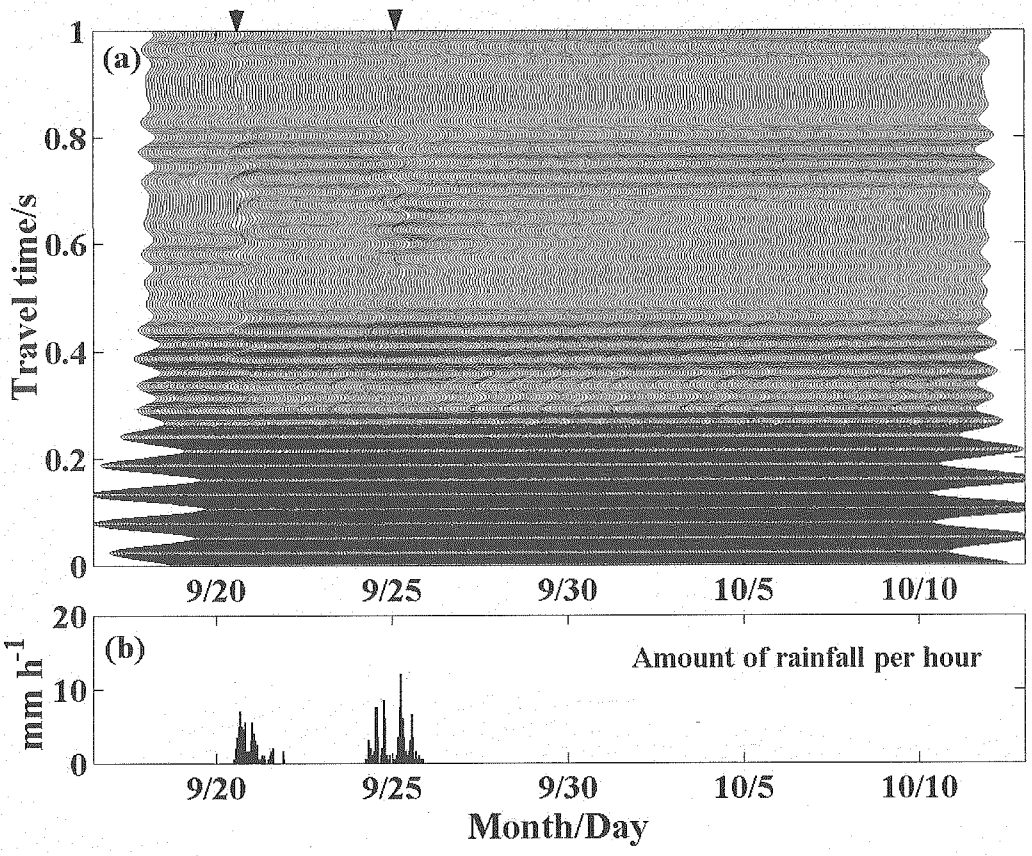

Figure 2.3.9 (a)Temporal variation of record sections of tT component at No.1 observation point. (b) Amount of rainfall per hour in observation area.

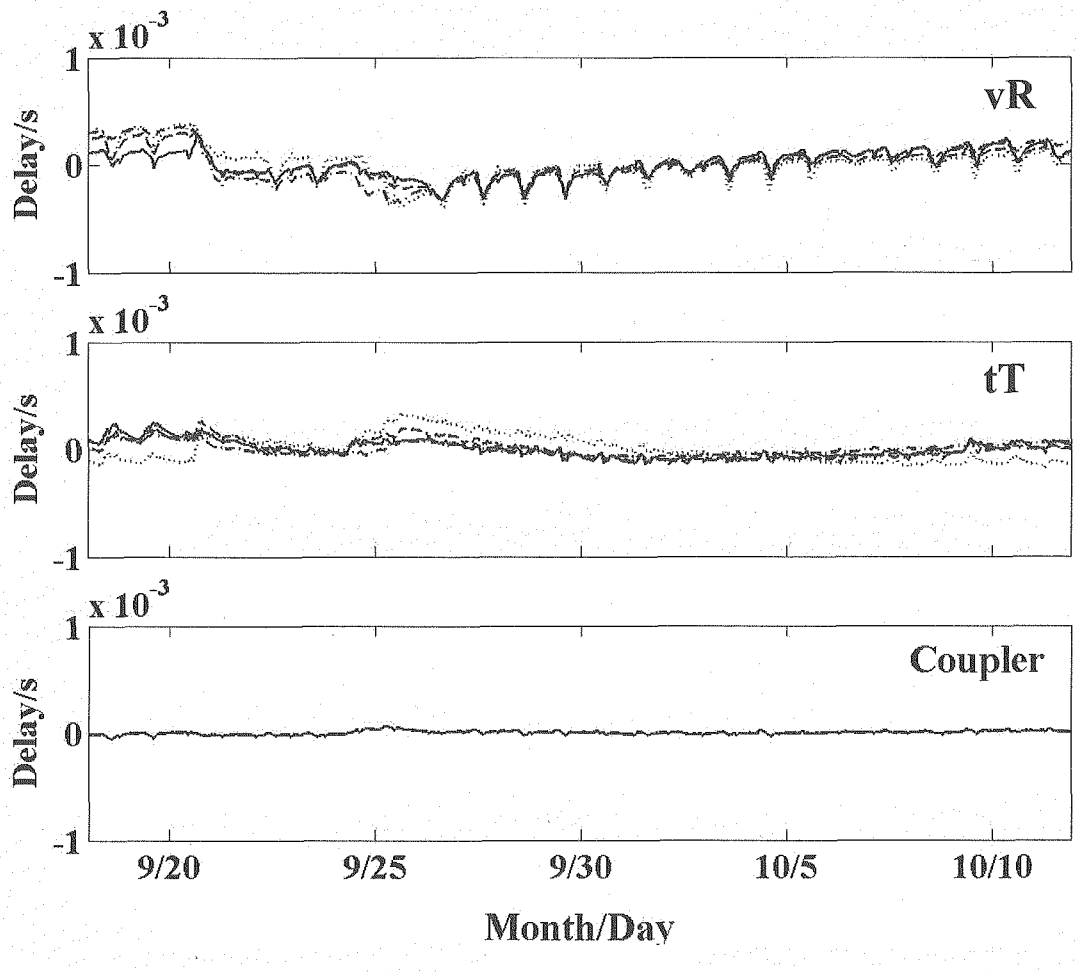

Figure 2.3.10 Temporal change of travel times of the direct S waves. vR and tT (solid lines:No.1, break lines:No.2,chained line:No.3, dotted line:No.4). "Coupler" in the bottom is seismic records measured by a seismometer on the concrete foundation of the source.

2.4 A dense seismic array for acquisition of high quality data in the ACROSS observation

2.4.1 Introduction

We are developing an active seismic monitoring methodology on the seismic ACROSS (Accurately Controlled Routinely Operated Signal System) as a system consisting of all the factors: signal transmission, observations, analysis and so on in order to detect any subtle change in space and time of physical properties in the Earth's interior, particularly in the seismogenic zone [1]. For the above purpose, we should map and/or image the geophysical structures and their heterogeneities in the Earth's crust and around the subduction zones. We therefore attempt to characterize such heterogeneities by the seismological parameters such as travel times, the seismic wave velocities, the propagating directions, the attenuation and the scattering of seismic waves by use of the high quality data in the seismic ACROSS observation.

It is well known that any observed data include noise and bias from various sources not only in time but also in space. The ACROSS is the best way to reduce noises in observed data in time and space. The noise in space is due to the scattering and/or multi-path effects in the heterogeneous subsurface layers and due to the different topological and geological conditions of receiver sites. The combination of an ACROSS source and/or an ACROSS source array, and receiver array(s) allow us to obtain data with high S/N (ratio of signal (information) to noise) and S/B (ratio of signal to bias) easily obtained by data-stacking in time and space domains and also by careful managements on all the technological components involved in the observation systems.

In this study, we briefly review our seismic array observation system by the seismic ACROSS and their specifications, and describe the latest results of array observation made towards our target.

2.4.2 Analyzing scheme

(1) Data acquisition to transfer functions

Fig.2.4.1 shows the flowchart of the data acquisition in the seismic ACROSS. A whole observation system in the seismic ACROSS is assumed to be a liner system, and we can obtain the characteristics of wave propagation path as a transfer function between a source and a receiver.

We have a few different ways to describe source characteristics. In the case of a fixed seismic ACROSS transmitter, the source characteristics, $F^{v}(\omega)$ [N], is described by the measurements of the position of a rotating eccentric mass [2]. It is also described by the measurements of ground motions around the transmitter in practice.

On the other hand, the observational response characteristics at a receiver are described through the several data processing as shown in Fig.2.4.1. First, the time series data, $v(t)$ [volt], by the ACROSS are obtained by a time-segment-stacking (TSS) method. The data, $v(t)$, in time domain are converted to the data, $V(\omega)$ [volt] in frequency domain by the Fourier transform. We obtain the reliable receiver's response characteristics, $V'(\omega)$ [m/s], after correcting the frequency response of the observation system, $Q(\omega)$ [volt/(m/s)], to the frequency data $V(\omega)$. Then the displacement data, $U(\omega)$ [m], can be obtained by multiplying the velocity data, $V(\omega)$ [m/s], by $1/(i\omega)$ (i.e., ω is an angular frequency and i is a unit of complex number). The site correction, $R(\omega)$, will be developed in future. In the frequency domain, there are two groups of the data: signal and noise. We can evaluate the noise-level-estimate independently by use of noise group. Such a noise-level-estimate can be used as a weight in the weighted stacking processing developed by Nagao et al. [3].

Finally, a transfer function, $H(\omega)$, is given by a division of the displacement data, $U(\omega)$, observed at a receiver by the transmitted force, $F(\omega)$, and its dimension is m/N. Since the signatures of seismic waves are different among the type of waves, such as P, S and surface waves, we need to evaluate a transfer function along a particular direction to clarify the characteristics of incident waves across a seismometer array. The manners of the observed displacement at a receiver relate to the ground motion or force excited by the transmitter at the source site. If we have two kinds of data sets obtained by clockwise/anti-clockwise rotations, it is possible to synthesize the liner motions along a particular direction. The direction for the seismic waves arriving at the receiver along a great-circle path, is called the radial direction (denoted by a subscript, r). On the other hand, the direction of motion perpendicular to the great-circle path is called transverse. The vibration in horizontal and vertical directions on the transverse plane is called t and z components, respectively. We define the transfer function, $H(\omega)$ (after here, (ω) is omitted), by a following 9-compoenent second-order tensor:

$$\begin{pmatrix} U_r \\ U_t \\ U_z \end{pmatrix} = \begin{pmatrix} H_{rr} & H_{rt} & H_{rz} \\ H_{tr} & H_{tt} & H_{tz} \\ H_{zr} & H_{zt} & H_{zz} \end{pmatrix} \begin{pmatrix} F_r \\ F_t \\ F_z \end{pmatrix}. \quad (2.4.1)$$

$\boldsymbol{F}=(F_r, F_t, F_z)$ and $\boldsymbol{U}=(U_r, U_t, U_z)$ represent the three-component forces excited at a source and the three-component displacement observed at a receiver, respectively. If the eccentric mass rotates only in the horizontal plane and the force, F_z, in the vertical direction is assumed to be zero, we only obtain six components of the transfer function. If the seismic waves propagate in a homogeneous and isotropic medium, the transfer functions H_{rr} and H_{zr} include a P-wave and a SV-wave arrivals while H_{tt} includes a SH-wave arrival.

(2) Detection of "wave element"

We analyzed the complex transfer functions by means of both the slant stack processing and the Sompi event analysis method [4] in order to obtain the travel times and propagating directions of the seismic waves. A slant stack processing is to emphasize plane wave propagation toward a particular direction by using a ray parameter and to reduce the spatial noise due to heterogeneities in the subsurface layer. And the Sompi event analysis method was developed to detect any 'wave element', which denotes the propagation along a particular ray path even in a narrow frequency band.

First, we defined a ray parameter, p, as follows: At a given point the direction cosine of the ray is given by

$$\frac{\sin\theta}{c} = const = p, \qquad (2.4.2)$$

where c and θ are a seismic velocity of the media along a travel path and an incident angle, respectively. The constant, $\boldsymbol{p}$, is called the ray parameter or horizontal slowness and varies from 0 (vertical travel path) to $1/c$ (horizontal travel path). For a prescribed reference point and a particular takeoff angle, a ray will have a constant ray parameter $\boldsymbol{p}$ along the entire path. If we observe seismic waves by a planar array, we also define a 2-D ray parameter as $\boldsymbol{p}=(p_x,p_y)$ along the horizontal X and Y axes, respectively. We handle only body waves. The range of ray parameter, p, is defined by a following equation:

$$|p| \le 1/(2df_{\max}) \qquad (2.4.3)$$

where f_{max} and d are the maximum frequency to be analyzed and an interval between the receivers, respectively.

Next, we calculate an array response function to evaluate the effect of the array's design, such as a shape and size of the array and the position of receivers [5]. The array response function, $R(\boldsymbol{p})$, is expressed by

$$R(\omega,\mathbf{p}) = \sum_{j=1}^{J}\sum_{l=1}^{J}\exp[i\cdot 2\pi\cdot\omega\mathbf{p}(\mathbf{r}_j-\mathbf{r}_l)]. \qquad (2.4.4)$$

$\boldsymbol{r}_j=(x_j,y_j)$ is the location of the j-th receiver site at (x_j,y_j).

We now describe the five steps of the analysis of the transfer functions to detect the seismic waves propagating along a particular direction with a particular ray parameter as follows:

STEP-1: We determine a range of ray parameter, $\boldsymbol{p}=(p_x, p_y)$, by Eq(2.4.3).

STEP-2: Stacking the transfer functions, $H(x_j,y_j,\omega)$, in space by a slant stack processing. Fig.2.4.3 illustrates the construction of the tau-p (i.e., τ-p) transform, that is, a slant stack processing (or plane-wave decomposition). It is assumed that a plane wave with a ray parameter, $\boldsymbol{p}$, propagates along the X axis. The summed-up (slant-stacked) seismic trace is shown in the left. The transform is completed by forming an entire suite of $\boldsymbol{p}$ by summing-up along numerous different slopes. That is, each seismic time trace of the transform is simply the sum of all input seismic trace taken along a particular slant. Although we describe the τ-$\boldsymbol{p}$ transform in time domain, in practice we operated it in frequency domain. The slant-stacked data, $F(\boldsymbol{p}, \omega)$, for an arbitrary ray parameter, $\boldsymbol{p}$, is expressed by

$$F(\mathbf{p},\omega)=\sum_{j=1}^{J}H(\mathbf{r}_j,\omega)\exp[i\omega\mathbf{p}\cdot\mathbf{r}_j] \quad (2.4.5)$$

where J is a number of traces.

STEP-3: Decomposing the travel time and amplitude of each wave element by using the Sompi Event Analysis (i.e., SEA) method. We show the relationship between a slant-stacked time trace with a ray parameter, $\boldsymbol{p}$, and the travel times, τ, detected by SEA. The travel time, τ, is consistent with the time of a peak of wave packet (i.e., a peak of the envelope) of the slant-stacked seismic trace.

STEP-4: Synthesizing an event time series with the travel times and the amplitudes of the wave elements obtained in STEP-3. In this case, the event time series are composed by several Lorenz functions.

STEP-5: Summarizing all the event time series on the space of ray parameter, $\boldsymbol{p}(p_x, p_y)$. It provides us the information of the elapsed time variations of the propagating direction and the amplitude (i.e., intensity) of the seismic waves across the array.

2.4.3 Observation and data

In this section, we overview our seismic array observation in Gifu prefecture, and show the results of analyses of the seismic array data.

1) Overviews of a dense seismic array observation

Fig.2.4.4 illustrates the maps of the seismic ACROSS source, the seismic array at Shobasama, and the surrounding situation of our test site. It is approximately 1 km distance between the seismic ACROSS transmitter and the aligned receivers' site. Our seismic array is located at one of the test sites of the Japan Nuclear Cycle Development Institute in Mizunami city, Gifu. Geological and geophysical structures in this area are well studied by means of geophysical explorations, which were conducted both in deep boreholes and subsurface (e.g., [6]). Soft sediments cover the subsurface around our array site with a thickness of a several meters, and the

Tertiary sedimentary rocks of the Mizunami Group and the basement rocks of the Toki granite Group lied under the soft sediments. An aperture of our array is 25 m x 25 m long and a span between the receivers is 5 m along each of X and Y axes. Our observation array comprises 36 moving-coil type three-component velocity seismometers, manufactured by Seismic Nail produced by GeoSpace, all of which were calibrated precisely by the secondary calibration method by Tsuruga et al. [7]. All seismometers are buried in the borehole at the depth of 1.8 m below the surface and the accuracies both of the direction and of the inclination of the settle are within 1 degree. We used time-segment-stacking-system type recorders names PAVEC MD-8464, which has 64 channels with a 24-bit A/D converter and is sampled by synchronization with a GPS clock timings. We have two receiver groups in the array to avoid data loss by accident. In this study, we only use the data from one of two groups named ARRAY-B. The array observation has been conducted since April 2003, and we obtained the data which included several ACROSS signals transmitted from the fixed seismic ACROSS transmitter, called FIT1, from Apr. 15, 2003 to Jan. 28, 2004 (i.e., the 4th transmission trial) [2].

Fig.2.4.5(a) shows the amplitude and phase spectral data of the source characteristics, $F^{v}(\omega)$ [N]. The direction of the rotation of the mass changes automatically every hour. Fig.2.4.5(b) shows the spectra of the observed displacement data, $U(\omega)$, which have a 100 sec-long segment and were recorded with a sampling rate of 1000 Hz for the stacking period of 3400 sec. The noise is supposed to be line spectra with every 0.01 Hz spacing in the frequency domain and the series of signal exist at line spectra with every 0.05 Hz separation because the modulation period of the FM transmission is 20sec. Noise level is estimated from the amplitudes in the frequency band neighboring to the signal, and its level is smaller than 1/100 of the signal (i.e., signal-to-noise ratio (S/N) is larger than 100). The displacement spectra obtained by stacking for about 12 days (283.5 hours) shown in Fig.2.4.5(c). In the case that the stacking period is 288 times larger than a fundamental stacking period (i.e., 3400 sec), the S/N is expected to be about 17 times larger than that obtained by stacking for 3400 sec. The S/N level in practice is to be approximately 10 and is less than theoretical value because of the mixing of the large impulse noise in time. It, however, is surprised to attain an extremely high quality data with an S/N larger than 10^3 although they are obtained by a simple stacking. This indicates that ACROSS technology is robust to noise. In the following section, we analyzed the data stacked in time for about 12 days.

Fig.2.4.6 shows complex spectral data of the transfer functions H_{tt} and their time traces obtained at 18 sites of the ARRAY-B. All time series were converted by the inverse Fourier transform. Black and gray lines represent the real and imaginary parts of complex spectral data, respectively. Amplitudes are normalized by the maximum amplitude of the data in each diagram. They are characterized by the followings: in both frequency and time domain, their amplitudes and phases are extremely different each other probably due to the heterogeneities in the subsurface layer around the array. Such fluctuation of data in space is called 'spatial noise'. It is

clearly found that the site with such a large spatial noise is not appropriate for any observation, even for the seismic ACROSS. We, however, show a trial to suppress the spatial noise by the array observation and our analysis scheme.

2.4.4 Analyses

In this section, we show the results of analyses using the transfer function H_{tt} in the frequency range from *16* to *20* Hz, in which the S/N is relatively higher than 10^2.

First, we determined the range of ray parameter, $\boldsymbol{p}(p_x, p_y)$, by Eq(2.4.3) and calculated an array response function by Eq(2.4.4) shown in Fig.2.4.7. Symbol, +, represents a grid point of a pair of (p_x,p_y). Gray-scaled color represents the intensity of the array response function normalized by the maximum one within the draw. The range of ray parameter to be searched is $|p_x| \leqq 2.5\times10^{-3}$ s/m and $|p_y| \leqq 2.5\times10^{-3}$ s/m, assuming that the distance between the receivers and the maximum frequency are $d=10$ m and $f_{max}=20.0$ Hz, respectively. An interval of searching grid is $\Delta p=2.5x10^{-4}$ s/m for both the axes. The resolution on the ray parameter space (i.e., $\boldsymbol{p}$-space) is not so high in this trial. The grid interval of ray parameters should be changed corresponding to the target of the investigation. Although an array response function represents in the wave-number space, we here show the ray parameter space corresponding to the frequency of *20* Hz as we easily found the effect of array design in the $\boldsymbol{p}$-space. A peak at the origin of the coordinate has a side robe parallel to both the X and Y axes due to the effect of a limited size of the array. The side robe band width with a half of the peak amplitude is 7.5×10^{-4} s/m.

Next, we show the results of the Sompi event analysis corresponding to the STEP-2 to STEP-4, respectively, in Fig.2.4.8. The mean power density of the wave elements decomposed by SEA is maximum when all the traces were slant-stacked with a pair of ray parameter $(p_x,p_y)= (-7.5x10^{-4}, 2.5x10^{-4})$. The top trace in the diagram (a) is the complex spectra whose real and imaginary parts are represented by black and gray lines, respectively, and it corresponds to a slant-stacked data, $F(\boldsymbol{p},\omega)$, in STEP-2. Three traces below the top represent each wave element decomposed by the SEA method and the wave element denoted by #1 has the largest amplitude among them (STEP-3). And then the bottom in the diagram (a) is the residue between the original trace (i.e., slant-stacked data) and the trace reproduced by three wave elements. It is clearly found that the wave element #1 is the most major element for the original trance and its travel time is estimated to be 1.067 sec. Fig.2.4.8 (b) shows the relationship between the slant-stacked time trace, $f(p,\omega)$, and the event time series, $g(p,\omega)$, composed by three wave elements in STEP-4. The amplitudes of the slant-stacked time traces vary in time with the frequency of about 18 Hz, which is the center of the analyzed frequency range. The travel times of the wave elements exist discretely in time and they are consistent with the peak times of the amplitude (or envelope) of the slant-stacked data.

Finally, we obtained the elapsed time variations of the directions and the amplitude of the incident wave elements in STEP-5 shown in Fig.2.4.9. Diagrams of (a) ~ (i) represent each time cross- section of the function $g(\boldsymbol{p},t)$ with an interval of *0.01* sec from *1.03* to *1.11* sec. The wave propagates from the origin point $p=(0,0)$ to an arbitrary point of $\boldsymbol{p}$, which represents as a vector $\boldsymbol{p}=(p_x,p_y)$. An apparent velocity, c_a, is obtained by an inverse of the absolute value of $\boldsymbol{p}$, that is, $c_a=1/|\boldsymbol{p}|$. The arrow line in the diagram (a) represents the direction of the wave propagation toward the direction of S54.9°E from the source to the receiver array. The darkness of image corresponds to the amplitude of wave element, and it is scaled by the maximum amplitude of wave element #1 shown in Fig.2.4.8. It is found that the grids with the large amplitude value for the travel time of *1.06* to *1.07* sec corresponding to the cross-sections (d) and (e). They might be related with the wave element #1 whose travel time is *1.067* sec and the ray parameter is $\boldsymbol{p}(px,py)=(-7.5\times10^{-4},2.5\times10^{-4})$. The wave element #1 propagated toward the direction of S 88°E (i.e., nearly from west to east) with the apparent velocity of *1.26* km/sec. If a shear wave velocity in the subsurface layer is assumed to be 1 km/sec, this wave penetrates to the array's surface with an angle of 52 degrees from the vertical direction.

2.4.5 Discussion

We here focus on the elapsed time variations of propagating waves through the array as shown in Fig.2.4.9. The wave groups around $(p_x,p_y)=(-5.0\times10^{-4},-2.5\times10^{-4})$ in the time cross-section of *1.05* sec are a bit larger and propagated along the direction of S26.6W nearly from the source to the receivers. On the contrary, the other wave groups are found in the time cross-sections from the arrival time from *1.07* to *1.09* second. Their ray parameters are distributed around that of the maximum wave element #1 represented by a symbol, *, in Fig.2.4.9. Their arrival times are not so different from that of the wave element #1 while their absolute values are a bit larger. These later phases of the waves might be the secondary waves which are composed of an ensemble of waves scattered by the heterogeneities over the observation area. It is necessary to improve the analysis methods and schemes to discuss about the scattered waves more detail. And it is also important to compare these results with other information obtained by the calculation of the wave fields with a real geological and geophysical structure model in future. However, the most important result in this study is that several wave elements are clearly detected from extremely non-uniform data observed at the strongly heterogeneous site such as our array site. And we also conclude that our array usefully works as a spatial filter and a detector of wave element. Moreover, we confirm that the seismic ACROSS signals and its technology are quite effective to suppress noise in space and time. Consequently we have the important and challenging subjects to discuss the characteristics of transfer functions or characteristics of the propagating path of the seismic wave across the array in detail. The major subjects are as follows:

(a) To obtain the accurate determination of the model parameters (e.g., complex travel time and amplitude by SEA), we should improve and develop the analysis method and also observe the high S/N data.

(b) Both to estimate the site characteristics of the subsurface around the observation site and to suppress the noise in space due to the heterogeneities of the subsurface, we should develop a new analysis methodology and scheme.

(c) To develop the practical method to construct an optimum array for the seismic ACROSS observation, we need to assess the ability of array observation by comparing the other array located at the different geological structure.

(d) To interpret the results of analyses effectively, we need the information from the forward modeling of wave field and/or calculation of synthetic data with a real geological structure.

(e) To establish the methodology to map the distribution of heterogeneities in the 3D space of the Earth's interior by observing the scattered waves with many receiver arrays.

2.4.6 Summary

We are developing the methodology and the technology for observation and analysis of the seismic ACROSS signals effectively in order to construct the observation array with an appropriate design. In this paper, we introduce our first trial of construction and observation by a dense seismic array and report the latest results of analyses. Although our trial has just begun, the analyses of the high S/N transfer functions, that is, high quality data provide us much information about the subsurface. Moreover it suggests us the possibility and ability of the seismic ACROSS array observation not only to detect the heterogeneities in the subsurface but also to monitor the Earth's interior in future.

References

[1] Kumazawa, M., T. Kunitomo, Y. Yokoyama, T. Nakajima and K. Tsuruga, ACROSS: Theoretical and technical developments and prospect to future applications, Technical report, Japan Nuclear Cycle Development Institute, 9, 115-129, 2000.

[2] Kunitomo, T., and M. Kumazawa, Active Monitoring of the Earth's Structure by the Seismic ACROSS - Transmitting and Receiving Technologies of the Seismic ACROSS -, *Proc. 1st IWAM04,* 2004.

[3] Nagao, H., T. Nakajima, M. Kumazawa and T. Kunitomo: Optimum weighted stacking method for acquisition of the ACROSS transfer functions having the maximum signal-to-noise ratio, *Proc. 1st IWAM04,* 2004.

[4] Hasada, Y., M. Kumazawa, K. Tsuruga and T. Kunitomo: Travel time estimation from the data observed by ACROSS, *Proc. 1st IWAM04,* 2004.

[5] Capon, J.: High-resolution frequency-wavenumber spectrum analysis, Proc. IEEE, 57, 1408-1418, 1969.

[6] Ishikawa, K., Y. Mezaki, H. Suzuki, M. Kai, H. Watanabe, S. Fujimori and J. Ishikawa: Investigation program, in borehole MIU-2 for the Mizunami Under ground Research Laboratory project in the Shobasama site, *Report of Japan Nuclear Cycle Development Institute,* TJ7420 99-16, 1999.

[7] Tsuruga, K., M. Kumazawa, T. Kunitomo and N. Shigeta: Seismometers for ACROSS by ACROSS, *Chikyu Monthly,* Active Monitoring, 2004.

Kayoko TSURUGA[1], Takahiro KUNITOMO[2], Yoko HASADA[3], Mineo KUMAZAWA[2], Naotaka SHIGETA[4] and Junzo KASAHARA[5]

[1] The University of Tokyo

[2] Tono Geoscientific Research Unit, JAEA

[3] Nagoya University

[4] Horonobe Underground Research Unit, JAEA

[5] Japan Continental Shelf Survey, Co. Ltd.

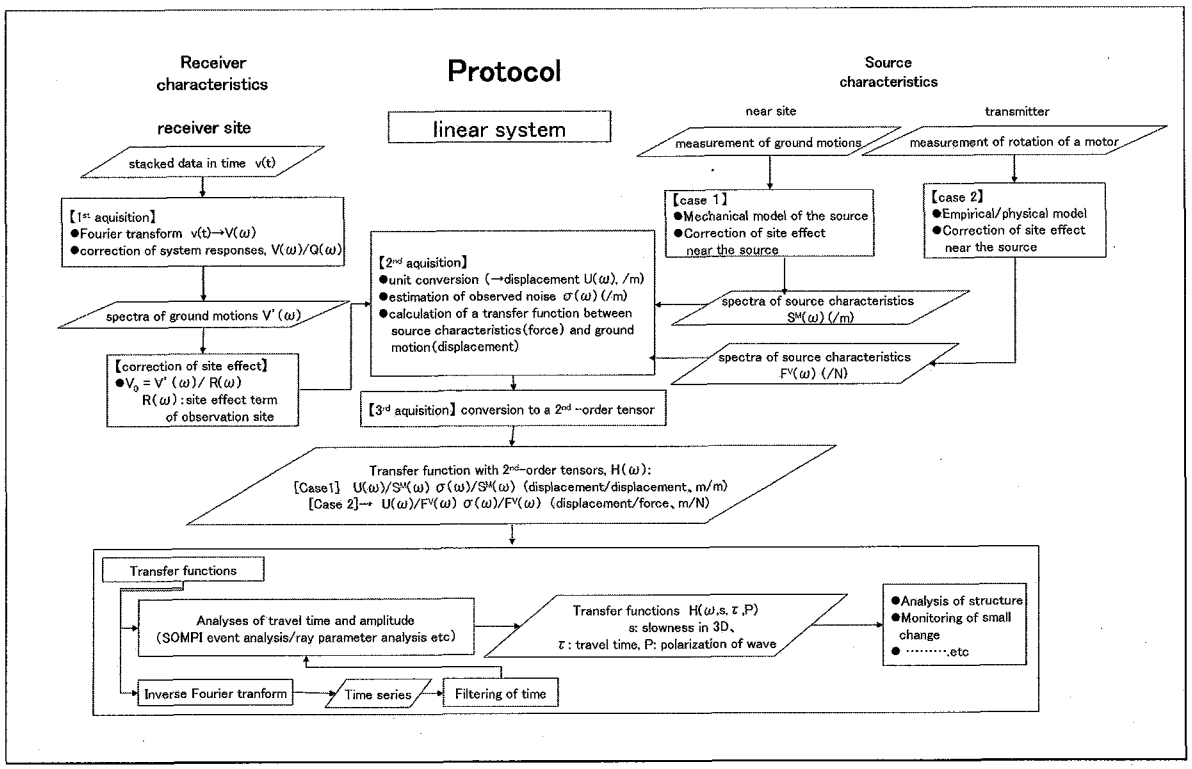

Fig.2.4.1 Flowchart of the data acquisition in the seismic ACROSS.

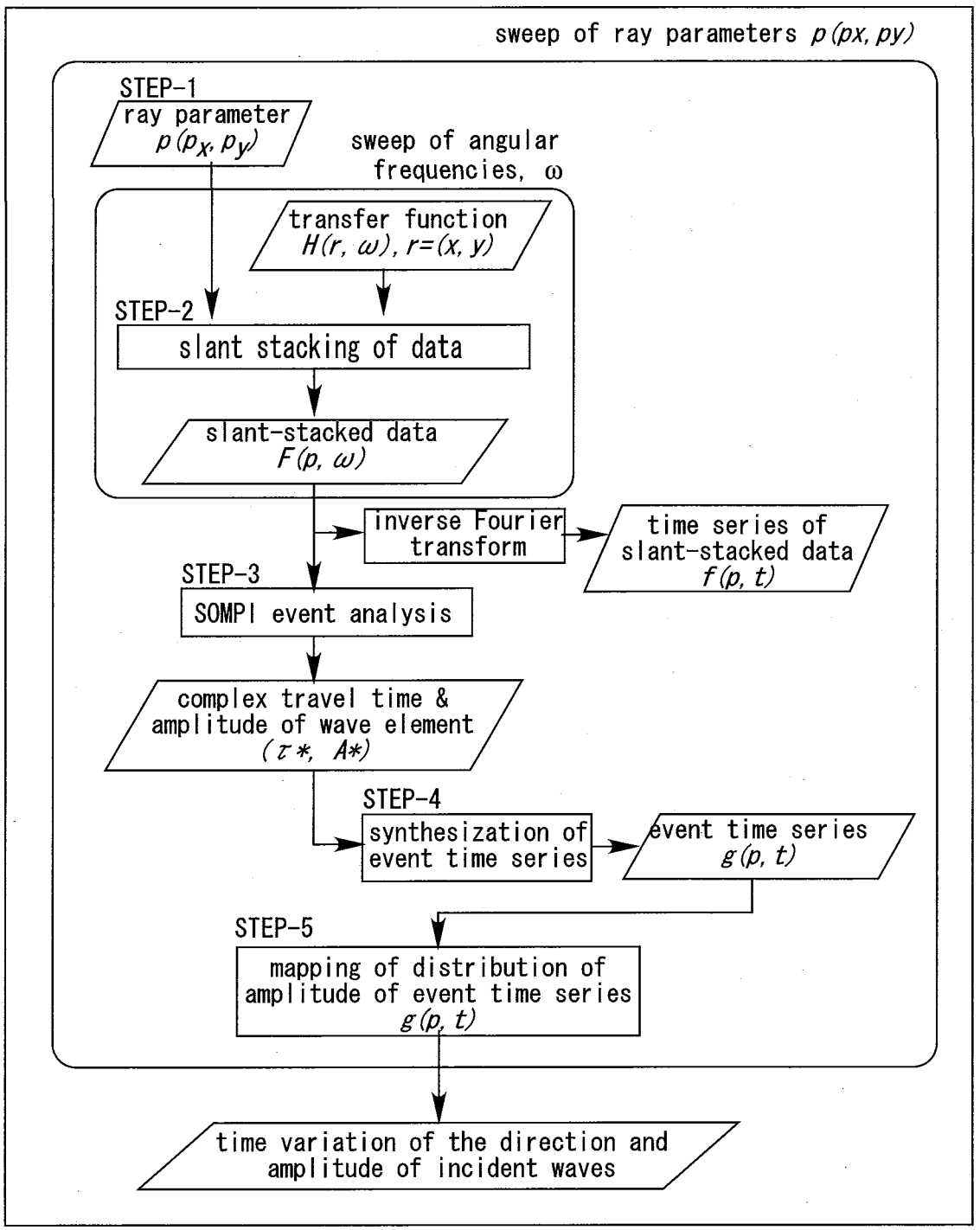

Fig.2.4.2 The analysis scheme to detect wave elements by SEA and investigate the temporal variations of intensity of the incident waves in a ray parameter space $\boldsymbol{p}(p_x, p_y)$.

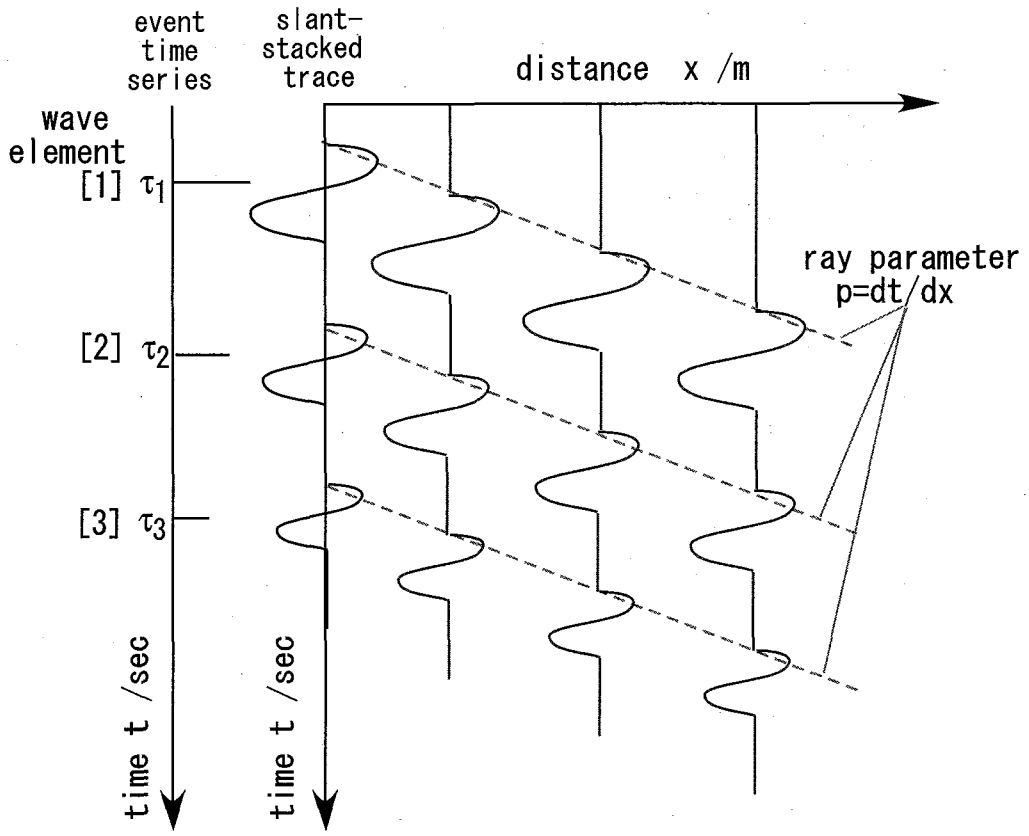

Fig.2.4.3 Construction of slant stack processing and relationship of travel times between a slant-stacked time trace and an event time series by SEA.

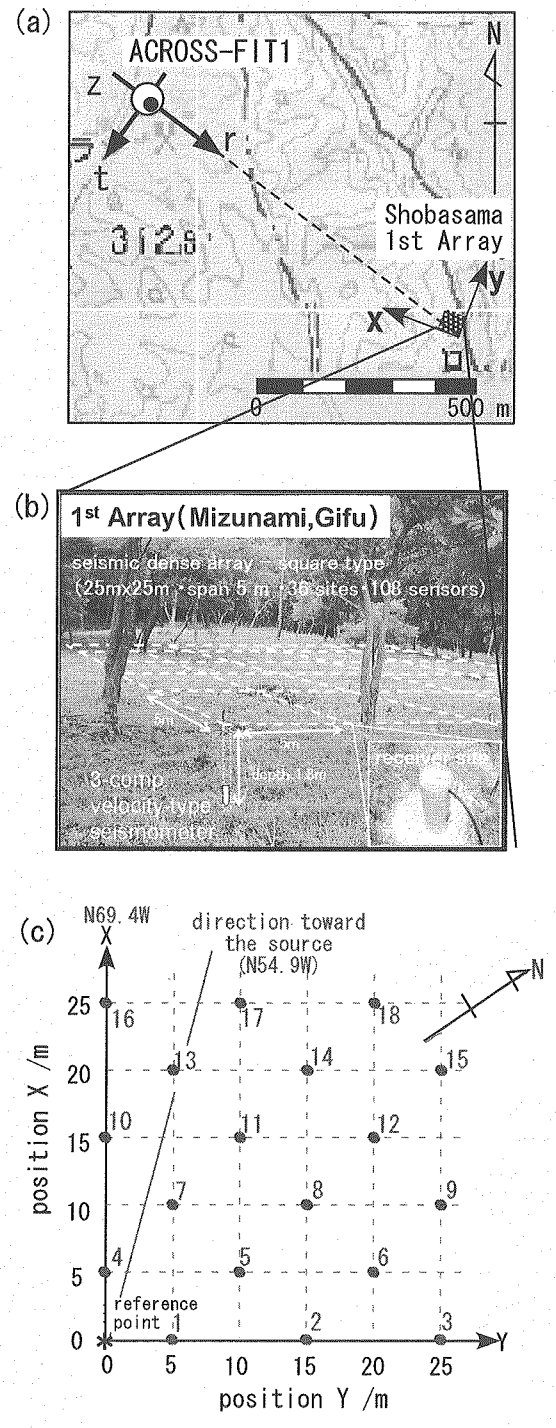

Fig.2.4.4 Location map of ACROSS observation site. (a) A fixed-type ACROSS transmitter, named FIT, is located at the distance of about 1 km from the array site toward the NNE direction. (b) An aperture length of the squared array is 25 m along the two axes (i.e., X and Y axes) and a span interval between receiver sites is 5 m. At each site, a three-component moving-coil velocity type seismometer is settled at the bottom of a borehole with a depth of 1.8 m below the surface. (c) 36 receiver sites divide into two groups (18 sites for each)

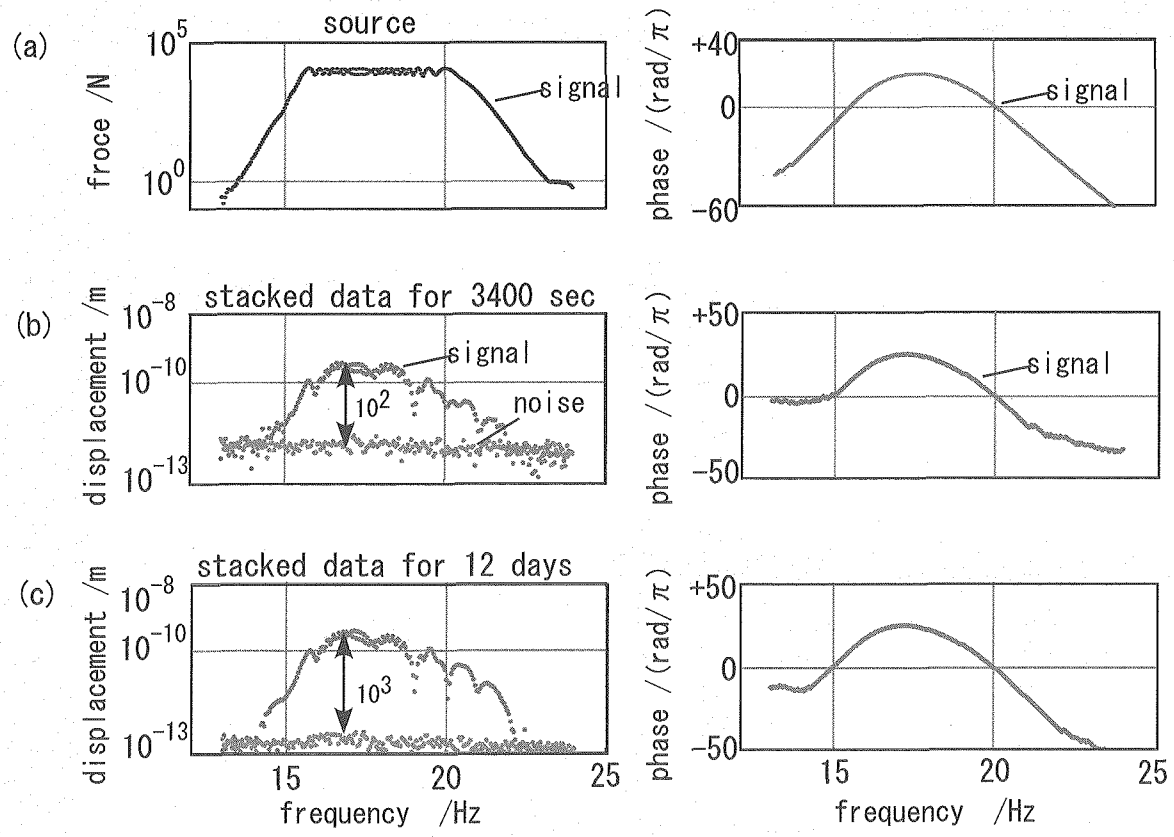

Fig.2.4.5 Diagrams of the amplitude and phase spectra observed at the source and the receiver. (a) Spectral data of the source characteristics during the period of the 4th transmission test from a fixed type ACROSS transmitter. The frequencies of transmitted signal modulated in the frequency range from 12.52 to 22.52 Hz for a fundamental modulation interval of 20 sec. (b) Spectra of observed displacement stacked for 3400 sec and its S/N is larger than 10^2. (c) Spectra of stacked data for about 12 days. Its S/N became larger than that of (b) but it didn't reach a ideal level which is 17 times larger than that of (b) at a basis of theory. However, its S/N achieves to extremely high value of 10^3 although large noise accidentally put into the data.

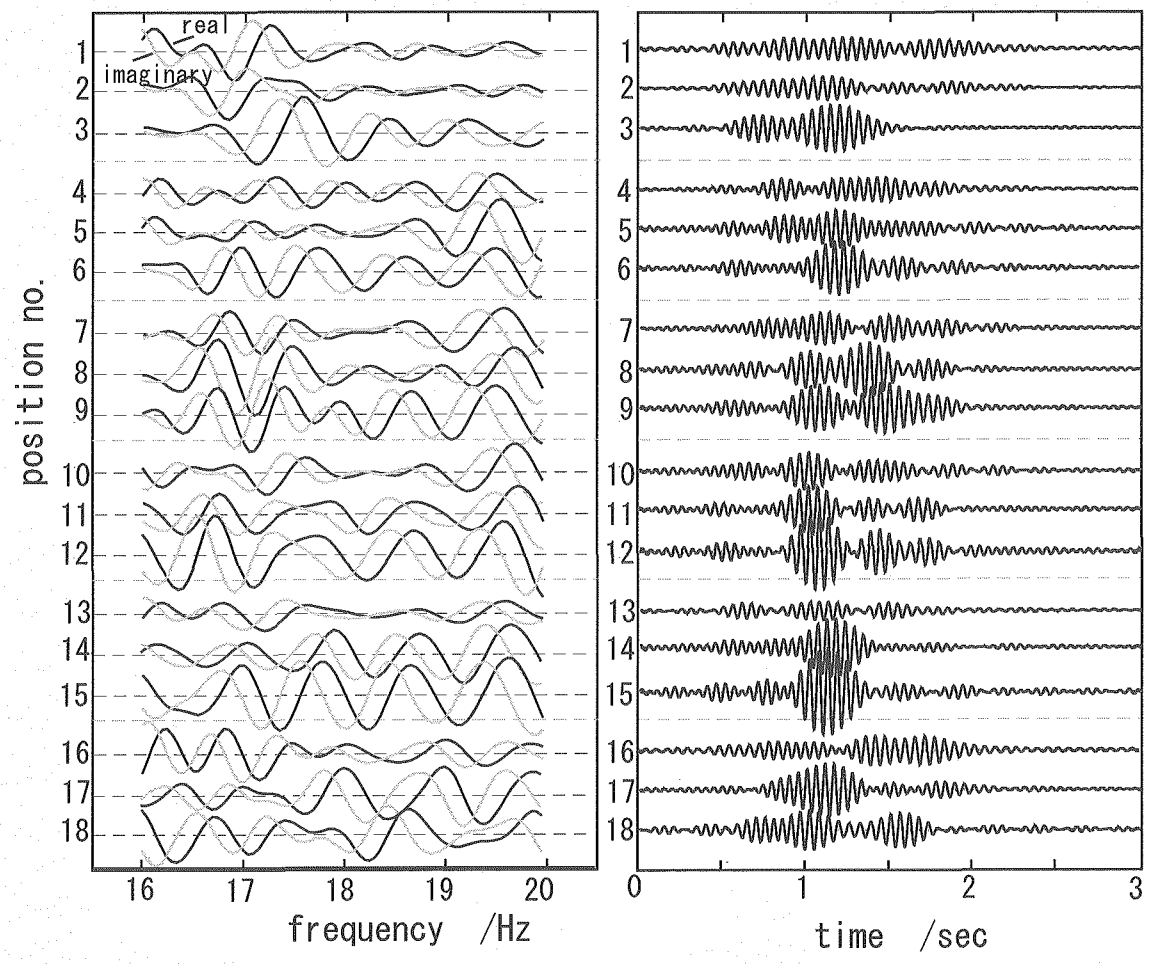

Fig.2.4.6 Diagrams of the complex spectra (left) of the transfer function H_{tt} and their time traces (right) at each receiver site in ARRAY-B. The amplitude of data are normalized by the maximum one of the 18 data in each domain. Every three plots from the top have a same coordinate value in the X direction of the array.

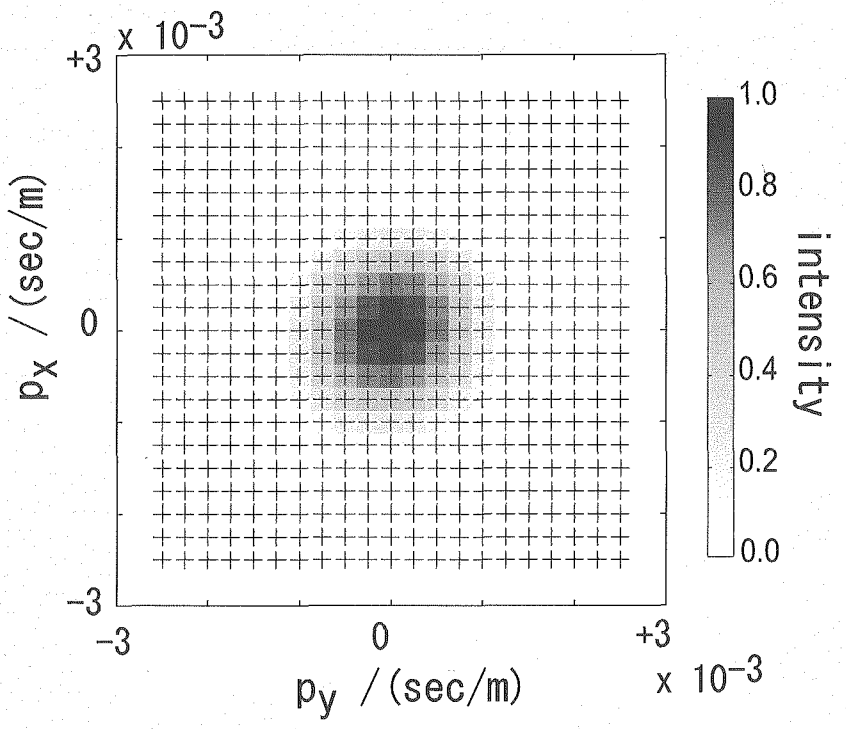

Fig.2.4.7 Space in the ray parameters (p_x,p_y) and an array response function. Symbol, +, represents a grid point with a pair of ray parameters (p_x, p_y) to calculate a slant-stacked data. The range of each ray parameter is limited from $-2.5x10^{-3}$ to $+2.5x10^{-3}$ sec/m. Because the array response function reflects the positions of receivers in the array, the resolution for detecting a propagating waves is relatively low along both X and Y directions.

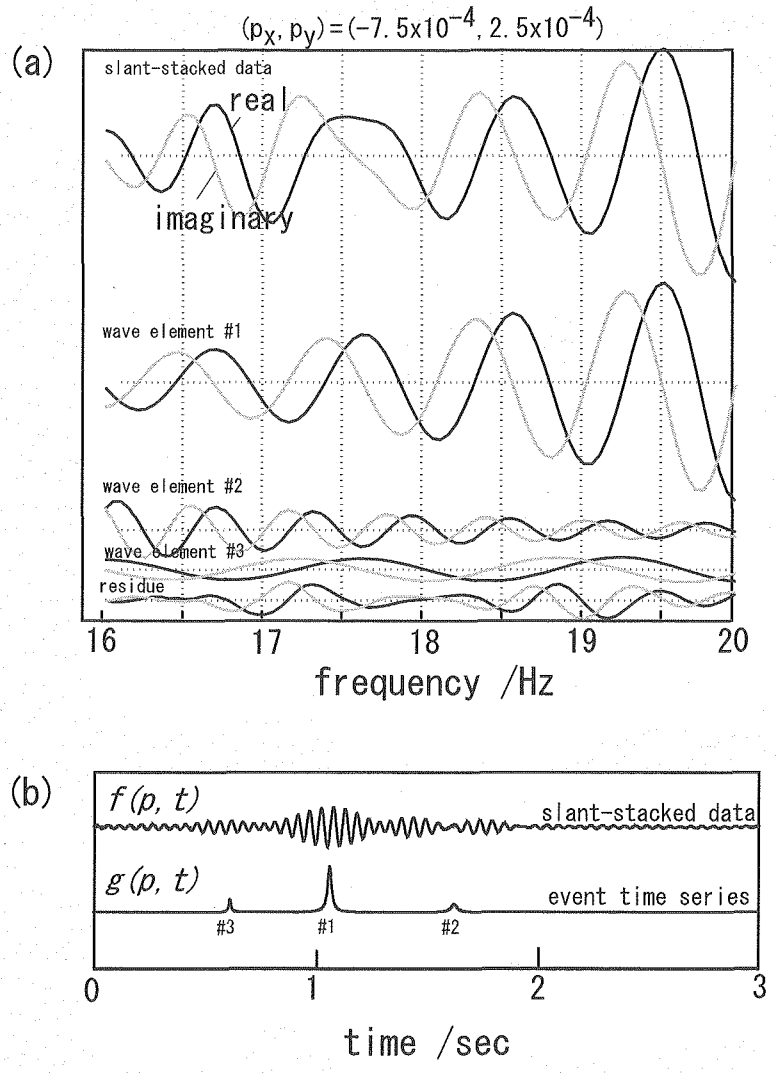

Fig.2.4.8 An example of the detections of three wave elements by Sompi event analysis from the slant-stacked spectral data. (a) Slant-stacked spectral data at the top of the diagram represents input data for Sompi event analysis and three plots in the middle of the diagram correspond to each wave element. The other plot at the bottom is a residue between the input and the calculated data. The maximum mean power density of the wave element is detected when the pair of ray parameter (p_x,p_y) is assumed to be ($-7.5x10^{-4}$, $2.5x10^{-4}$) and the most dominant wave element-1 arrives at the time of 1.067 sec. (b) Seismograms at the top of the diagram show the time traces converted from the slant-stacked data by an inverse Fourier transform. The series at the bottom show event series which are synthesized with the above three wave elements. The travel time detected by Sompi event analysis is consistent with the peak of amplitude in the above seismograms.

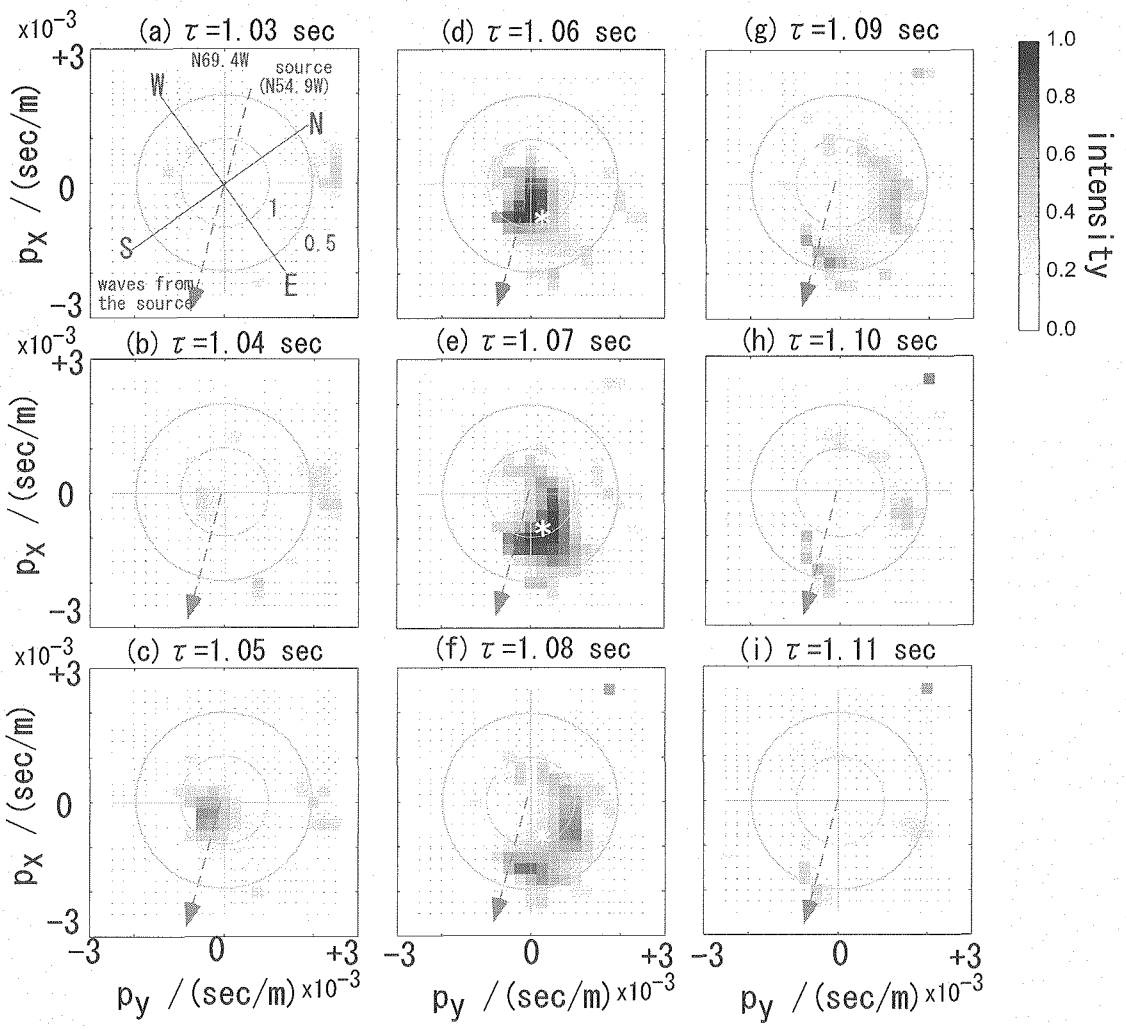

Fig.2.4.9 Elapsed time variations of amplitude of wave elements in the space of ray parameter $\boldsymbol{p}(p_x, p_y)$. Diagrams (a) to (f) correspond to the cross-sections of $g(\boldsymbol{p},t)$ with an interval of 0.01 sec in the travel time range from 1.03 to 1.11 sec.

3. EM-ACROSS

3.1 Overview of EM-ACROSS and its development

3.1.1 Introduction

Our research group has been developing a new observation system named 'ACROSS' (Accurately Controlled Routinely Operated Signal System) for a monitoring purpose of small change in the physical states in the ground. The essential points of this system are use of very accurate controlled periodic waves, and obtaining the transfer function with a high signal-to-noise ratio in frequency domain by means of a long period stacking [1]. To visualize the Earth's interiors there are two propagating waves, seismic and electromagnetic waves. The information derived from the each waves are independent. The method using electromagnetic waves is called EM-ACROSS (Electro-Magnetic Accurately Controlled Routinely Operated Signal System) [2]. In this paper we explain the feature of the EM-ACROSS, and examine the possibilities of the active monitoring using the electromagnetic waves.

3.1.2 Basic equation of electromagnetic field

The basic equation for the electro-magnetic phenomena with the time dependency of $\exp(i\omega t)$ is the Maxwell's equation,

$$\nabla \times \mathbf{H} = \mathbf{I} + i\omega\mathbf{D}, \quad \nabla \times \mathbf{E} = -i\omega\mathbf{B}, \tag{3.1.1}$$

where the physical parameters are related by the state equations,

$$\mathbf{I} = \sigma\mathbf{E}, \quad \mathbf{D} = \varepsilon\mathbf{E}, \quad \mathbf{B} = \mu\mathbf{H}. \tag{3.1.2}$$

In the above equation, $\mathbf{H}, \mathbf{I}, \mathbf{D}, \mathbf{E}$ and $\mathbf{B}$ are magnetic filed intensity, electric current density, electric displacement, electrical field intensity, and magnetic field strength, respectively. The physical parameters are electrical conductivity σ, dielectric permittivity ε, and magnetic permeability μ. Generally these physical parameters have heterogeneity, anisotropy, dispersion, nonlinearity and time dependency. The objective of the electromagnetic survey is to estimate all these properties from the observations of electric and magnetic field. In most electromagnetic explorations, following assumptions are made in order to simplify analysis; all media are linear, and the magnetic permeability is assumed to be that of free space [3].

Now we investigate the properties of Electromagnetic field. The propagation of electromagnetic disturbance in a uniform, dielectric and semi-conductive medium is governed by the Maxwell's equation

$$i\omega\mu\sigma\begin{pmatrix}\mathbf{E}\\ \mathbf{H}\end{pmatrix}+(i\omega)^2\mu\varepsilon\begin{pmatrix}\mathbf{E}\\ \mathbf{H}\end{pmatrix}=\nabla^2\begin{pmatrix}\mathbf{E}\\ \mathbf{H}\end{pmatrix}, \tag{3.1.3}$$

where the brackets means we can select $\mathbf{E}$ or $\mathbf{H}$. The left hand side of the equation shows that the propagation of the disturbance has two effects; wave propagation and diffusion. Assuming a plane wave traveling towards x direction in an infinite medium, we have a solution of Eq.(3.1.1) in frequency domain

$$\begin{pmatrix}\mathbf{E}\\ \mathbf{H}\end{pmatrix}=\begin{pmatrix}\mathbf{E}_0\\ \mathbf{H}_0\end{pmatrix}\exp(-ikx), \tag{3.1.4}$$

with a wave number k given by

$$k^2=\omega^2\mu(\varepsilon+\sigma/i\omega)=\omega^2\mu\varepsilon^*. \tag{3.1.5}$$

The real part of ε^* denote an effective dielectric permittivity, and the imaginary part is an effective electrical conductivity contributing to energy dissipation. When the real part is dominant, at frequency higher than $\sigma/(2\pi\varepsilon)$, the field behaves as 'wave field'. When the imaginary part is dominant at frequency, Eq.(3.1.3) reduces to a diffusion equation. The value $\sigma/(2\pi\varepsilon)$ represents the boundary between wave and diffusion field.

In the general electromagnetic surveys, different methods are applied for each frequency region. In the case of diffusion field, TDEM (Time Domain Electro Magnetic) method and CSMT (Controlled Source Magneto Telluric) method are mainly used, and the electrical conductivity structure in the ground is estimated. In the case of wave field, Ground Penetrating Radar is used, and dielectric permittivity structure is estimated [4].

Now we investigate the features of transfer function, which are acquired by EM-ACROSS observation. Assuming a uniform medium with the electrical conductivity σ=0.01[S/m] and relative dielectric permittivity ε_r=4, and a plane electromagnetic filed is propagating, the transfer function between source and receiver located 10[m] apart becomes as Figure 3.1.1. The boundary between diffusion and wave field is about 45MHz with these parameters. The features in this figure are; (1) the real and imaginary parts of the transfer function oscillate along the frequency in the 'wave'

region, (2) the amplitude of the transfer function decrease rapidly and the oscillation is not clear in the 'diffusion' region. These frequency dependencies have the information of the medium in which the signal has propagated. Yokoyama *et al.* [5] summarized the relation between an electromagnetic structure and the transfer function to clarify the physical meaning of the transfer function. The observed transfer function has the information of the underground structure and its physical parameters along the ray between the source and receiver.

The investigation of the electrical conductivity in the crust would be possible by the survey with low frequency. And the electrical conductivity is sensitive to the H_2O content in the ground.

3.1.3 Development of EM-ACROSS

In Figure 3.1.2, we show the schematic view of the procedure for the analysis in EM-ACROSS, and the relation between the procedure and the knowledge derived in the research at Tono Geoscience Center. As Kumazawa *et al.* [1] explained, ACROSS approach is the most robust observation against noise, we have developed both instruments and analyzing method to fit this framework.

We had developed the instruments for the survey with the frequency lower than 10kHz to investigate the electromagnetic properties in the crust. For the precise synchronization of the source and receiver, we use a GPS clock [6]. The precise time keeping enables us the transmission of signals with sharp spectrum [7].

As the analyzing method, we developed a method to determine the travel time of the propagating signal from the transfer function of the limited frequency range. This method which is called Sompi Event Analysis [8] is very useful tool in the analysis in the wave field [9]. The application for the diffusion field is examined by Nagao *et al.* [10].

The measurements of electromagnetic properties provide the essential information for the interpretation of the physical properties from the observed field. We also study this subject. The electrical conductivity in the crust is expected as (1) it is strongly dependent on the H_2O content and its condition, (2) electrical conductivity becomes larger near the surface due to the H_2O content, and in the deeper part of the crust due to the effect of temperature, and (3) electrical conductivity has large dispersion with frequency and has a variety corresponding to the materials. The directional cracks filled with H_2O might cause anisotropy in the electric properties of the material. Matsumoto *et al.* [11] studies the electromagnetic properties of rocks by experiments, and tries to

seen in the dielectric permittivity.

3.1.4 Emission of diffusion field from a dipole

To investigate the possibility of the active monitoring of the crust by electromagnetic waves, we study the propagation of the electromagnetic field in a uniform medium. The equations are

$$\begin{cases} H_\phi = \dfrac{I\ell}{4\pi r^2}(1+ikr)e^{-ikr}\sin\theta \\ E_\theta = \dfrac{I\ell}{4\pi(\sigma+i\omega\varepsilon)r^3}(1+ikr+(ikr)^2)e^{-ikr}\sin\theta \\ E_r = \dfrac{I\ell}{2\pi(\sigma+i\omega\varepsilon)r^3}(1+ikr)e^{-ikr}\cos\theta \end{cases} \tag{3.1.6}$$

In Figure 3.1.3 we show the amplitude of the electro-magnetic field as the function of frequency and distance between the source and the receiver. The physical parameters in the medium are; electrical conductivity σ=0.001[S/m], relative dielectric permittivity ε_r=4, and the magnetic permeability is equal to that of vacuum. The component of electric field is the same direction as the dipole, and that of magnetic field is the ϕ direction of the spherical coordinates. The position of the receiver is on the equator.

The signal amplitude is proportional to the dipole moment. This figure shows the case of dipole moment of 1[Am]. The dipole moment can be enlarged by using larger current or larger dipole length. The technically realizable current dipole would be the order of 10^5, the current is 100[A] and the dipole length is 1[km].

In Figure 3.1.3, we showed the boundary between the near field and far field, and also the line on which the signal amplitude of plane wave becomes 1/e (Skin depth). These lines are independent on the dipole moment. The boundary between near and far field is important for CSMT method, because they mainly use the electromagnetic field of far field.

From the measurement of electromagnetic noise at observation site, we can estimate the signa-to-noise ratio (SNR) at the observation site. This means we can estimate the time to acquire the necessary SNR, or can adjust the amplitude of dipole moment. The feature in this figure is, the signal amplitude becomes larger with smaller frequency, but this relation becomes weaker at most lower frequency. This is related the characteristics that near field becomes dominant. The term $1/r^3$ has much more

effective than $\exp(-ikr)$. For the electromagnetic survey up to 10 [km] in the crust, it is essential to use and analyze the near field.

Meanwhile there is the time delay of the signal propagation even when the near field is dominant. We can estimate the travel time as this figure, and we would know the necessary instruments to observe the travel time. In Figure 3.1.4 we show the apparent travel time of the signal between the source and receiver. Because this travel time was calculated from the phase difference in the small frequency range, it represents the group velocity in a sense. The sign of the travel time changes with frequency in the figure for the electric field. This comes from the reason that the frequency dependencies of the near and the far field are different (see the second equation of Eq.(3.1.6)). Only electric field has the term $1/r^3$ so this term affects the sign of the travel time.

3.1.5 Summary

We introduced the overviews of the EM-ACROSS method as a method in frequency domain to investigate the electrical characteristics of the ground. In the survey of the ground, the transfer function acquired by the EM-ACROSS method has characteristic dispersion, which is usually small in the Seismic-ACROSS method.

We have developed the equipments and the theory for the EM-ACROSS at the Tono Geoscience Center. A trial observation has been carried out at around the Tono Mine campus of JNC (currently JAEA, [8]). We have been operating the Seismic-ACROSS in the same campus [13]. We are trying to observe and analyze both data, and trying to investigate the possibility that we can detect the change of the stress and the state of the H_2O from the observations of the EM-ACROSS.

From the estimation of the propagation of electromagnetic waves in the crust, the survey using the near filed is inevitable. To establish the analysis in the near field is one of the important subjects. The analysis of the near field becomes a mode analysis in generally. The mode analysis is suitable to investigate the averaged properties near the source. On the other hand, ray path analysis is suitable at higher frequencies to resolve the fine structure in the medium. We need to use these contrastive analyses properly in accordance with the objectives of the surveys.

We also find out the possibilities that the electric properties of rocks have dielectric dispersion, which are not caused by the diffusion nor structure in the ground [11]. We need a numerical code which can calculate the electromagnetic field in medium with any dielectric dispersion. The development of this code is the one of the important subject in the EM-ACROSS.

References

[1] Kumazawa, M., T. Kunitomo, Y. Yokoyama, T. Nakajima, and K. Tsuruga, ACROSS: Theoretical and technical developments and prospect to future applications, *JNC Technical Review*, 9, 115-129, 2000. (in Japanese)

[2] Ogawa, K. and M. Kumazawa, Towards the continuous remote sensing of H2O, tectonic stress and physical states in the Earth's crust by means of acoustic and electromagnetic ACROSS, Abstract at the seismological society of Japan 1996 fall meeting, 45, 1996. (in Japanese)

[3] Ward, S.H. and G. W. Hohmann, Electromagnetic theory for Geophysical Applications, in applied geophysics Vol.1, edited by M.N. Nabighian, pp.131-312, Society of exploration geophysicists, Oklahoma, 1987.

[4] Society of Exploration Geophysicists of Japan, Handbook of Geophysical Exploration, Chapter 5-7, Society of Exploration Geophysicists of Japan, Tokyo, 1998.

[5] Yokoyama Y., M. Kumazawa, T. Nakajima, Transfer function measured by electromagnetic sounding with an accurately controlled signal, *Earth Planets Space*, 54, 459-472, 2002.

[6] Nakajima, T., T. Kunitomo, M. Kumazawa, Y. Yokoyama, Development of EM-ACROSS and its field test, *Bull. Eathq. Res. Inst. Univ. Tokyo*, 75, 413-428, 2000.

[7] Nakajima, T., T. Kunitomo, H. Nagao, M. Kumazawa, and N. Shigeta, Long-term operation of the EM-ACROSS and derived transfer function in the diffusion field region, *JAEA Research*, 2007-033, 3.2, 84-95, 2007.

[8] Hasada, Y., H. Kumagai and M. Kumazawa, Autoregressive modeling of transfer functions in frequency domain to determine complex travel times, *Earth Planets Space*, 53, pp. 3-11, 2001.

[9] Yokoyama, Y., M. Kumazawa, and T. Nakajima, A decomposition method of the electromagnetic transfer function using ray model and autoregressive-type model – the case of horizontal layered structure -, *Bull. earthq. Res. Inst. Univ. Tokyo*, 75, 393-411, 2000.

[10] Nagao, H., T. Nakajima, Y. Hasada,, M. Kumazawa, and T. Kunitomo, Detection of a reflected wave by application of the Sompi event analysis method to EM-ACROSS transfer functions, *In the Proceedings of the " st International Workshop on Active Monitoring in the Solid Earth Geophysics (IWAM04)"*, Task Group for Active Monitoring, Mizunami, Japan, 2004.

[11] Matsumoto, M., N. Shigeta, M. Kumazawa, and T. Nakajima, Complex dielectric permittivity spectroscopy using ACROSS measurement system, *JAEA-Research*, 2007-033, 3.3, 96-105, 2007.

[12] Nagao, H, T. Nakajima, M. Kumazawa, and T. Kunitomo, Optimum weighted stacking method for acquisition of the ACROSS transfer functions having the maximum signal-to-noise ratio, *JAEA-Research*, 2007-033,4.1,106-119,2007.

[13] Kunitomo, T.and M. Kumazawa, Active monitoring of the Earth's structure by the seismic ACROSS – Field examples at the Tono mine ACROSS experimental site -, *In the Proceedings of the "1st International Workshop on Active Monitoring in the Solid Earth Geophysics (IWAM04)"*, Task Group for Active Monitoring, Mizunami, Japan, 2004.

Takahiro NAKAJIMA[1], Mineo KUMAZAWA[1], Naotaka SHIGETA[2], Takahiro KUNITOMO[1], Hiromichi NAGAO[3], and Hiroshi MATSUMOTO[4]

[1] Tono Geoscientific Research Unit, JAEA

[2] Horonobe Underground Research Unit, JAEA

[3] Japan Agency for Marine-Earth Science and Technology

[4] Toyama University

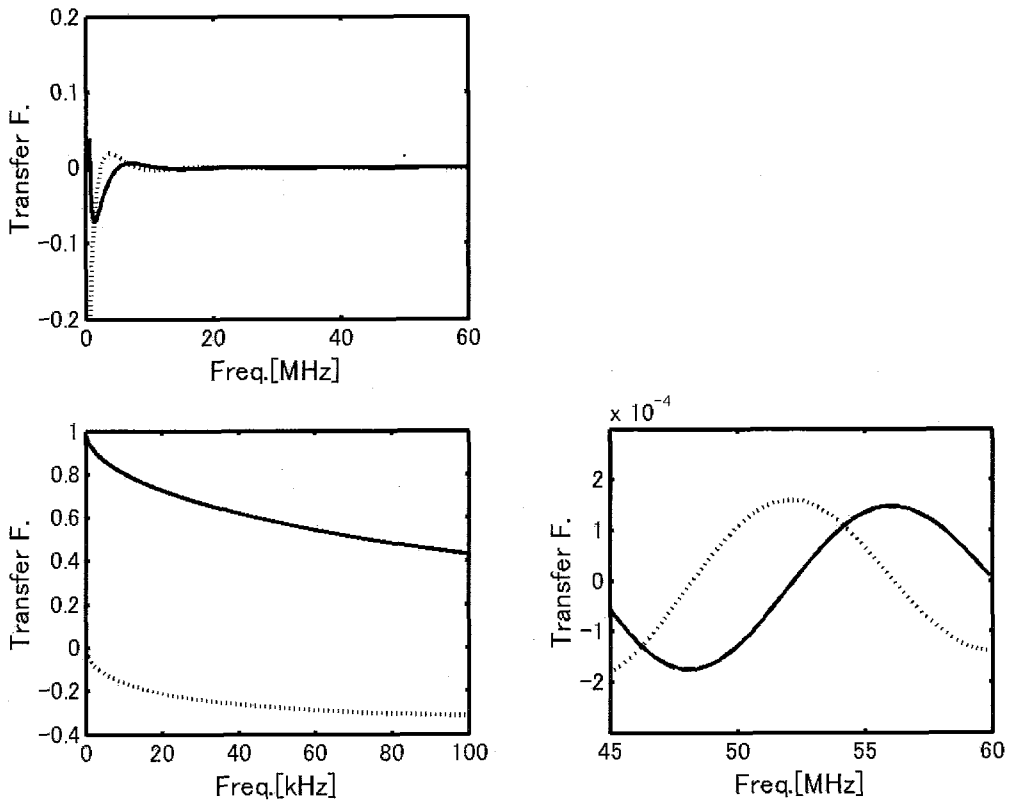

Figure 3.1.1 Transfer function of the electromagnetic field propagating in the uniform medium. The solid/dashed line shows real/imaginary part, respectively. (a) shows the transition of diffusion and wave field, and (b)/(c) shows the diffusion/wave field, respectively.

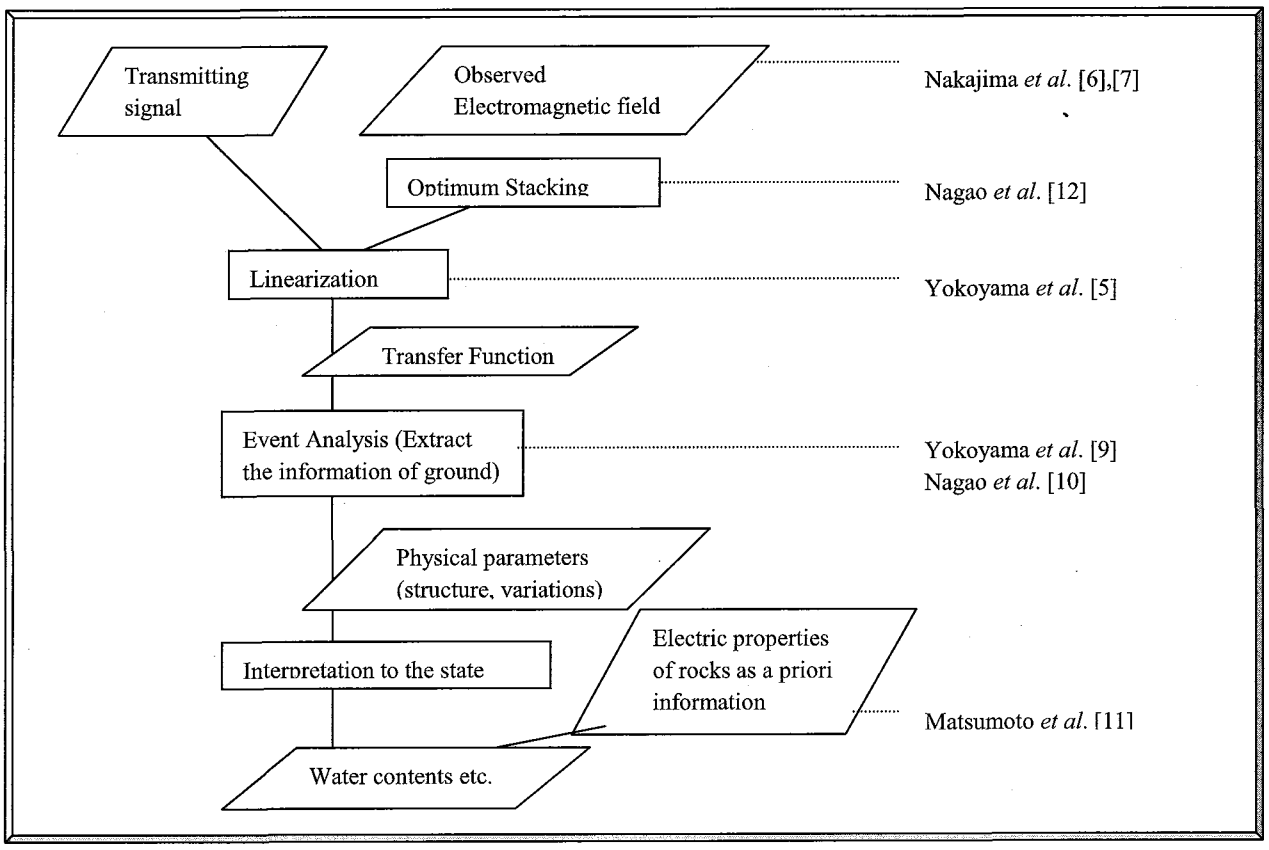

Figure 3.1.2 Flow chart of the investigation by the EM-ACROSS. Knowledge obtained during the development of the EM-ACROSS method and their relations in the flows are also shown. In the figure, boxes represent manipulations and parallelograms show data which we handle.

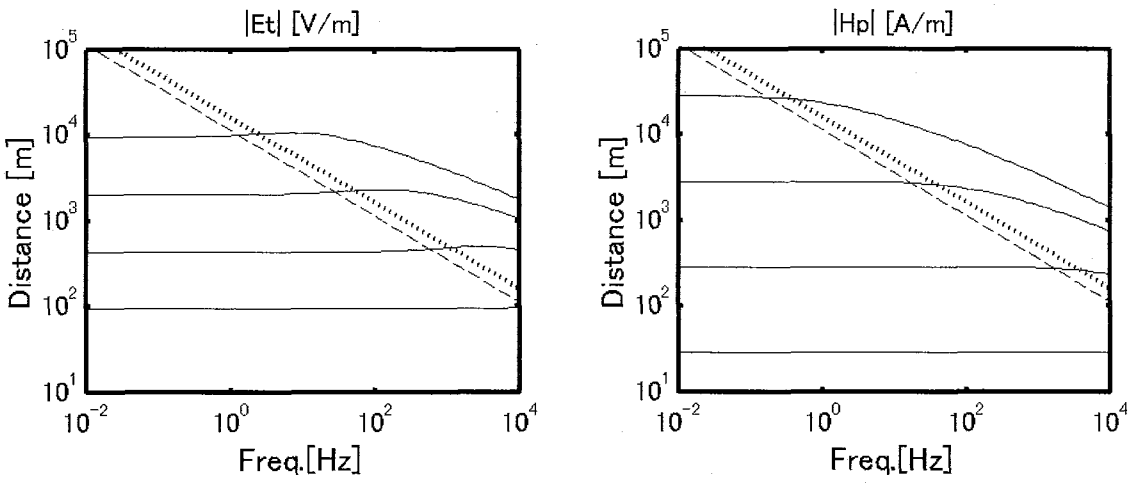

Figure 3.1.3 The signal amplitude of the electromagnetic field emitted by the current dipole of 1Am. (a)/(b) represents the amplitude of electric/magnetic field as the function of frequency and distance between the source and the receiver. The physical parameters in the medium are; electrical conductivity σ =0.001[S/m], relative dielectric permittivity ε_r =4, and the magnetic permeability is equal to that of vacuum. The broken lines are the boundary between the near field and the far field, and on the dashed lines the signal amplitude of plane wave becomes 1/e (Skin depth). The values in the figure show the value of contour in the unit of [V/m] in (a) and [A/m] in (b).

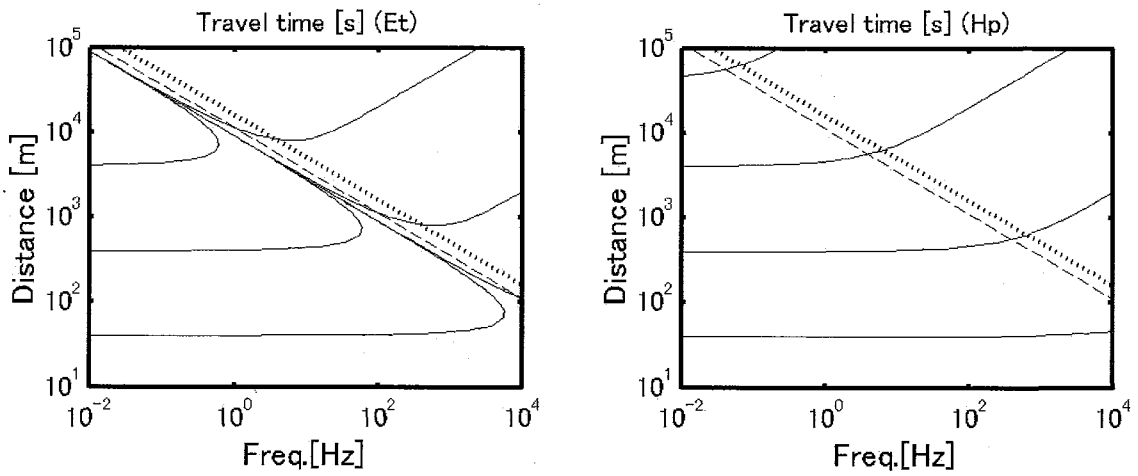

Figure 3.1.4 The apparent travel time between the source and receiver by the electromagnetic field emitted by a current dipole. (a)/(b) represents the contour as the function of frequency and distance. The values in the figure are the apparent travel time with the unit of milli-seconds. The physical parameters and the meaning of lines are the same as Figure 3.1.3.

3.2 Long-term operation of the EM-ACROSS and derived transfer function in the diffusion field region

3.2.1 Introduction

We have developed and tested a new electromagnetic controlled source method, which is called ACROSS (Accurately Controlled Routinely Operated Signal System). This characteristic feature of this approach is the use of accurately controlled waves to determine the accurately controlled electromagnetic waves to determine the accurate transfer function between source and observed signal. From the observed transfer function, the information of the underground structure is extracted out. In this method, we transmit accurately controlled sinusoidal waves to acquire the transfer function of better Signal-to-Noise Ratio (SNR) at all time, we can use this to detect the temporal variation of the physical and chemical state of the Earth [1]. Ogawa and Kumazawa [2] suggested to use both seismic and electromagnetic waves to visualize the Earth's interior. Nakajima *et al.* [3] summarized the features of the method using electromagnetic waves. In this study we shows the results of the EM-ACROSS in the diffusion field region. The trail observations are carried out at Tono area as an active monitoring of the electrical conductivity of this area.

3.2.2 Observation system

The test site locates around Tono mine campus of JNC (Figure 3.2.1). We use GPS clocks (TrueTime XL-DC) for the synchronization between the source and receivers [4].

(1) Transmitting system

We use electrical current dipole for the transmitting electromagnetic waves. We settled three grounded electrodes at Tono mine, and the spacing between electrodes is 150m (Figure 3.2.2). The three electrodes can be used to investigate the anisotrophy around the source. The transmitting signal is designed to be appropriate for the survey. The signal is generated by an arbitrary waveform generator, which the time base is synchronized with the GPS clock. Moreover this signal is amplified by a power amplifier, which outputs the current proportional to the designed signal. Using this transmitter with function generator and power amplifier, we can avoid the effect of higher harmonics of the transmitting signal. Transmitting current and the differences of electric potentials between the electrodes are monitored to use when the transfer function is calculated, and to examine the change of surroundings near the source. The monitored signals are also recorded together with the timing of GPS clock.

The configurations of the amplifier are; maximum output current is 10A, maximum output voltage is 200V, frequency range is from DC to 10kHz. The configurations of the recorder are; maximum channel is 16, sampling rate is 1kHz (maximum 10kHz), A/D resolution is 16 bits.

(2) Receiving system

The receiver is placed at the Shouba-sama of JNC (currently JAEA), located at 700m distance from the source. We observe magnetic field of 3 components and electric field of horizontal 2 components. The magnetic field is measured by the fluxgate magnetometer (Bartington MAG-03). For the electric field measurements we use Pb-$PbCl_2$ electrodes, and the distance between the electrodes are 33m. The recorder is the same configuration as the monitor of the source. We corrected the frequency dependency of the amplifiers and recorders after the verification of the equipments.

3.2.3 Long-term operation test

(1) Design of the transmitting signal

The transmitting signal is designed by the summation of several sinusoids of different frequencies. To investigate the details of the transfer function in a limited frequency range, and to grip the crude trend of the transfer function, we select following signals. The number in the table below represents the frequency of the signals.

Range 1: 35.0, 37.5, 40.0 [Hz]

Range 2: 125.0, 127.5, 130.0, 132.5, 135.0 [Hz]

Range 3: 362.5, 365.0, 367.5, 370.0, 372.5 [Hz]

From the consideration of the dispersion of the diffusion field, the mean frequency of each Range was selected as the mean frequencies of Range 1 and Range 2 is about 3 times and those of Range 1 and Range 3 is 9 times. The small differences from the proportion are the reason to aviod the coincidence of the signal and higher modes of the signals with smaller frequencies.

After the consideration of the decrease of the amplitude in higher frequency, the relative amplitude of the signal in each range is selected as 1:2:2. The initial phase of each signal in time domain is determined as the amplitude of total signal becomes minimum as Yokoyama *et al.* [5] did.

The spectrum of the actually transmitting signal is shown in Figure 3.2.3. The highest common measure of the frequencies of source signal is 2.5Hz, so we designed and transmitted the signal of the period of 0.4 s. In the spectral peaks of this and its higher modes can be seen. The amplitude of these peaks are, however, are four figures smaller than the designed signals. The noise level around the signals is five figures smaller, so very accurate transmission of the signal was realized.

(2) Received signal

We checked the performance of stacking. We transformed the observed signals from the time domain to the frequency domain. In Figure 3.2.4 (a)(c), we show the amplitude spectrum of the electromagnetic field. The signals in Range 2 can be faintly identified. We calculated the averaged spectrum, and by the use of optimum stacking method [6]. This optimum stacking can acquire the highest SNR data regardless the sudden noise or daily change of noise level. In Figure 3.2.4 (b)(d), we show the stacked results. By the optimum stacking, the noise level decreases, and high SNR results are acquired. The amplitudes of the signals are almost constant before and after the stacking except for the uncertainty of the noise at 100 sec data. The peaks of each signal are very sharp, showing that the accurate synchronization was realized through the stacking period.

The stacking of the whole frequency range is shown in Figure 3.2.5. The 13 signals are identified in both magnetic and electric field data. The peaks near 60Hz and its higher modes come from power line noise. Although the observed signals are smaller than the power line noise, the signals can be identified.

The results of electric field have better SNR than those of magnetic field. One of the reasons is that the noise level from the instruments is lower in the electric field measurements. Another reason is the observed electromagnetic field is in the near field region, and the near field term of the electric field is larger than that of magnetic field [7].

3.2.4 Characteristics in the observed transfer function

We show the transfer function acquired by the continuous operation. As the transmitting signal for the calculation of the transfer function we use the current, because it is the source of the electromagnetic field. The observed signals are electric and magnetic fields. The units of the transfer functions are, therefore, [(V/m)/A] for the electric field measurements, and [T/A] for the magnetic field.

(1) The averaged transfer function

In Figure 3.2.6 we show the transfer function of the stacked data as in the previous section. This figure shows the averaged values during the observation period and their confidence limits. It is common that the amplitudes at higher frequencies become smaller. However the phases have different features. These differences are thought to be come from followings;

1) the difference between electric and magnetic fields.
2) the differences in the tensor elements of the transfer function.
3) the difference of frequency dependency of near and far field.
4) the heterogeneity of the electric properties of the ground.

To obtain the more information, the change of the excitation direction is the one of the method. Using the three electrodes at Tono mine, we can transmit the electromagnetic field in any direction. From these results, we can obtain the tensor transfer function. This has information about heterogeneity or anisotropy in the ground. Although we presume the presence of lateral heterogeneity or anisotropy, we do not have enough observation points to describe them at this time yet. For the interpretation which explains the observed data very well, we also need a computation tool for the wave propagation in the arbitrary heterogeneity and dispersion [8].

(2) Temporal variations

In order to investigate the temporal variation of the transfer functions, we examine them every two hours. As one of the examples we examine the temporal changes of the phases of the transfer functions in 'Range 2' of the EW component of electric field (E_E). In Figure 3.2.7 we show the temporal change of the average of the 5 signals and their averaged slope in the frequency range with their confidence limits. The slope has a relation to the travel time from the source to receivers. As shown in Figure 3.2.7 we could not observe the transfer function in the period from 11th to 16th, and after 29th, July 2003. They are caused by the power failure caused by thunders. As the temporal variations we can see the meaningful changes in the average of phases, because the confidence limit is smaller than the amplitude of temporal variations.

To investigate the correlations among the temporal variation and other natural phenomena, we compare them with the rainfall in the test site. As shown in Figure 3.2.7 the average phase delayed a few percent just after the rainfall. Meanwhile we cannot see the correlation between the difference rate and the rainfall. The slope has large error because it is calculated from the difference of the phases. Nevertheless of the large error, the average of phase and the slope might have different information for the state in the ground. To see the relation, we need the observation with better SNR.

3.2.5 Summary

We carried out the continuous operation of EM-ACROSS at Tono area, and acquired the transfer function with their confidence limits. We also tested the transmission of the designed signal. By the accurately control of the transmitting signal, we obtained the transfer function with good SNR. From the results of the operation for one month, we could see temporal variation in the phase of transfer function. Although the changes are small as 1% of the averaged value, they are smaller than the confidence limit of averaged value. We could conclude that the variation is meaningful. We found these variations correlated with the rainfall.

We are improving the system by solving the problems through the continuous operation. Meanwhile we are trying to estimate the underground structure and investigate the reasons for the temporal variations. Tono area has explored the detailed geology by the boring up to 1 km. It is

known that there is a clear unconformity of the tertiary Mizunami group and the granite formation at about 100 m depth. We are trying to estimate this unconformity by our system. There are proper frequencies for the survey of this structure. Our system is adjustable for this purpose.

We have developed a method of 'ray-path' analysis using the transfer function of limited frequency range [9, 10, 11]. This method works in the wave field very well, and the transfer function obtained in this study is in the region of diffusion filed and also has near field, we need to develop an analyzing method, which is applicable to this region.

Concerning the temporal variation, we can obtain the transfer function with the confidence limit. We found the correlation between the measured value and the rainfalls. This correlation will be a noise to detect the changes in the deeper underground. Therefore the investigation of the changes near the surface is important for the detection of the change in the ground. To obtain and compare the independent data, we are doing the observation of the Seismic ACROSS at the same site [12]. We will compare both results to understand the nature of the temporal changes.

References

[1] Kumazawa, M., T. Kunitomo, Y. Yokoyama, T. Nakajima, and K. Tsuruga, ACROSS: Theoretical and technical developments and prospect to future applications, *JNC Technical Review*, **9**, 115-129, 2000. (in Japanese)

[2] Ogawa, K. and M. Kumazawa, Towards the continuous remote sensing of H2O, tectonic stress and physical states in the Earth's crust by means of acoustic and electromagnetic ACROSS, Abstract at the seismological society of Japan 1996 fall meeting, 45, 1996. (in Japanese)

[3] Nakajima, T., M. Kumazawa, N. Shigeta, T. Kunitomo, H. Nagao, and M. Matsumoto, Overview of EM-ACROSS and its development, *JAEA-Research*, 2007-033, 3.1, 73-83, 2007.

[4] Nakajima, T., T. Kunitomo, M. Kumazawa, Y. Yokoyama, Development of EM-ACROSS and its field test, *Bull. Eathq. Res. Inst. Univ. Tokyo*, **75**, 413-428, 2000.

[5] Yokoyama, Y., M. Kumazawa, T. Kunitomo, and T. Nakajima, Waveform of digital signal for a 3-D electric structure sounding using accurately controlled electromagnetic waves, *Bull. Eathq. Res. Inst. Univ. Tokyo*, **75**, 375-392, 2000.

[6] Nagao, H, T. Nakajima, M. Kumazawa, and T. Kunitomo, Optimum weighted stacking method for acquisition of the ACROSS transfer functions having the maximum signal-to-noise ratio, *JAEA-Research*, 2007-033, 4.1, 106-119, 2007.

[7] Ward, S.H. and G. W. Hohmann, Electromagnetic theory for Geophysical Applications, in applied geophysics Vol.1, edited by M.N. Nabighian, pp.131-312, Society of exploration geophysicists, Oklahoma, 1987.

[8] Kumazawa, M, K. Tsuruga, N. Shigeta, T. Nakajima and T. Nagai, Treatise of discontinuity in wave equation to derive linear system equation for computation of wave field, *In the Proceedings of the "1st International Workshop on Active Monitoring in the Solid Earth Geophysics (IWAM04)"*, Task Group for Active Monitoring, Mizunami, Japan, 279-281, 2004.

[9] Yokoyama, Y., M. Kumazawa, and T. Nakajima, A decomposition method of the electromagnetic transfer function using ray model and autoregressive-type model – the case of horizontal layered structure -, *Bull. Earthq. Res. Inst. Univ. Tokyo*, **75**, 393-411, 2000.

[10] Hasada, Y., H. Kumagai and M. Kumazawa, Autoregressive modeling of transfer functions in frequency domain to determine complex travel times, *Earth Planets Space*, **53**, pp. 3-11, 2001.

[11] Nagao, H., T. Nakajima, Y. Hasada,, M. Kumazawa, and T. Kunitomo, Detection of a reflected wave by application of the Sompi event analysis method to EM-ACROSS transfer functions, *In the Proceedings of the "1st International Workshop on Active Monitoring in the Solid Earth Geophysics (IWAM04)"*, Task Group for Active Monitoring, Mizunami, Japan, 245-248, 2004.

[12] Kunitomo, T. and M. Kumazawa, Active monitoring of the Earth's structure by the seismic ACROSS - Field examples at the Tono mine ACROSS experimental site -, *In the Proceedings of*

the "1st International Workshop on Active Monitoring in the Solid Earth Geophysics (IWAM04)", Task Group for Active Monitoring, Mizunami, Japan, 181-184, 2004.

Takahiro NAKAJIMA[1], Takahiro KUNITOMO[1], Hiromichi NAGAO[2], Mineo KUMAZAWA[1], and Naotaka SHIGETA[3]

[1] Tono Geoscientific Research Unit, JAEA

[2] Japan Agency for Marine-Earth Science and Technology

[3] Horonobe Underground Research Unit, JAEA

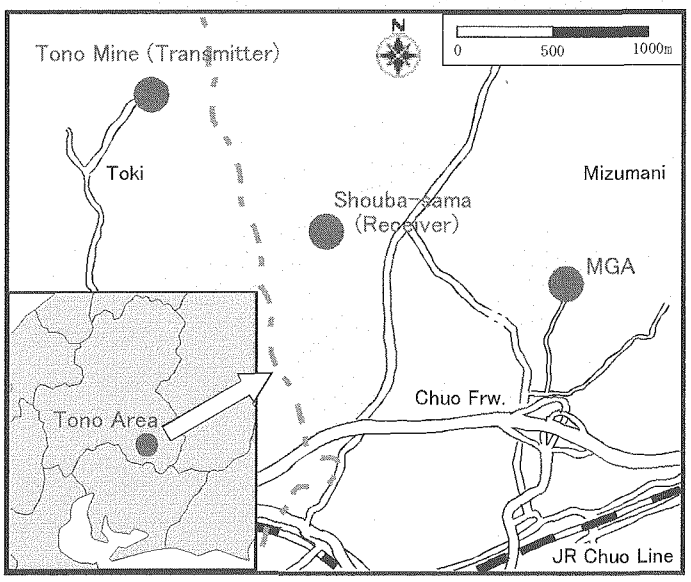

Figure 3.2.1 Tono test site, the arrangement of transmitter and receiver.

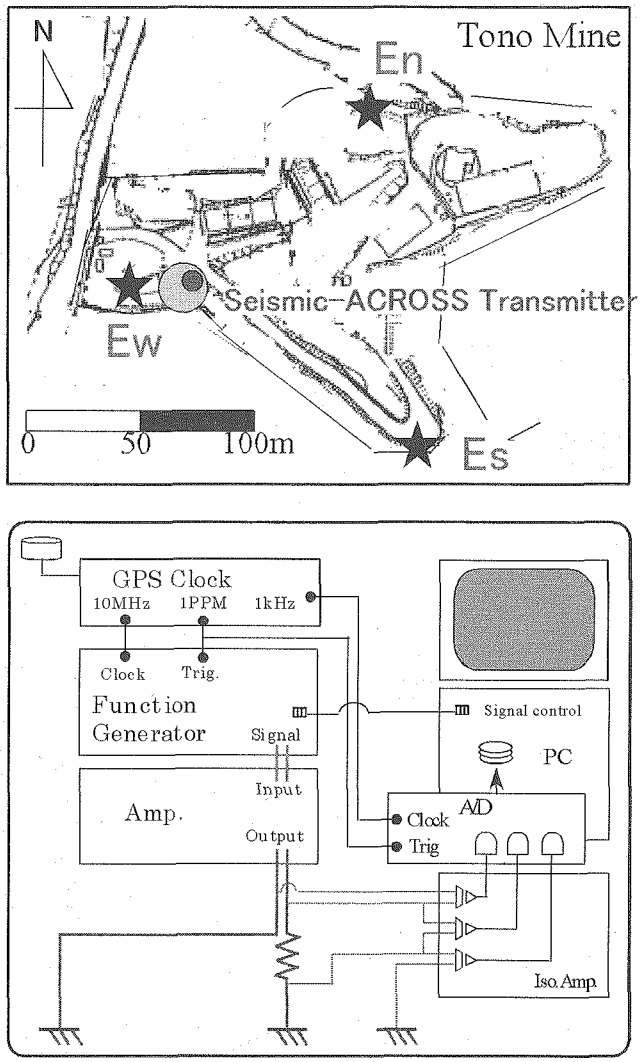

Figure 3.2.2 The layout of transmitting electrodes and schematic view of the transmitting and monitoring system.

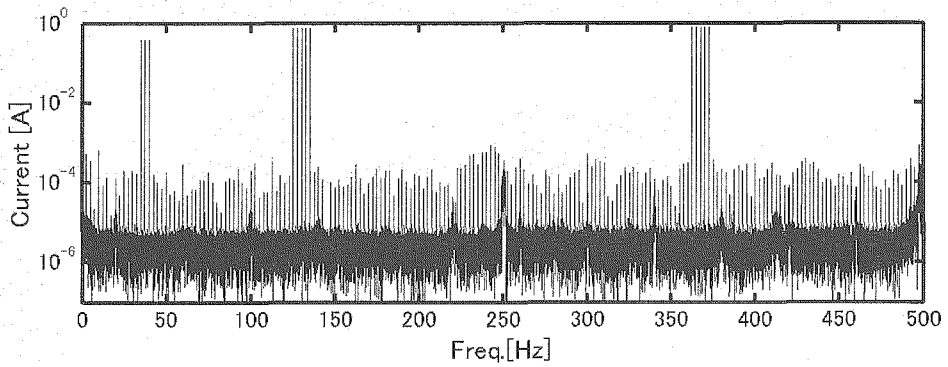

Figure 3.2.3 Amplitude spectrum of the transmitting signal.

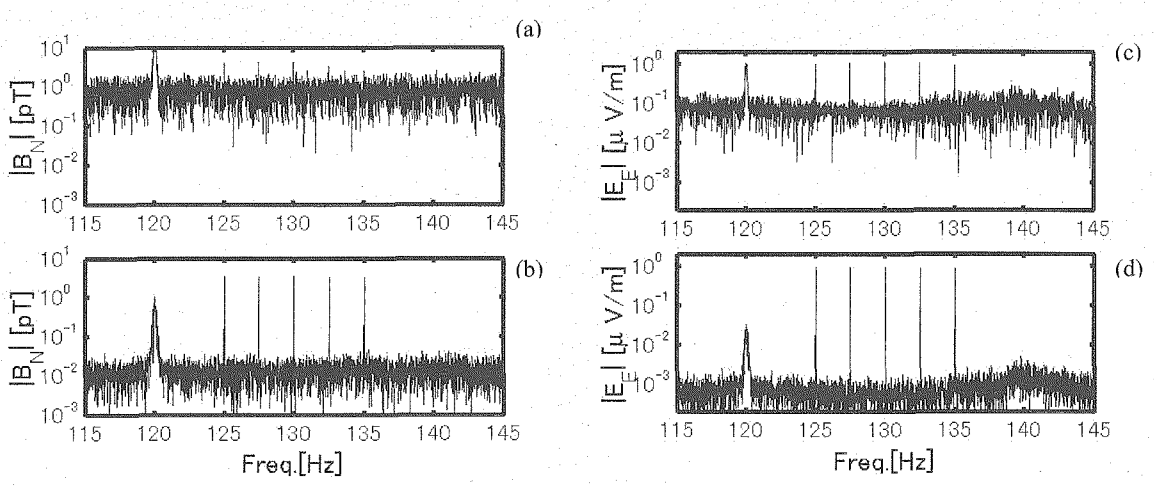

Figure 3.2.4 The amplitude spectrum of observed magnetic and electric field. (a), (b) are N-components of magnetic field, and (c), (d) are the E-components of electric field. (a), (c) represent the spectrum from 100 sec data, and (b), (d) show those of 181 hours stacking data.

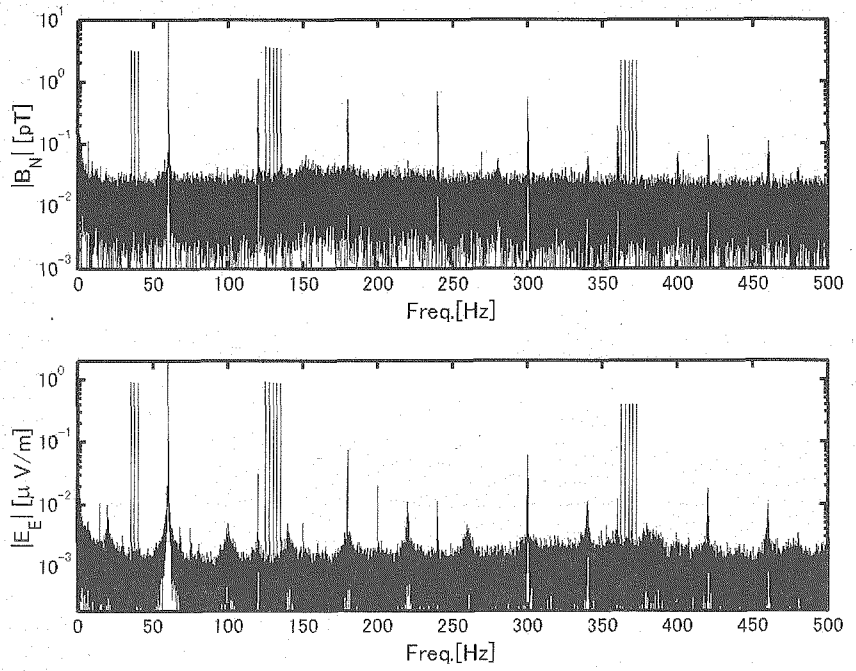

Figure 3.2.5 The amplitude spectrum of observed magnetic (B_N) and electric field (E_E). Peaks at 60Hz and their higher modes are caused by the commercial power supply.

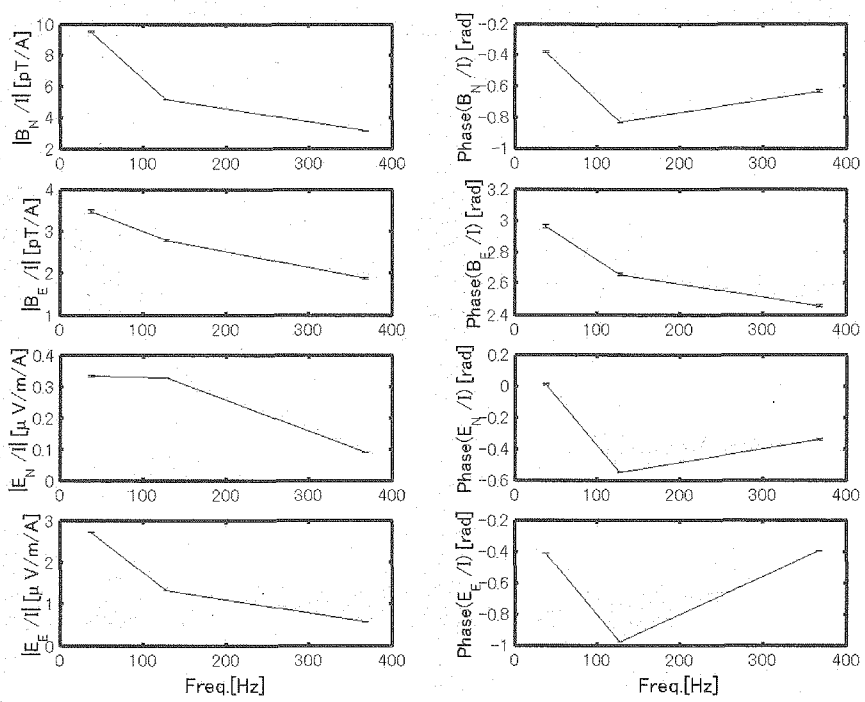

Figure 3.2.6 Observed transfer function after 181 hours stacking. The left hand side shows amplitudes and right hand side represents phases. From the top, N-component and E-component of magnetic field, and N-component and E-component of electric field are showed. The confidence limits of the data are also showed but they are small especially in the case of the electric fields.

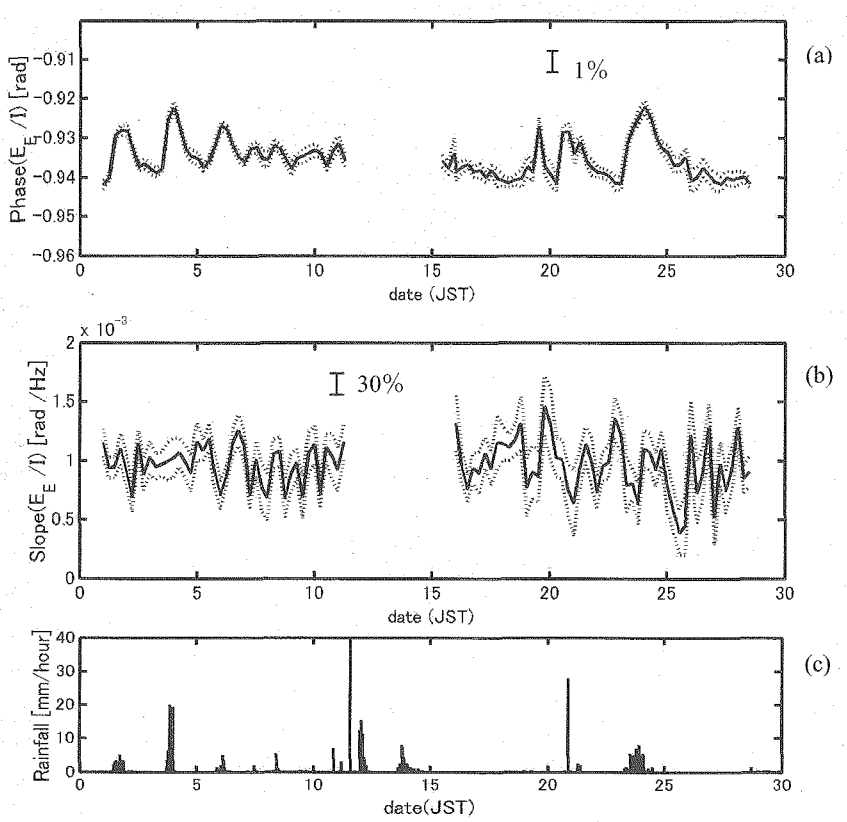

Figure 3.2.7 Temporal variation of the phase of E-component of electric field observed in July 2003. (a) is the average of Range 2, (b) is the slope in the range, and (c) is the rainfall at the site. The date is represented by the local time.

3.3 Complex dielectric permittivity spectroscopy using ACROSS measurement system

3.3.1 Introduction

Complex dielectric permittivity $\varepsilon^* = \varepsilon + \sigma/j\omega$ of rocks drastically changes by including water [1-3], where ε, σ and j are dielectric permittivity, electric conductivity, and imaginary unit. Our motivation of studying ε^* is the presence of a peculiar behavior in the real part ε: It may appear to go up to incredibly large values at lower frequencies, whereas the reliability of the previous data appears lacking. The large value of ε suggests that the large amount of electric energy is stored when the dissipative electric current exists. If such a phenomena exists in nature, there are some important implications in geophysical problems, since there have been debates on the electromagnetic precursors to the earthquakes, for example. One may raise such a question: Could the large value of ε be a source of electromagnetic emission?

Measurement of ε, however, is difficult because the moist rocks is a very good conductor; contribution of $\sigma/j\omega$ tending dominant at the lower frequencies below a few hundreds kHz, in particular. Measured value of ε in ε^* can be biased due to the electric noise, polarization of electrodes [4, 5], or the electric leak current due to stray capacitances and many other unknown factors. Therefore, we studied all the possible sources of difficulty in the reliable measurement of ε^*, and we have been tried to establish such a reliable and precise method that is appropriate for our purpose.

Complex dielectric permittivity itself is measured usually using the impedance spectrum analyzer available commercially for the measurements of any electric object with two or four terminals. Most of them are well designed to pose with even nonlinear response characteristic. However, the direct use of such a convenient product leads to some deficits for the present measurement aiming at the linear property under low electric field strength corresponding to natural condition. They are (1) difficult to measure very low impedance as in the case of moist rocks, (2) involving nonlinear electric property; and (3) lacking the appropriate method of error estimation. To overcome the factor as above we have developed a measurement system by introducing the concept of ACROSS (Accurately Controlled Routinely Operated Signal System [6]).

We have found that the measured complex dielectric permittivity is easily biased by polarization of potential electrode even by four electrode method [5] at frequency range lower than 1 kHz. We noted that the polarization is induced at the potential electrodes even by very small electric current flowing through sample-electrode interface, when the conduction mechanism is different between sample and electrode. In order to suppress this effect, we have developed the potential electrodes consisting of ionically conductive material instead of metallic electrode [5].

On the basis of the previous works noted above, we describe the new system for the measurement

of complex dielectric permittivity. The results of measurements on bentnite and three different samples of moist granular rock analogue are shown. The basic characteristics of dielectric dispersion are discussed for the relevant materials.

3.3.2 Complex dielectric permittivity

Electric property of a material is phenomenologically described by the equivalent circuit consisted of conductance σ and capacitance ε connecting parallel. In the case of moist rocks, ε is dependent on frequency while σ is usually independent on frequency. Electric current density i induced by alternating electric field of angular frequency ω and amplitude of electric field E is given as

$$i = \sigma^* E = j\omega\varepsilon^* E = (\sigma + j\omega\varepsilon)E, \tag{3.3.1}$$

$$\varepsilon^* = \sigma^*/j\omega = \varepsilon + \sigma/j\omega = \varepsilon - j\varepsilon'', \tag{3.3.2}$$

The ratio of real and imaginary parts of ε* is related to dielectric loss angle δ as a measure of energy loss by tanδ or energy storage by cotδ.

$$\cot\delta = \varepsilon/\varepsilon'' = \omega\varepsilon/\sigma. \tag{3.3.3}$$

Cotangent of δ represents the ratio of displacement and conduction currents. It represents propagation characteristics of electromagnetic field; diffusion wave when $\cot\delta << 1$, and ordinary wave when $\cot\delta >> 1$.

Electric property of moist rocks is usually described by resistivity $\rho = |\sigma^*|^{-1}$ or impedance corresponding to complex resistivity $\rho^* = \sigma^{*-1}$. We use ε* so that the frequency dependence of ε is plainly presented. We also employ cotδ to describe the characteristics for EM field propagation expected for a material.

There are a variety of spectra type of ε* and cotδ depending on materials. A material has ε and σ independent on frequency in a certain frequency range. Figure 3.3.1(a) shows spectra of ε* and cotδ for the model of ε and σ independent on frequency. Debye type dielectric dispersion occurs if a material shows dielectric polarization responding to electric field with a time constant τ, which is called relaxation time. Figure 3.3.1 (b) shows spectra of ε* of Debye type dispersion, and dielectric permittivity increases at frequency f_c, where f_c is called characteristic frequency and given as $f_c = 1/\tau$. The model of 1/f-type dielectric dispersion is shown in Figure 3.3.1(c).

3.3.3 Overview of the measurement system

Figure 3.3.2 shows the overview of the developed measurement system. Sinusoidal voltage generated by a function generator (Agilent Technology 33120A) is supplied to the sample via buffer amplifier. To measure the induced electric current, we used current-voltage conversion circuit. The circuit has some advantages in reduction of the electric leak current through stray capacitance, since one of the sample edge is imaginary grounded via an OP amp. The potential difference between the potential electrodes is measured by the differential amplifier (Burr-Brown INA114) with a high input impedance ($> 10^9\ \Omega$). Input voltage is digitized by an A/D converter board (National Instruments DAQ-Card 6062E) and is stored in the computer. The combination of the A/D converter and a multiplexer on the A/D board enables us to measure up to seven impedances in series simultaneously.

Obtained digital data are processed by the procedure based on the method of ACROSS. First we obtain $V'(\omega)$, $I'(\omega)$ and their SNR. The admittance Y is given by

$$Y = I'(\omega)/V'(\omega). \tag{3.3.4}$$

The error of $|Y|$ and ϕ (phase of Y) in the unit of radian is calculated as

$$\delta(Y) = |Y|/snr', \tag{3.3.5}$$

$$\delta(\phi) = 1/snr', \tag{3.3.6}$$

where snr′ is the smaller one of either SNR for $V'(\omega)$ or for $I'(\omega)$.

The complex dielectric permittivity ε^* is

$$\varepsilon^* = Y/\kappa, \tag{3.3.7}$$

where κ (=S/d) is a factor given by the cross section S and the thickness d of the sample.

3.3.4 Measurement and results

Figure 3.3.3 shows how electrodes were installed to the sample. A small piece of agar-agar plate was inserted in the sample as a potential-detecting part, and electric lead is placed at the distant edge of the agar-ager plate. This method suppresses surely disturbances caused by the contact of metallic electrodes and the sample of ionic conductor [5]. Stainless mesh was used as the current electrode just for convenience.

Applied sinusoidal voltage signal is 5 V in double amplitude. The time period of data acquisition is set to be 256 cycles of sinusoidal signal above 10 Hz, and 16 cycles below 10 Hz. Figure 3.3.4 shows an example of raw data on the moist bentonite at 10 Hz in (a) and (b), and that at 0.01 Hz in

(c) and (d). We note spectrum in (b) and (d) that spectral line of the signal is well separated from noise and overtones, whereas considerable higher harmonics involve at low frequency. Further we note that S/N is high enough for the present work.

The measurements are made on the moist granular samples of quartz, calcite, and glass as moist rock analogue, and bentonite as a representative of clay in order to know the difference and similarity of the results among different materials. The granular samples are consisted of coarse grains with uniform size. Calcite grains of about 5 mm in diameter and quartz grains of 2mm in diameter were moistened by 2 wt % of 10^{-5} mol/l NaCl (aq). Glass beads of 1mm in diameter were moistened by 0.15 wt % of 10^{-3} mol/l NaCl (aq). Bentonite was moistened with pure water of 33 wt %.

Figure 3.3.5 shows the results of measurements on the samples above. The imaginary part is surely in reciprocal proportion to frequency for all the samples to satisfy a model with conductivity independent of frequency. Another feature common to the four samples is that the real part ε tends nearly to be in reciprocal proportion to frequency at the lower frequency. A straightforward conclusion is the 1/f type dielectric dispersion is a common nature of the moist silicate materials.

3.3.5 Discussion

Moist granular samples of calcite, quartz and glass showed 1/f type dielectric dispersion. We claim that the 1/f dielectric dispersion observed here is the bulk property of the sample and due neither to the polarization induced at and around the electrodes nor to the measurement circuitry.

The present granular samples do not contain metallic or sulfide minerals, which are known to induce strong dielectric dispersion by electrochemical effect. Therefore, the physical mechanism of 1/f type dispersion is a subject of our relevant concern. One hypothesis proposed by Lesmes and Morgan [1] has not clarified yet and it is discarded, since it demands a specific grain size distribution to account for the continuous characteristic frequency spectrum of Debye type dispersion with a single relaxation peak. Even if wide distribution of all possible spatial scales is considered in the aggregate of spheres with uniform grain size, it appears very difficult to create the explanation on the basis of Debye model for the granular samples.

Bentonite clay shows nearly the 1/f type dielectric dispersion, whereas phenomenological features are a little different from that of granular samples: Both real and imaginary parts are larger by 4 order of magnitude with the phase angle larger only by a factor of 2 or 3. Bentonite has been known to show dielectric dispersion with the broadened Debye type as indicated by spectrum of ε*[7]. Since the measurement error becomes larger below 1 Hz in the present case, and we reserve any discussion on this subject until better data comes out.

As far as granular silicate materials concern, the presence of 1/f type dielectric dispersion is certainly existent. Whereas there has never been presented any reasonable explanation on the

mechanism of 1/f type dispersion in detail, we can state at least a phenomenological feature of the mechanism; there should be some electrochemical reaction, which proceeds with a constant rate as suggested by a factor 1/f under the constant driving force. The phase angle is 0.01~0.02, indicating that 1~2 % of ohmic loss is stored in the sample. Under the constant electric field, the stored energy increases in proportional to time elapsed. Simple extrapolation leads to the infinitely large amount of energy, so that there should be a limit, and the strict 1/f law will fail at the very low frequency (after a long period of time). Therefore, the experimental data on the deviation from the 1/f law would be one of the potential clues to clarify the physical mechanism.

3.3.6 Conclusion

Peculiar phenomena called '1/f type' dispersion in complex dielectric permittivity is studied very carefully on the moist rock analogues after the extensive and intensive improvement of the measurement system. In summary, we conclude that the 1/f type dielectric dispersion or alike, is surely existent in most of rocks; not only silicate but carbonate materials. Therefore, the storage of large amount of electric energy is shown to be possible in the most crustal rocks, and this would raise a question on their geophysical significance. The understanding of the physical mechanism is left for the future study down to the lower frequency on the moist materials with an appropriate texture.

References

[1] D. P. Lesmes and F. D. Morgan, Dielectric spectroscopy of sedimentary rocks. *J. Geophy. Res.* **106**, 13329-13346, 2001.

[2] L. Chilidze, Y. Gueguen, and C. Ruffet, Electrical spectroscopy of porous rocks: a review-I. Theoretical models. *Geophys. J. Int.*, **137**, 1-15, 1999.

[3] L. Chilidze, Y. Gueguen, and C. Ruffet, Electrical spectroscopy of porous rocks: a review-II.Experimental results and interpretation. *Geophys. J. Int.*, **137**, 16-34, 1999.

[4] G. R. Olhoeft, Low frequency electrical properties, *Geophysics*, **50**, 2492-2503, 1985.

[5] H. Matsumoto, N. Shigeta, M. Kumazawa and T. Nakajima, Study of dielectric dispersion of ionic conductors as a possible observables of ACROSS, *AGU 2003 Fall Meeting*, San Francisco, 2003.

[6] M. Kumazawa, T. Kunitomo, Y. Yokoyama, T. Nakajima and K. Tsuruga, ACROSS: Theoretical and technical developments and prospect to future applications, *JNC Technical Review*, **9**, 115-129, 2000.

[7] W. H. Pelton, S. H.Ward, P. G. Hallof, W. R. Sill and P. H. Nelson, Mineral Discrimination and Removal of Inductive Coupling with Multifrequency IP, *Geophysics*, **43**, 588-609, 1998.

Hiroshi Matsumoto[1], Naotaka Shigeta[2], Mineo Kumazawa[3], and Takahiro Nakajima[3]

[1] Toyama University

[2] Horonobe Underground Research Unit, JAEA

[3] Tono Geoscientific Research Unit, JAEA

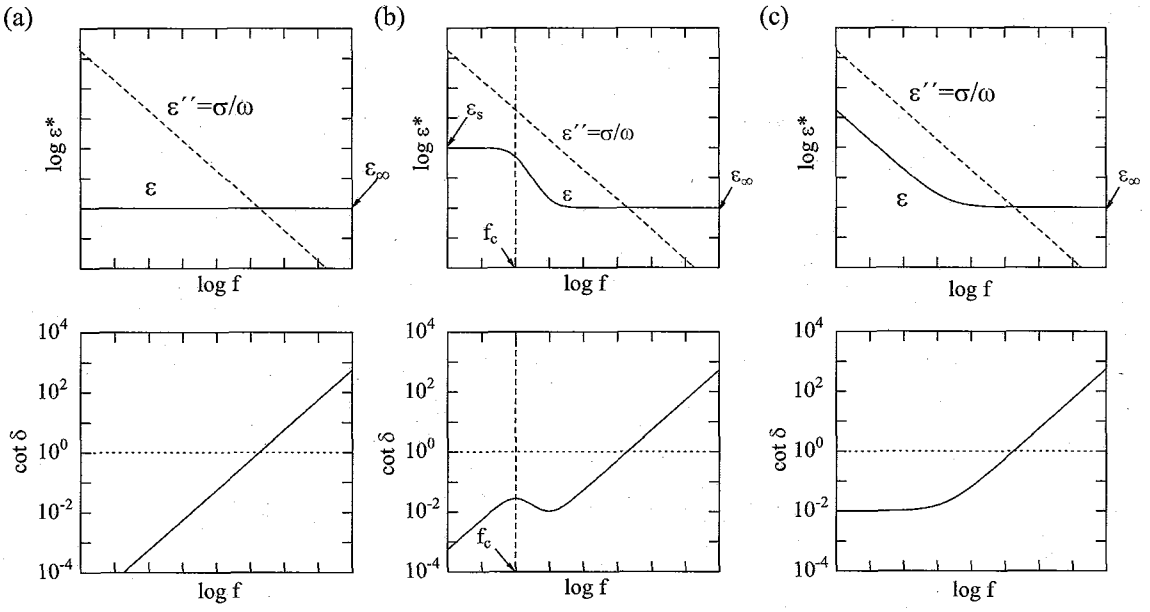

Figure 3.3.1 Models of frequency dependence of complex dielectric permittivity $\varepsilon^* = \varepsilon + \sigma/j\omega = \varepsilon - j\varepsilon''$ (upper column) and cot δ(lower column), where ε, σ, ω and δ are dielectric permittivity, electric conductivity, angular frequency and a dielectric loss angle, respectively. (a) the model with frequency-independent ε and σ are (b) Debye type dielectric dispersion, and (c) 1/f type dielectric dispersion. Characteristic frequency f_c of dielectric dispersion is indicated in (b).

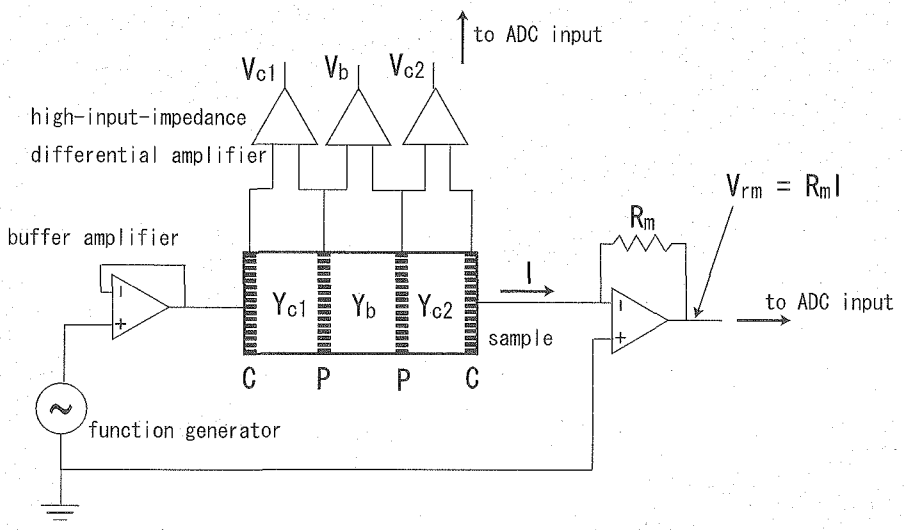

Figure 3.3.2 The electric circuit used for complex dielectric permittivity measurement. Current electrodes (C) and potential electrodes (P) are attached to the sample. Input voltage is generated by a function generator and is supplied to the sample via buffer amplifier. Potential difference between electrodes is measured by differential amplifier, and electric current flowing through the sample is measured by current-voltage conversion circuit. Analog signals are digitized by an A/D converter and the digitized data are stored in a computer.

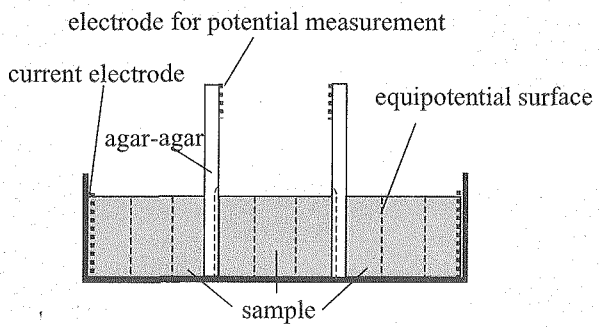

Figure 3.3.3 Method of electrode installation employed in this study. Stainless mesh was used as current electrodes. Potential of the sample was measured by metal electrode attached on the edge of agar-agar plate inserted in the sample.

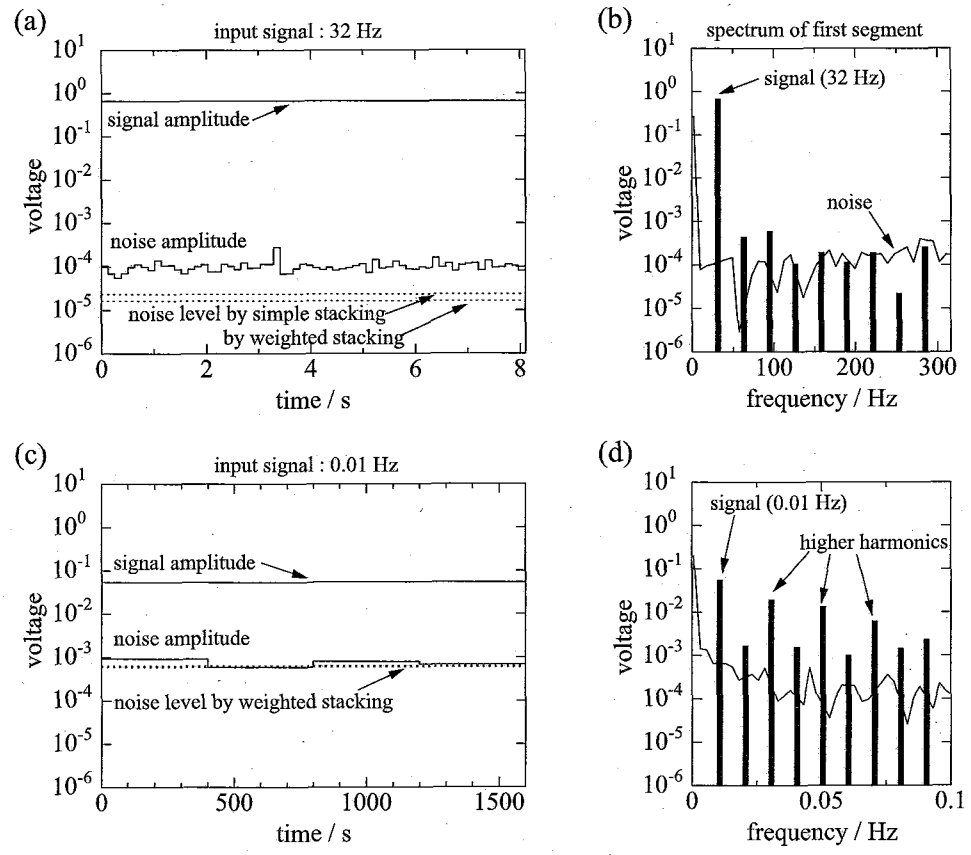

Figure 3.3.4 Signal and noise in the voltage between the potential electrodes during the complex dielectric permittivity measurements. (a),(b) are the results when the input signal is 32Hz, and (c),(d) are the case of 0.01Hz. Left panels show the stability of signal and noise. The dotted lines in the right panel indicate the noise levels of stacked data obtained by weighted stacking and non-weighted stacking. One segment includes four sinusoidal cycles; 0.125sec for 32Hz, and 400sec for 0.01Hz. The right panels show the spectra calculated from one segment data. The vertical lines represent the input signal and its higher harmonics, and the thin lines show the envelopes of the noise spectrum.

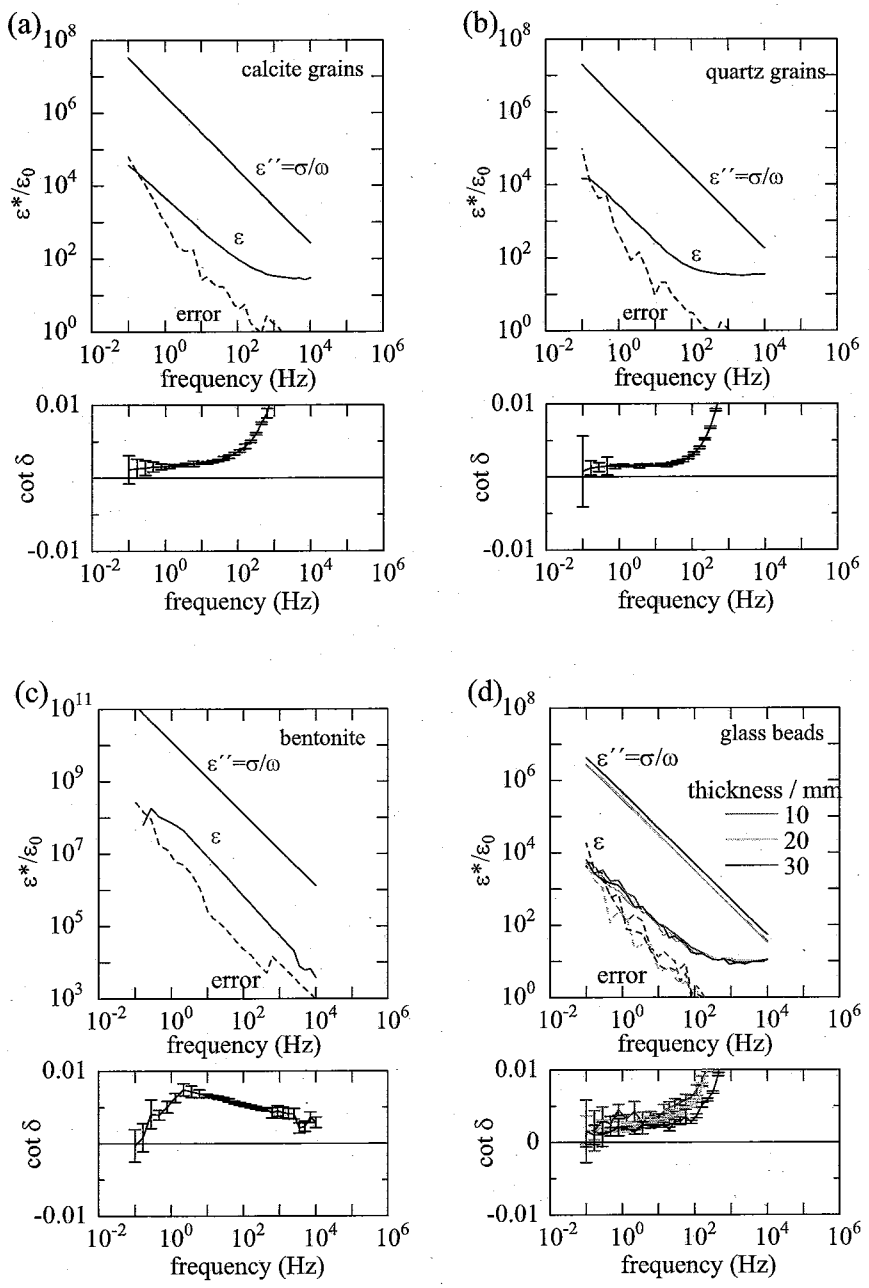

Figure 3.3.5 Dielectric dispersion observation. (a) calcite grains of diameter about 5 mm with 10^{-5} mol/l NaCl (aq) by 2 wt %, (b) quartz grains of 1 mm with 10^{-5} mol/l NaCl (aq) by 2 wt %, (c) bentonite with pure water by 33 wt %. (d) glass beads of 1 mm with 10^{-3} mol/l NaCl, measured for samples of 10, 20, 30 mm in thickness. Upper and lower columns show complex dielectric permittivity and cot δ, respectively, where δ is loss angle; a measure of energy loss by tanδ (see eq.(3.3.3)).

4. Theory of data analysis and modeling

4.1 Optimum weighted stacking method for acquisition of the ACROSS transfer functions having the maximum signal-to-noise ratio

4.1.1 Introduction

Accurately Controlled Routinely Operated Signal System (ACROSS) is such a new sounding method for underground structures that is organized to be robust against noise. [9] and [4] suggested the concept of ACROSS, and its theory and equipments are being developed in Tono Geoscience Center, Japan Nuclear Cycle Development Institute (TGC/JNC), and in Nagoya University. A controlled seismic or electromagnetic signal with a set of line spectra is transmitted from a source on the Earth's surface, and the transfer functions from the source to receivers are determined, which will be analyzed in the frequency domain by using the Sompi event analysis method [1][3][11] to clarify the underground structures. The received signal is divided into time segments, and they are successively stacked for a long period of time to obtain a transfer function having a large signal-to-noise ratio (SNR). All the system elements of ACROSS are precisely synchronized with the Global Positioning System (GPS) clocks.

The purpose of this paper is to devise an optimum method for the signal level estimation in received ACROSS data in order to obtain a transfer function having the maximum SNR even if the noise level changes with time and depends on frequency. The traditional method is a simple average of the whole data, and this method requires the stationarity in signal and noise levels during a observation period in order to increase the SNR with the stacking time. However, ACROSS is in operation not only at nighttime but also at daytime, when the noise level produced by human activities seems much larger than that at nighttime. The SNR decreases extremely when noisy data is added. The deletion of data acquired at noisy time is often used to improve the SNR. For example, only data obtained at nighttime are used in an electromagnetic sounding method such as the magnetotelluric (MT) or controlled source magnetotelluric (CSMT) method. However, the daytime data must contain a signal although the signal level is smaller than the noise level, and these data are thought to be available with a suitable method. Some weighted stacking methods have been applied to obtain optimum use of noisy data. [2] used a weighted stacking method for received seismic ACROSS data, in which the weight for a segment is defined as the reciprocal of the maximum amplitude in the time domain. This method is effective to reject a segment which contains a sudden event such as an earthquake. Here we propose the optimum weighted stacking method (OWSM) by using noise level as a measure of weight on the theoretical basis of the maximum likelihood principle to attain the maximum SNR of transfer function. We also suggest a new method for the noise level estimation, which is necessary to determine the optimum weight. The derivation of the

OWSM and the noise level estimation method from the maximum likelihood method are mentioned in Section 2. We report, in Section 3, the results of the application of these methods to real seismic and electromagnetic data obtained by a long-term observation test of ACROSS at Tono, Gifu, Japan.

4.1.2 Methodology

(1) Derivation of Optimum Weighted Stacking Method

In order to increase the SNR of a transfer function, continuously received ACROSS data are divided into time segments, and then the segments are successively stacked. Suppose that a time series of data in a segment is $x(j\Delta t)$, where Δt is the sampling time and K is the number of data, i.e., the time length of the segment becomes to be $T = K\Delta t$. Some peaks related to the source signal should appear in both real and imaginary parts of the finite Fourier series

$$z(k\Delta f) = \frac{1}{K}\sum_{j=1}^{K} x(j\Delta t)\exp\left[-i\frac{2\pi(j-1)(k-1)}{K}\right] \quad (k = 1, 2, \cdots, K) \ , \tag{4.1.1}$$

where $\Delta f = 1/T$ is the mesh width of frequency. We call each frequency at which a peak appears "signal channel," and other frequency "noise channel." Note that not only signal but also noise is included in a signal channel. Here we derive the optimum method for the signal level estimation from the maximum likelihood principle, which attains the SNR in each signal channel maximum. The probability density function (PDF) for the k-th channel in the m-th segment is given by

$$p_{mk}(z) = \left(\frac{1}{\sqrt{2\pi n_{mk}^2}}\right)^2 \exp\left[-\frac{|z - s_{mk}|^2}{2n_{mk}^2}\right] \ , \tag{4.1.2}$$

where s_{mk} and n_{mk} are the signal and noise levels, respectively, i.e., $s_{mk} = 0$ for a noise channel. This PDF is a two-dimensional normal distribution function with variances n_{mk} and covariances zero because a Fourier component z is considered to have independent two parameters, i.e., real and imaginary parts. In this paper, we assume that the signal level is stationary during an observation period, i.e., $s_{mk} = s_k$. Therefore equation (4.1.2) is rewritten as

$$p_{mk}(z) = \left(\frac{1}{\sqrt{2\pi n_{mk}^2}}\right)^2 \exp\left[-\frac{|z - s_k|^2}{2n_{mk}^2}\right] \ . \tag{4.1.3}$$

When M is assumed to be the number of segment obtained during an observation period, the likelihood function of the received data is given by

$$L=\prod_{m=1}^{M} p_{mk}(z_{mk})=\left(\frac{1}{2\pi}\right)^{M}\cdot\prod_{m=1}^{M}\frac{1}{n_{mk}^2}\cdot\exp\left[-\sum_{m=1}^{M}\frac{|z_{mk}-s_k|^2}{2n_{mk}^2}\right] \quad , \tag{4.1.4}$$

where $z_{mk}=z(m\Delta f)$ is a realized value of the Fourier component at the k-th channel in the m-th segment. The log-likelihood function becomes

$$\log L=-M\log 2\pi-\sum_{m=1}^{M}\log n_{mk}^2-\frac{1}{2}\sum_{m=1}^{M}\frac{|z_{mk}-s_k|^2}{n_{mk}^2}=-M\log 2\pi-\sum_{m=1}^{M}\log n_{mk}^2-\frac{1}{2}\sum_{m=1}^{M}\frac{(z_{mk}^R-s_k^R)^2+(z_{mk}^I-s_k^I)^2}{n_{mk}^2}, \tag{4.1.5}$$

where R and I, respectively, denote the real and imaginary parts of a complex number. To obtain $s_k=s_k^R+is_k^I$ which attains this equation maximum,

$$\frac{\partial\log L}{\partial s_k^R}=\sum_{m=1}^{M}\frac{z_{mk}^R-s_k^R}{n_{mk}^2}=0, \quad \frac{\partial\log L}{\partial s_k^I}=\sum_{m=1}^{M}\frac{z_{mk}^I-s_k^I}{n_{mk}^2}=0 \quad . \tag{4.1.6}$$

Solving these equations, the optimum estimation of the signal level is given by

$$s_k^R=\sum_{m=1}^{M}\frac{z_{mk}^R}{n_{mk}^2}\Big/\sum_{m=1}^{M}\frac{1}{n_{mk}^2}, \quad s_k^I=\sum_{m=1}^{M}\frac{z_{mk}^I}{n_{mk}^2}\Big/\sum_{m=1}^{M}\frac{1}{n_{mk}^2} \quad . \tag{4.1.7}$$

Consequently, we obtain

$$s_k=\sum_{m=1}^{M}\frac{z_{mk}}{n_{mk}^2}\Big/\sum_{m=1}^{M}\frac{1}{n_{mk}^2} \quad . \tag{4.1.8}$$

This equation means that the optimum estimation of the signal level is given by an optimum weighted stacking method (OWSM), and the optimum weight for each signal channel in each segment is inverse proportion to the square of noise level at the signal channel, that is,

$$w_{mk}=\frac{1}{n_{mk}^2}\Big/\sum_{m'=1}^{M}\frac{1}{n_{m'k}^2} \quad . \tag{4.1.9}$$

Of course, this weight satisfies $0<w_{mk}<1$ except for the ultimate and unrealistic case that the noise level is zero or infinity. This means that the SNR of stacked data is always increasing even if a segment having a large noise level is added. Note that the OWSM is derived without an assumption that "stacking."

(2) Estimation of Noise Level at a Signal Channel

According to equation (4.2.9), it is necessary to estimate the noise level included in each signal channel in each segment in order to obtain the optimum weight. However the noise level cannot be estimated only from the signal channel. Here we propose a new method for the noise level estimation by using noise channels around the signal channel. ACROSS signals are designed so that these noise channels are always produced around each signal channel. Recalling equation (4.1.3), the PDF for each noise channel is given by

$$p_{mk}(z)=\left(\frac{1}{\sqrt{2\pi n_{mk}^2}}\right)^2 \exp\left[-\frac{|z|^2}{2n_{mk}^2}\right] \quad . \tag{4.1.10}$$

Here it is assumed that the noise level in a signal channel k_0 is estimated from noise channels in the range of $k_0-k' \le k \le k_0+k'$. The likelihood function is given by

$$L=\prod_{k=k_0-k'}^{k_0+k}{}' p_{mk}(z_{mk})=\left(\frac{1}{2\pi}\right)^{K'} \cdot \prod_{k=k_0-k'}^{k_0+k'}{}' \frac{1}{n_{mk}^2} \cdot \exp\left[-\sum_{k=k_0-k'}^{k_0+k'}{}' \frac{|z_{mk}|^2}{2n_{mk}^2}\right] , \tag{4.1.11}$$

where K' is the number of noise channels used for the noise level estimation, and Π' and Σ' denote a production and summation for noise channels (i.e., excluding signal channels), respectively. The log-likelihood function becomes

$$\log L=-K'\log 2\pi-\sum_{k=k_0-k'}^{k_0+k'}{}' \log n_{mk}^2-\frac{1}{2}\sum_{k=k_0-k'}^{k_0+k'}{}' \frac{|z_{mk}|^2}{n_{mk}^2} \quad . \tag{4.1.12}$$

Here we give a frequency-dependent model for n_{mk}, i.e., $n_{mk}=n_m(k;\theta)$, where θ is a vector of model parameters. To obtain the optimum parameters of the model, calculate $\partial \log L/\partial\theta=0$, and we have

$$\sum_{k=k_0-k'}^{k_0+k'}{}' \left[\frac{|z_{mk}|^2}{n_m(k;\theta)^3}-\frac{2}{n_m(k;\theta)}\right]\frac{\partial n_m(k;\theta)}{\partial\theta}=0 \quad . \tag{4.1.13}$$

This equation is non-linear in general, and the solution can be obtained not analytically but numerically. The numerical process takes too much computational time, and it is not practical to give a complicated model when there are many segments to be stacked. Therefore we give the simplest model for n_{mk}, i.e., $n_{mk}=n_m$, assuming that the noise level is stationary in a narrow band of frequency. In this case, equation (4.1.13) can be solved analytically, and we have

$$n_m = \sqrt{\frac{1}{2K'} \sum_{k=k_0-k'}^{k_0+k}{}' |z_{mk}|^2} \quad . \tag{4.1.14}$$

The noise level is estimated by $1/\sqrt{2}$ of the root-mean-square of spectrum amplitudes in the noise channels. Taking both the real and imaginary parts of a Fourier component into consideration, the noise level should be estimated by $\sqrt{2}n_m$ in the amplitude domain, i.e., the root-mean-square of spectrum amplitudes in the noise channels.

Note that it is difficult from the statistical point of view to derive an optimum range of noise channels k' used for the noise level estimation because it is impossible to compare two likelihood functions obtained from different number of noise channels. From this reason, the range k' is *a priori* given in this paper, in which noise level is thought to be stationary.

4.1.3 Application of weighted stacking method

In this section, the OWSM derived in Section 2 and other stacking methods used in various underground explorations are applied to real ACROSS data obtained by a long-term observation test at Tono, Gifu, Japan [6]. Then we compare the SNR in a signal channel of stacked data obtained by (1) simple stacking method (SSM), which is an ordinary averaging stacking of whole data, (2) nighttime stacking method (NSM), which is an ordinary averaging stacking using only data at nighttime, (3) inverse weighted stacking method (IWSM), which is a weighted stacking using a weight defined as the reciprocal of the maximum amplitude in the time domain in each segment [2], and (4) the OWSM.

(1) Application to Seismic ACROSS Data

A long-term seismic ACROSS observation test has begun from October 2002 at Tono, Gifu, Japan. Figure 4.1.1 shows the location of Tono Mine, where three seismic ACROSS transmitters [5] are located, and five Hi-net observatories (Yaotsu, Kasugai, Hiraya, Takagi, and Fujimi) operated by National Research Institute for Earth Science and Disaster Prevention, Japan, where the ACROSS signals are expected to be observed. The distance of each observatory from Tono Mine is 11.1, 17.0, 38.6, 61.7, and 115 kilometers, respectively. In this test, one of the seismic transmitters called "FIT No.1" radiates a frequency-modulated (FM) signal. The frequency of this FM signal changes temporally with a period of 20 seconds, and this changing frequency is in the range of 18.52 ± 0.50Hz [7]. Another transmitter called "FIT No.3" radiates, at the same time with FIT No.1, a sinusoidal signal with a frequency of 25.00Hz. Signal channels are produced in every 0.05Hz for FIT No.1 signal, i.e., 18.52Hz, 18.52 ± 0.05Hz, 18.52 ± 0.10Hz, $\cdots$, and in 25.00Hz for FIT No.3 signal.

Figure 4.1.2 shows the time series of noise level included in a signal channel of 18.37Hz estimated for each observatory by equation (4.1.14). It can be confirmed that the noise level has a

clear daily variation at each observatory, and the noise level at daytime is several times larger than that at nighttime. As mentioned in Section 2, this noise level estimation is necessary to determine the optimum weight for each segment used in the OWSM.

Figure 4.1.3 shows the signal and noise levels at each signal channel of stacked data at each Hi-net observatory. The stacked data are obtained from the up-down component of the velocity field, and four stacking methods raised in the beginning of this section are applied. The data stacking started at 18h on October 28 (Japan Standard Time), and ended at 18h on November 8, 2002, i.e., the stacking period is 11 days. The length of a time segment is $T = 100$ seconds and the sampling time is $\Delta t = 0.01$ second, i.e., the number of segments is up to 9504. It can be confirmed from Figure 4.1.3 that the noise level obtained by the OWSM is smaller than those obtained by other stacking methods for each signal channel at each observatory. The signal levels at most of signal channels are much larger than the noise levels obtained by the OWSM at the nearest four observatories (i.e., Yaotsu, Kasugai, Hiraya, and Takagi), and the signal levels at some signal channels overcome the noise levels at Fujimi. On the other hand, the signal levels at most of signal channels are below the noise levels obtained by the SSM, NSM, and IWSM at Hiraya, Takagi, and Fujimi.

Figure 4.1.4 shows the growth curve of the SNR at this signal channel obtained by each stacking method. The SNR obtained by the SSM decreases suddenly by stacking a segment of 19h36m40s-19h38m20s on November 3, 2002, when the noise level is extremely large as shown in Figure 4.1.2. An earthquake (*M*3.7, epicenter: 35° 7'N, 137° 47'E, depth: 45km, occurrence time: 19h37m52.5s) is reported to occur, and the decrease of SNR is thought to be an influence of this event. Because the occurrence time of the earthquake corresponds to daytime according to the definition of daytime in this paper, the NSM does not stack this segment and the SNR is not influenced by this event. It is worth noting that the IWSM and OWSM do not decrease the SNRs in spite of the stack of this segment. The SNR obtained by the OWSM is confirmed to be larger than that obtained by the other stacking methods. The SNR at Fujimi obtained by the OWSM exceeds 1 at this signal channel, so that it is possible to conclude that the FM signal at 18.37Hz reaches to Fujimi more than 100km far from the transmitter.

(2) Application to Electromagnetic ACROSS Data

A long-term test of the electromagnetic ACROSS has begun from November 2002 as well as the seismic ACROSS. The electromagnetic source is generated by a current dipole located at Tono Mine with a length of 100m, and the current intensity is 10 amperes at maximum [9]. In this test, sinusoidal signals with frequencies of 125.0, 127.5, 130.0, 132.5, and 135.0Hz are transmitted. This source signal is designed so that the maximum amplitude does not become so large by shifting the initial phase of each signal component [10]. A receiver locates at Shobasama with a distance of 700m from the transmitter, and three components of the magnetic field (northward component B_X, eastward component B_Y, and downward component B_Z) and two components of the electric field

(northward component E_X and eastward component E_Y) are observed. The electromagnetic data used in this paper are obtained from 16h on June 27 to 24h on July 9, 2003, i.e., the stacking period is about 12 days. The length of a time segment is $T = 100$ seconds and the sampling time is $\Delta t = 0.001$ second. The number of segments is up to 8833 after rejecting segments which contain obvious errors. Figure 4.1.5 shows the time series of noise level estimated at a signal channel of 125.0Hz by equation (4.1.14). Contrary to the case of seismic wave data shown in Figure 4.1.2, the noise level in nighttime is several times larger than that in daytime. Because the height of the ionosphere in daytime becomes to be lower than the nighttime, more electromagnetic waves in the atmosphere are considered to be absorbed in the ionosphere in daytime. This may be the reason of the lower noise level in the daytime shown in Figure 4.1.5. Figure 4.1.6 shows the growth curve of SNR at the signal channel of 125.0Hz of stacked data. The SNR obtained by the OWSM is not so different from those obtained by the SSM and IWSM for the magnetic field while the difference is remarkable in the electric field. This is because the difference of the noise level in the magnetic field is not so large between in daytime and nighttime although the difference is remarkable in the electric field. It is confirmed that the SNR obtained by the OWSM is the largest as the case of the seismic ACROSS.

4.1.4 Conclusions

We showed theoretically that the best estimation of the signal level at a signal channel in received ACROSS data is the OWSM, and the optimum weight is inverse proportion to the square of noise level at the signal channel. It is necessary to estimate the noise level in order to determine the optimum weight, and we suggested a new method for this noise level estimation. The noise level is estimated from noise channels produced around the signal channel, and the optimum estimation is shown to be the root-mean-square of the spectrum amplitudes at the noise channels. We applied OWSM to real ACROSS data obtained by a long-term observation test at Tono, Gifu, Japan, and the SNR obtained by the OWSM is confirmed to be larger than those obtained by the other stacking methods used so far. It is concluded that observation of ACROSS in noisy time is as invaluable as in quiet time because the noisy data contribute to increase the SNR of a transfer function by using the OWSM.

4.1.5 Acknowlegement

We are grateful to Junzo Kasahara, Naotaka Shigeta, Kayoko Tsuruga, Yoko Hasada, and Hiroshi Matsumoto for their invaluable comments. We used seismic wave data obtained at Hi-net observatories operated by National Research Institute for Earth Science and Disaster Prevention, Japan.

References

[1] Hasada, Y., H. Kumagai, and M. Kumazawa, Autoregressive modeling of transfer functions in frequency domain to determine complex travel times, *Earth Planets Space*, **53**, 3-11, 2001.

[2] Ikuta, R., K. Yamaoka, K. Miyakawa, T. Kunitomo, and M. Kumazawa, Continuous monitoring of propagation velocity of seismic wave using ACROSS, *Geophys. Res. Lett.*, **29**, doi: 10.1029/2001GL013974, 2002.

[3] Kumazawa, M., Y. Imanishi, Y. Fukao, M. Furumoto, and A. Yamamoto, A theory of spectral analysis based on the characteristic property of a linear dynamic system, *Geophys. J. Int.*, **101**, 613-630, 1990.

[4] Kumazawa, M., A new light and new eye to look into the solid Earth and a potential monitoring methodology of geodynamic states; Introduction to ACROSS, *Abstracts of International Workshop on Frontiers in monitoring science and technology for earthquake environments*, **A1**, 1998.

[5] Kunitomo, T., K. Yamaoka, S. Inoue, N. Ikeda, S. Watanabe, and M. Kumazawa, Micro-hertz control technology of frequency-modulated rotary type transmitter to radiate a set of plural sinusoids with a 20 tonf in amplitude, *Abstracts of International Workshop on Frontiers in monitoring science and technology for earthquake environments*, **AP1-2**, 1998.

[6] Kunitomo, T., M. Kumazawa, and K. Yamaoka, The broadcast station of ACROSS signals on seismic observation networks for monitoring the Earth's crust, the start at Tono mine, *Abstracts of IUGG Meeting 2003, Sapporo*, 2003a.

[7] Kunitomo, T. and M. Kumazawa, Optimum FM signal for monitoring the underground states by means of the seismic ACROSS, *Abstracts of IUGG Meeting 2003*, Sapporo, 2003b.

[8] Nakajima, T., T. Kunitomo, M. Kumazawa, N. Shigeta, and H. Nagao, Observations of the transfer function using an electromagnetic sounding system, EM-ACROSS, *Abstracts of IUGG Meeting 2003, Sapporo*, 2003.

[9] Ogawa, K. and M. Kumazawa, Towards the continuous remote sensing of H_2O, tectonic stress and physical states in the Earth's crust by means of acoustic and electromagnetic ACROSS, *Proceedings of fall meeting of the Seismological Society of Japan*, p45, 1996 (in Japanese).

[10] Yokoyama, Y., M. Kumazawa, T. Kunitomo, and T. Nakajima, Waveform of digital signal for a 3-D electric structure sounding using accrately controlled electromagnetic waves, *Bull. Earthq. Res. Inst. Univ. Tokyo*, **75**, 375-392, 2000 (in Japanese).

[11] Yokoyama, Y., M. Kumazawa, and T. Nakajima, Transfer function measured by electromagnetic sounding with an accurately controlled signal, *Earth Planet Space*, **54**, 459-472, 2002.

Hiromichi NAGAO[1], Takahiro NAKAJIMA[2], Mineo KUMAZAWA[2], and Takahiro KUNITOMO[2]

[1] Japan Agency for Marine-Earth Science and Technology,

[2] Tono Geoscientific Research Unit, JAEA

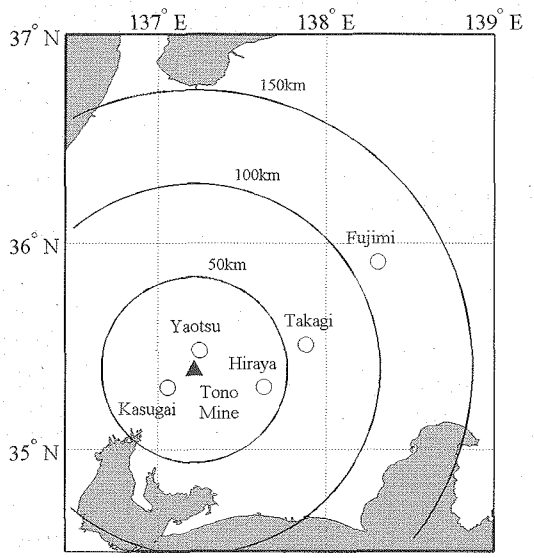

Figure 4.1.1 Location of Tono Mine (solid triangle) and five Hi-net observatories (circle). Both seismic and electromagnetic ACROSS transmitters are located at Tono Mine. The seismic wave data obtained at above Hi-net observatories are used in this paper.

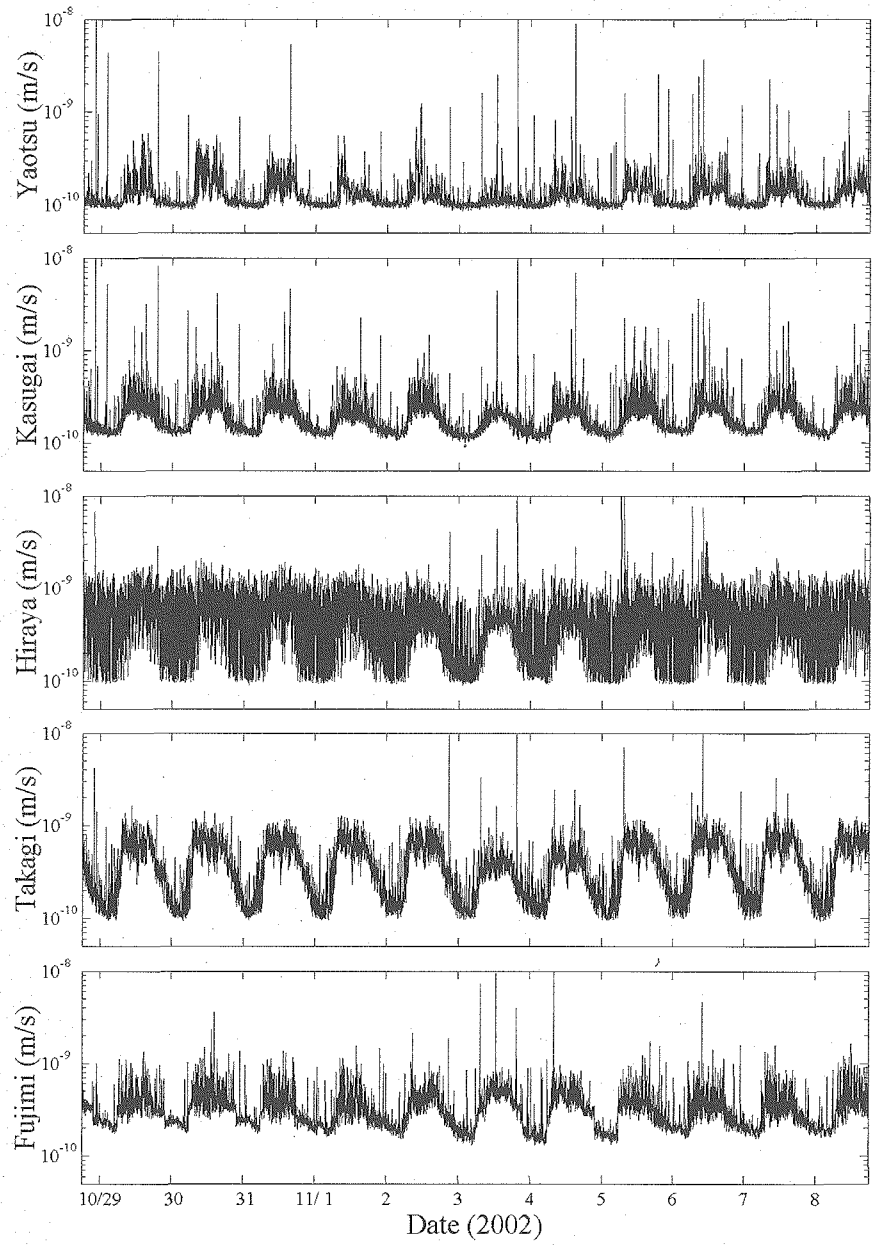

Figure 4.1.2 The time series of noise level included in a signal channel of 18.37Hz at each Hi-net observatory shown in Figure 4.1.1. Each dataset is the up-down component of the velocity field, and the noise level is estimated by equation (14).

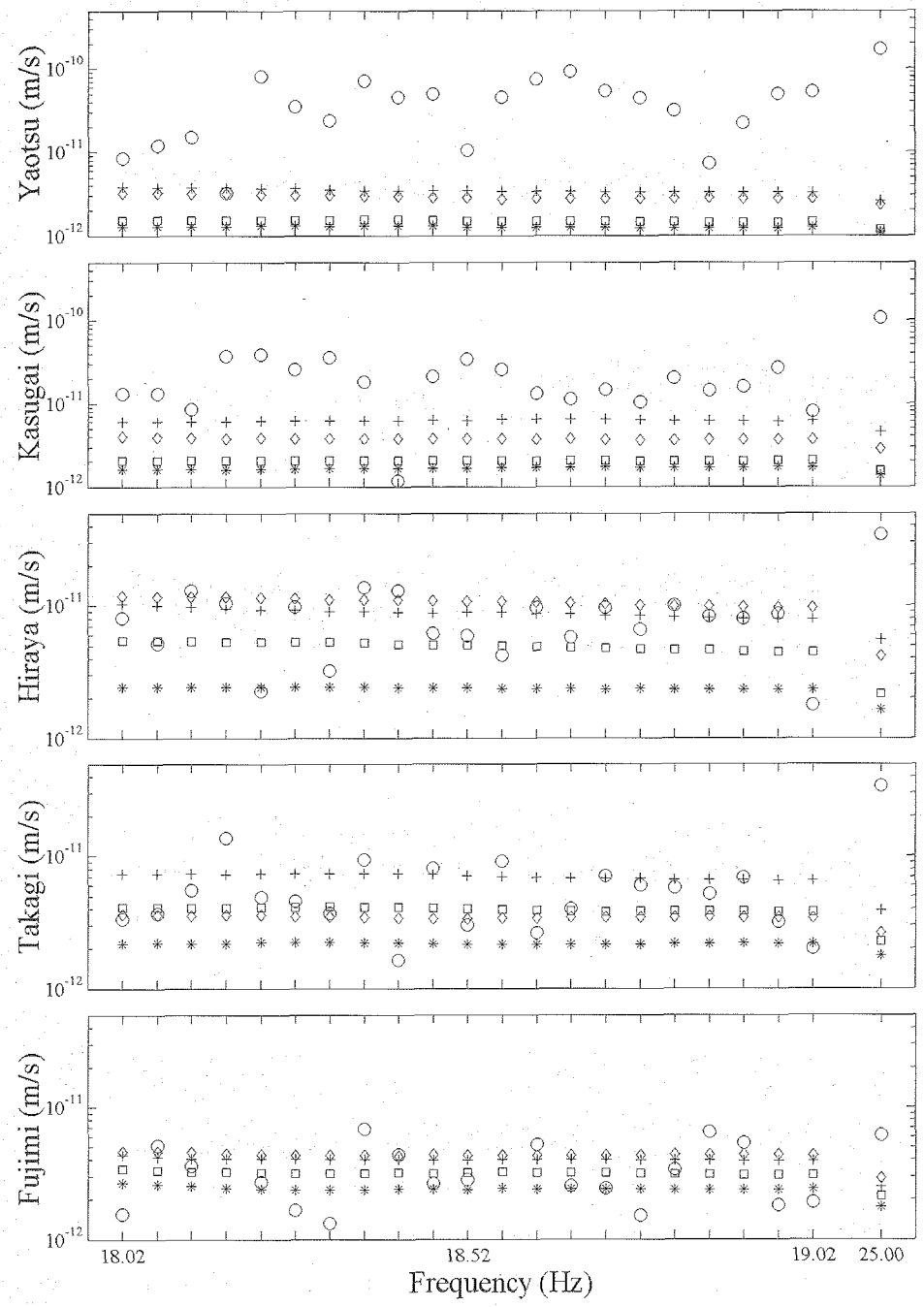

Figure 4.1.3 Signal level (circle), and noise levels obtained by SSM (plus), NSM (diamond), IWSM (square), and OWSM (star) at each signal channel in stacked seismic wave data.

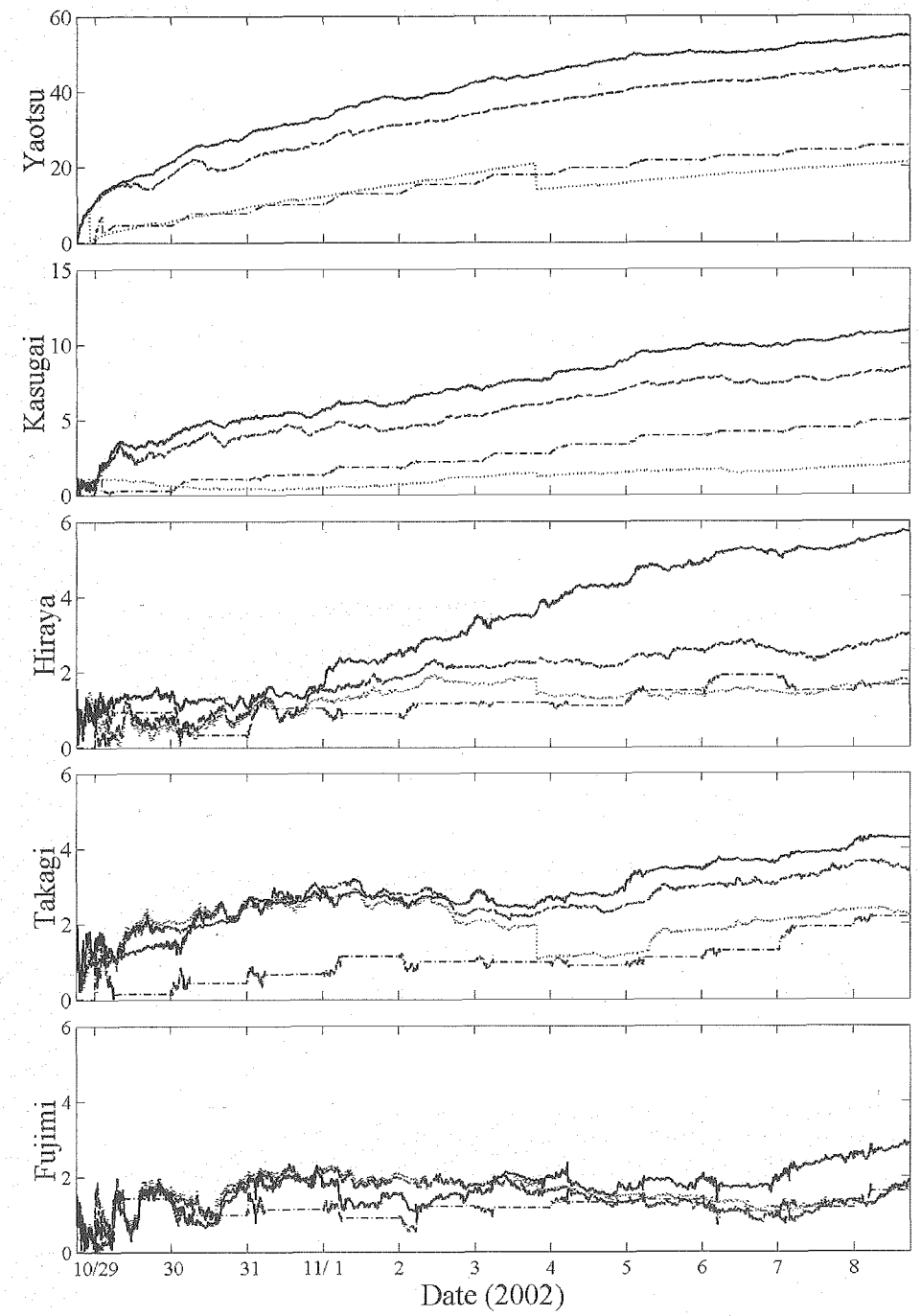

Figure 4.1.4 The growth curve of SNR at a signal channel of 18.37Hz obtained from the up-down component of the velocity field at each Hi-net observatory. The curves obtained by SSM (dotted line), NSM (chain line), IWSM (dashed line), and OWSM (solid line) are shown.

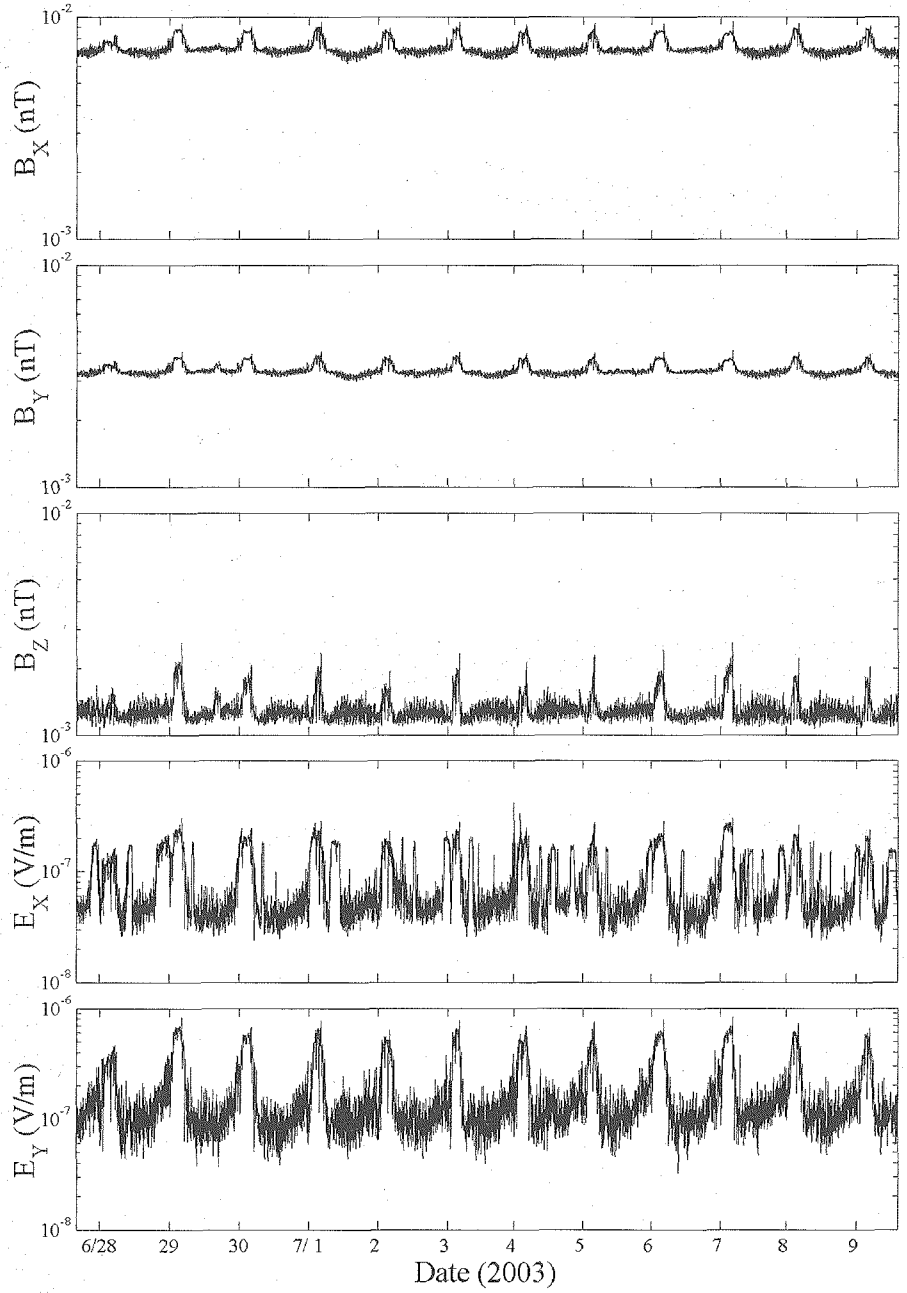

Figure 4.1.5 The time series of noise level included in a signal channel of 125.0Hz in each component of electromagnetic data obtained at Shobasama. The noise level is estimated by (14).

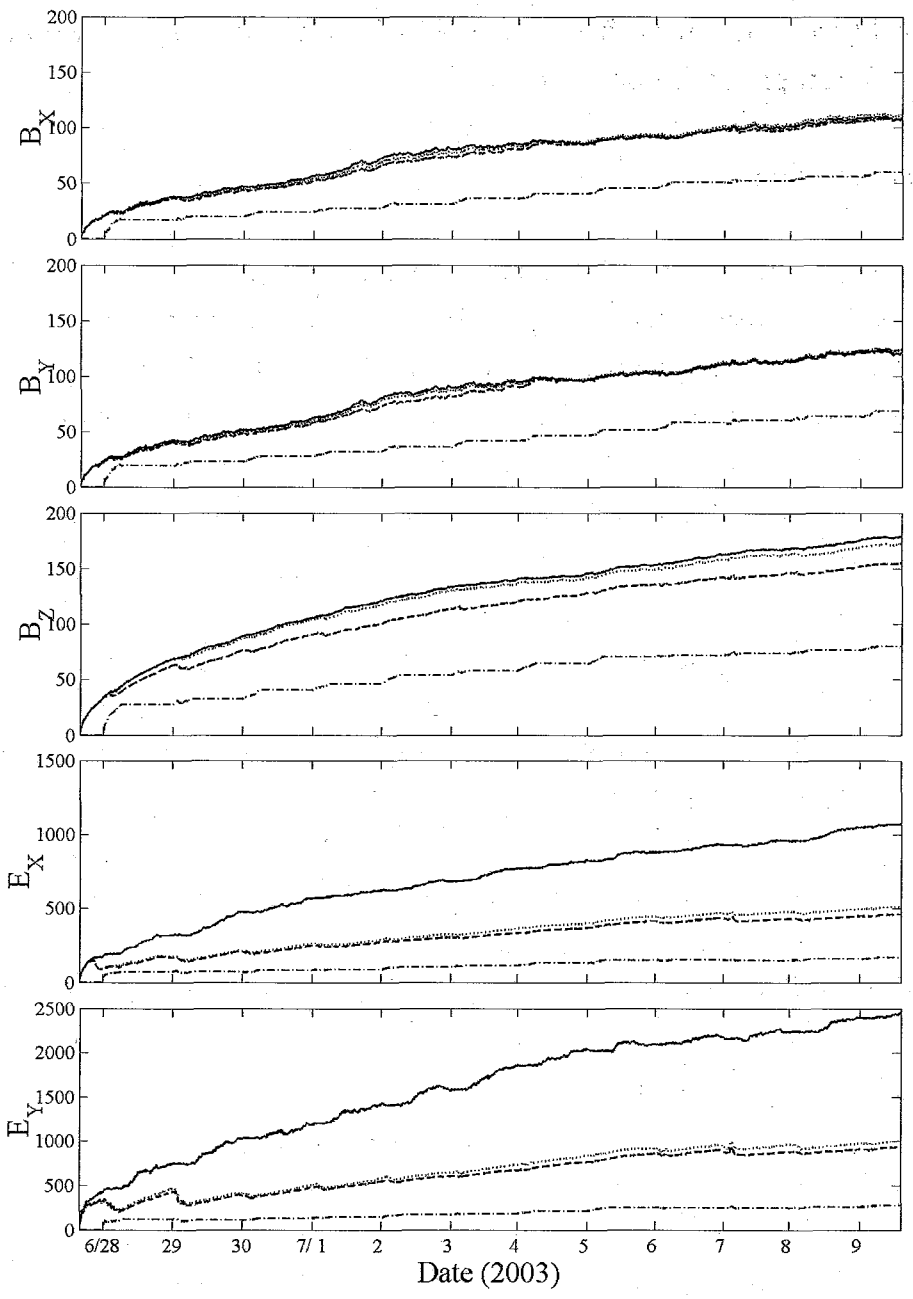

Figure 4.1.6 The growth curves of SNR at a signal channel of 125.0Hz of stacked electromagnetic ACROSS data obtained at Shobasama.

4.2 Travel time estimation from a transfer function in frequency domain: the revised Sompi event analysis

4.2.1 Introduction

ACROSS (Accurately Controlled Routinely Operated Signal System) is a subsurface exploring/monitoring system whose concept of data acquisition is distinctive, and data obtained by the system are complex discrete frequency series within limited band width [1]. To utilize the ACROSS system, it is required to establish a series of analysis method, by which the subsurface structure is estimated from observed frequency-domain data. As the first step, we have developed a method to extract 'events' localized in time domain from frequency-domain data, which is called the Sompi event analysis [2].

In this method we assume that the complex frequency sequence to be analyzed is a transfer function between the source input and the receiver output sampled at discrete frequencies. Through a kind of autoregressive modeling in frequency domain, we obtain a set of 'events' characterized by complex travel time and complex amplitude, where the former expresses travel time and attenuation, and the latter amplitude and phase angle.

Though the validity of the Sompi event analysis is confirmed through various numerical tests especially for analysis of dispersive wave, there are some problems in practical application. Here we introduce a revised procedure by means of weighted least squares fitting, which is based on maximum likelihood estimation.

4.2.2 Modeling transfer functions

(1) Model of pulse sequence

In observation by ACROSS, we measure the transfer function at a set of plural frequencies in limited band. A transfer function, which indicates how much sinusoidal wave is amplified and delayed in phase during transmission through some linear system as a function of frequency, is obtained by dividing output signal of the system by its input signal. An impulse response function is Fourier transform of the transfer function.

Supposing a certain medium with neither dispersion nor attenuation, we consider that the waveform $f(t)$ observed at a certain distance from a source is represented as superposition of delayed pulses which are similar to the source time function $f_0(t)$,

$$f(t)=\sum_{m=1}^{M} A_m f_0(t-\tau_m), \tag{4.2.1}$$

where A_m and τ_m are the amplification factor and the delay time of M-th wave arrival, respectively. In frequency domain, the Fourier transform of $f(t)$ is described using the source spectrum $F_0(\omega)$ as

$$F(\omega) = \sum_{m=1}^{M} A_m e^{-i\omega\tau_m} F_0(\omega) . \tag{4.2.2}$$

The transfer function between the source spectrum and the observation spectrum is obtained as

$$H(\omega) = \frac{F(\omega)}{F_0(\omega)} = \sum_{m=1}^{M} A_m e^{-i\omega\tau_m} , \tag{4.2.3}$$

which is corresponding to the impulse response function

$$h(t) = \sum_{m=1}^{M} A_m \delta(t - \tau_m) . \tag{4.2.4}$$

The transfer function in eq. (4.2.3) contains exponential of imaginary numbers, whose real and imaginary parts are cosine and sine functions. Figures 4.2.1a and 4.2.1b shows impulse response functions composed of one impulse and the corresponding transfer functions. The oscillation 'frequency' in the complex transfer function is equal to the delay time in the impulse response function.

In order to consider attenuation and phase shift, it is useful to introduce complex values for both of amplification factor and delay time. We define the complex amplitude

$$\alpha_m = A_m e^{i\phi_m} \tag{4.2.5}$$

and the complex travel time

$$q_m = \tau_m + i\upsilon_m . \tag{4.2.6}$$

Then we have a model for transfer functions as

$$H(\omega) = \sum_{m=1}^{M} \alpha_m e^{-i\omega q_m} , \tag{4.2.7}$$

with corresponding impulse response function being

$$h(t)=\frac{1}{\pi}\sum_{m=1}^{M}\Re\left[\frac{i\alpha_m}{t-q_m}\right], \tag{4.2.8}$$

where $\Re$ indicates to take the real part. Figures 4.2.1c and 4.2.2d shows examples for eqs. (4.2.7) and (4.2.8).

The transfer function defined by eq. (4.2.7) is superposition of decaying or growing sinusoids. The growth rate is given by υ_m, which is required to be negative for the energy not to diverge to infinity. The constraint for real $h(t)$ is $H(\omega)=H^*(-\omega)$ for negative ω, where * denotes the complex conjugate.

Each pulse in eq. (4.2.8) has the form of a linear combination of Lorentz function and its Hilbert transform, and then we refer to the content of the square bracket as 'complex Lorentzian'. When $\phi_m=0$, the pulse becomes a Lorentz function whose half-value width is $-2\upsilon_m$. This function has long tails on both side of the peak, which seems to violate causality. An attenuating medium necessarily involves dispersion to satisfy causality (see e.g. [3]).

(2) Modeling dispersive wave

Here we consider a homogeneous dispersive media for convenience. A transfer function is written using frequency dependent wave number $k(\omega)$ and propagating distance x,

$$H(\omega)=\alpha e^{-ik(\omega)x}. \tag{4.2.9}$$

Expanding $k(\omega)$ into Taylor series around ω_0 up to the first order as

$$k(\omega)=k(\omega_0)+\left.\frac{\partial k}{\partial\omega}\right|_{\omega=\omega_0}(\omega-\omega_0)=\frac{\omega_0}{c(\omega_0)}+\frac{\omega-\omega_0}{u(\omega_0)}, \tag{4.2.10}$$

we obtain the transfer function

$$H(\omega)=\alpha e^{-i\omega_0\frac{x}{c(\omega_0)}}e^{-i(\omega-\omega_0)\frac{x}{u(\omega_0)}}=\tilde{\alpha}e^{-i(\omega-\omega_0)\tilde{q}}, \tag{4.2.11}$$

where $c(\omega_0)$ and $u(\omega_0)$ denotes phase velocity and group velocity at the frequency ω_0, respectively. Eq. (4.2.11) is similar to eq. (4.2.7) with the complex amplitude and the complex travel time defined as

$$\tilde{\alpha}=\alpha e^{-i\omega_0\frac{x}{c(\omega_0)}}, \qquad \tilde{q}=\frac{x}{u(\omega_0)}. \tag{4.2.12}$$

This indicates that the complex travel time obtained by our method is not related to the phase velocity but to the group velocity.

Thus our model defined by eq. (4.2.7) is approximately adaptable for a dispersive wave if the frequency range of the data to be analyzed is narrow enough. It is effective to divide the data into some segments with band width suitable to the frequency dependency inherent in the data when we are to analyze highly dispersive waves.

4.2.3 Basic algorithm

(1) Modeling observed data

We assume that the observed transfer function X_j consists of the signal sequence H_j and the noise sequence E_j.

$$X_j = H_j + E_j \qquad (j = 1, \ldots, N), \tag{4.2.13}$$

where the real and the imaginary parts of E_j are independently obey the same normal distribution $N(0,\sigma_j^2)$, whose variance depends on the frequency. In case of ACROSS observation, errors of measured transfer function can be evaluated by taking root mean squares of data at the vicinal frequencies of the transmitted signals. The estimated error of the transfer function ε_j is assumed to be proportional to the noise standard deviation σ_j.

The signal sequence H_j is superposition of decaying sinusoids as stated above,

$$H_j = \sum_{m=1}^{M} \alpha_m e^{-2\pi i(j-1)\Delta f q_m} . \tag{4.2.14}$$

The parameters to be determined are the complex travel times q_m, the complex amplitudes α_m. Because the order of model M is also unknown, we change M in arbitrary range and attempt to find the optimum model.

(2) Determine initial parameters with the Sompi method

Hasada et al. [2] proposed a procedure to determine complex travel times and complex amplitudes from observed transfer function by means of the Sompi method, which is based on autoregressive modeling. As autoregressive approach has difficulty in dealing with variable noise distribution, first we obtain initial values of q_m on the assumption of constant noise distribution.

The signal sequence composed of decaying sinusoids should satisfy the following homogeneous autoregressive (AR) equation of order M.

$$\sum_{l=0}^{M} a_l H_{j-l} = 0 , \tag{4.2.15}$$

where $\boldsymbol{a} = \{a_0, \ldots , a_M\}$ is a complex AR coefficient vector. We determine $\boldsymbol{a}$ by minimizing the fitting error

$$\frac{1}{N-M} \sum_{j=M+1}^{N} \left| \sum_{l=0}^{M} a_l X_{j-l} \right|^2 \rightarrow \min , \tag{4.2.16}$$

under a constraint to obtain non-zero $\boldsymbol{a}$,

$$\boldsymbol{a} \cdot \boldsymbol{a}^* = 1 . \tag{4.2.17}$$

Minimization of eq. (4.2.16) with the condition eq. (4.2.17) using Lagrangian undetermined multiplier λ leads to an eigenvalue problem,

$$\mathbf{P}\boldsymbol{a} = \lambda \boldsymbol{a} . \tag{4.2.18}$$

Here **P** is non-Toeplitz Hermitian autocovariance matrix

$$P_{ml} = \frac{1}{N-M} \sum_{j=M+1}^{N} X_{j-l} X_{j-m}^* = P_{lm}^* \qquad (l, m = 0, \ldots , M). \tag{4.2.19}$$

Solving eq. (4.2.18), M eigenvectors are obtained. We adopt the eigenvector $\boldsymbol{a}$ corresponding to the minimum eigenvalue since λ means the noise power.

In order to the convert AR coefficient vector $\boldsymbol{a}$ to a set of the complex travel times, we should solve the characteristic equation,

$$\sum_{l=0}^{M} a_l z^{-l} = 0 , \tag{4.2.20}$$

where z is the unit time shift operator ($zH_j = H_{j+1}$). M characteristic solutions $z_1, \ldots , z_M$ of eq. (4.2.20) is related to complex travel times by

$$z_m = e^{-2\pi i \Delta f q_m} , \tag{4.2.21}$$

and then we have M initial values of complex travel time,

$$q_m^0 = \frac{i \ln z_m}{2\pi\Delta f} . \tag{4.2.22}$$

The initial values of complex amplitude α^0_m are determined by least squares fitting. If we have estimated error of X_j, weighted least squares fitting provides more accurate estimation.

$$\sum_{j=1}^{N} w_j \left| X_j - \sum_{m=1}^{M} \alpha_m^0 e^{-2\pi i(j-1)\Delta f q_{0m}} \right|^2 \to \min \tag{4.2.23}$$

The weight w_j is defined in terms of maximum likelihood procedure as follows,

$$w_j = \frac{1}{\varepsilon_j^2} \Big/ \sum_{k=1}^{N} \frac{1}{\varepsilon_k^2} . \tag{4.2.24}$$

(3) Improve parameters by weighted least squares fitting

Next, we attempt to improve parameters by weighted least squares fitting, through linearization of model about small variation of parameters δq^0_m and $\delta\alpha^0_m$.

$$\sum_{j=1}^{N} w_j \left| \delta X_j - \sum_{m=1}^{M} \left(\delta\alpha_m - 2\pi i \alpha_m^0 \delta q_m \right) e^{-2\pi i(j-1)\Delta f q_m^0} \right|^2 \to \min , \tag{4.2.25}$$

where

$$\delta X_j = X_j - \sum_{m=1}^{M} \alpha_m^0 e^{-2\pi i(j-1)\Delta f q_m^0} . \tag{4.2.26}$$

Therefore we have final model parameters $q_m = q^0_m + \delta q_m$ and $\alpha_m = \alpha^0_m + \delta\alpha_m$.

The uncertainty of parameters is estimated by error propagation.

(4) Determine the number of wave elements

The model order or the number of wave elements is determined by means of two-parameter AIC (Akaike's Information Criterion) proposed by Matsuura *et al.* [4].

For an AR order M, we determine q_m and α_m and sort wave elements in descending order of the mean power densities (MPD) defined as

$$MPD_m = \frac{1}{N}\sum_{j=1}^{N}\left|\alpha_m e^{-2\pi i(j-1)\Delta f q_m}\right|^2 . \tag{4.2.27}$$

Then, the complex amplitudes for the first M_0 wave elements are recalculated by least squares fitting. We denote this revised model as MODEL(M, M_0).

The definition of AIC is

$$AIC = -2l(\hat{\theta}) + 2k , \tag{4.2.28}$$

where $l(\hat{\theta})$ is the maximum logarithmic likelihood and k is the number of free parameters. The two-parameter AIC of MODEL(M, M_0) is given by

$$AIC(M, M_0) = 2N\ln 2\pi\hat{\sigma}_0^2 - \sum_{j=1}^{N}\ln w_j + 2N + 8M_0 \tag{4.2.29}$$

where $\hat{\sigma}_0^2$ is the maximum likelihood estimate of noise variance per unit weight calculated by

$$\hat{\sigma}_0^2 = \frac{1}{2N}\sum_{j=1}^{N} w_j\left|X_j - \sum_{m=1}^{M_0}\alpha_m e^{-2\pi i(j-1)\Delta f q_m}\right|^2 . \tag{4.2.30}$$

We can determine the optimum MODEL(M, M_0) by searching the minimum AIC for a certain range of both M and M_0.

4.2.4 Numerical test

To test the effect of revised procedure, we analyze a synthetic transfer function by both of the previous Sompi event analysis [2] and the present method. We synthesized the transfer function by three decaying sinusoids and a frequency-dependent random noise sequence. The sampled frequency range is 15~19.95Hz with the interval of 0.05Hz. Figure 4.2.3 shows the synthetic data composed of three wave elements at 0.1s, 1.0s, and 4.0s. The frequency dependency of the noise sequence is shown in Figure 4.2.4.

We have scanned the AR order from 1 to 7, and found optimum models MODEL (7, 4) for the previous procedure and MODEL (7, 3) for the revised one, respectively. AIC of all models are shown in Figure 4.2.5. The final model obtained by the revised method has substantially smaller AIC, indicating the validity of parameter improvement by weighted least squares fitting, where as some models obtained by the revised method have quite large values of AIC, which suggest the instability of calculation.

In Figure 4.2.6 we plot the largest three wave element obtained by both methods. As AIC indicates, it is clarified that the revised procedure using weighted least squares fitting gives better estimation.

4.2.5 Discussion and conclusion

We propose the revised Sompi event analysis for estimation of travel time from a transfer function in frequency domain. In the Sompi event analysis the observed transfer function is modeled as an autoregressive process, and decomposed into wave elements. As an autoregressive model is based on a solution of wave equation, the physical significance of the model is clear. However, extended modeling is necessary in cases of existence of multiple reflections or resonance.

By repeating weighted least squares, several advantages are generated; (1) Maximum likelihood estimation of complex travel times is realized, (2) Identification of wave elements among the different data sets is possible, (3) The errors of the results are easily evaluated by error propagation. On the other hand, there is serious instability in the calculation of least squares. To overcome this problem, some procedure of non-linear optimization may be available.

References

[1] M. Kumazawa, T. Kunitomo, Y. Yokoyama, T. Nakajima and K. Tsuruga, ACROSS: Theoretical and technical developments and prospect to future applications, *Technical report, Japan Nuclear Cycle Development Institute,* **9**, pp. 115-129, 2000 (in Japanese).

[2] Y. Hasada, H. Kumagai and M. Kumazawa, Autoregressive modeling of transfer functions in frequency domain to determine complex travel times, *Earth Planets Space*, **53**, pp. 3-11, 2001.

[3] K. Aki and P. G. Richards, *Quantitative seismology: Theory and methods*, Freeman and Co., 932 pp., 1980.

[4] T. Matsuura, Y. Imanishi, M. Imanari and M. Kumazawa, Application of a new method of high-resolution spectral analysis, "Sompi," for free induction decay of nuclear magnetic resonance, *Appl. Spectrosc.*, **44**, pp. 618-626, 1990.

[5] Y. Hasada, M. Kumazawa, K. Tsuruga and T. Kunitomo, Traveltime estimation from the data acquired in frequency domain by ACROSS: Sompi Event Analysis, *Chikyu Monthly, Special issue "Active Monitoring"*, 2004 (in press) (in Japanese).

Yoko HASADA[1], Mineo KUMAZAWA[2], Kayoko TSURUGA[3] and Takahiro KUNITOMO[2]

[1] Nagoya University,

[2] Tono Geoscientific Research Unit, JAEA

[3] Ocean Research Institute, the University of Tokyo

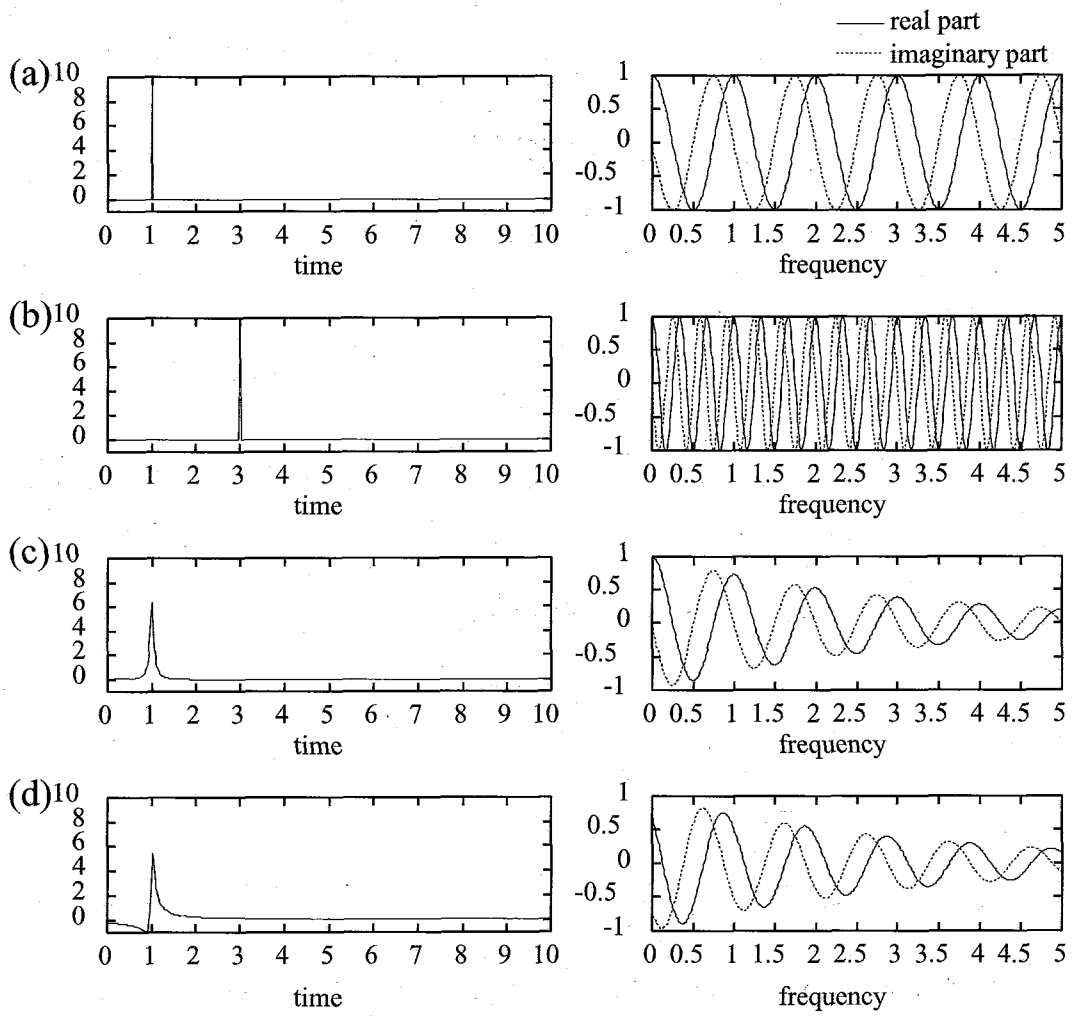

Figure 4.2.1 The impulse response functions (left) and the corresponding transfer functions in frequency domain (right) for a non-dispersive medium without attenuation (a and b) and with attenuation (c and d).

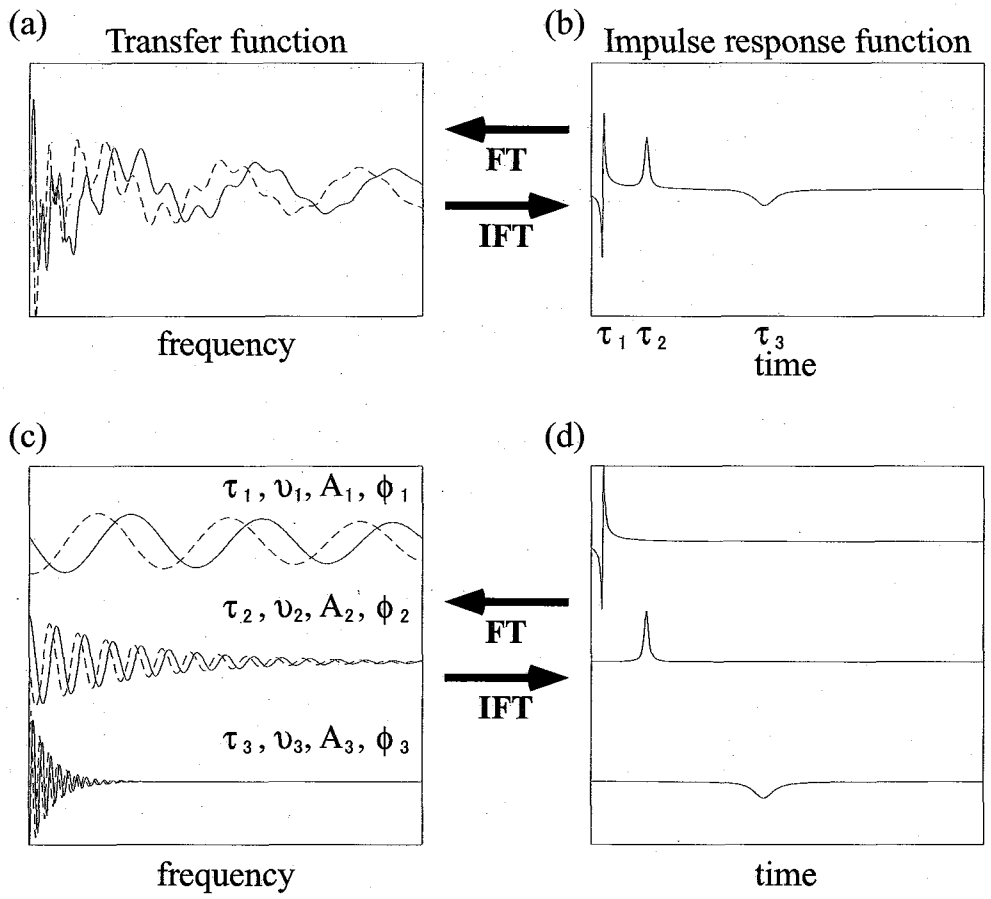

Figure 4.4.2 Schematic image of a model in the Sompi Event Analysis. (a) is an example transfer function composed of three decaying sinusoids shown in (c). (b) is the corresponding impulse response function. The three waves in (c) are corresponding to three pulses in (d). The impulse response functions in (b) and (d) are calculated by complex Lorentzian model and are not Fourier transform of (a) and (c).

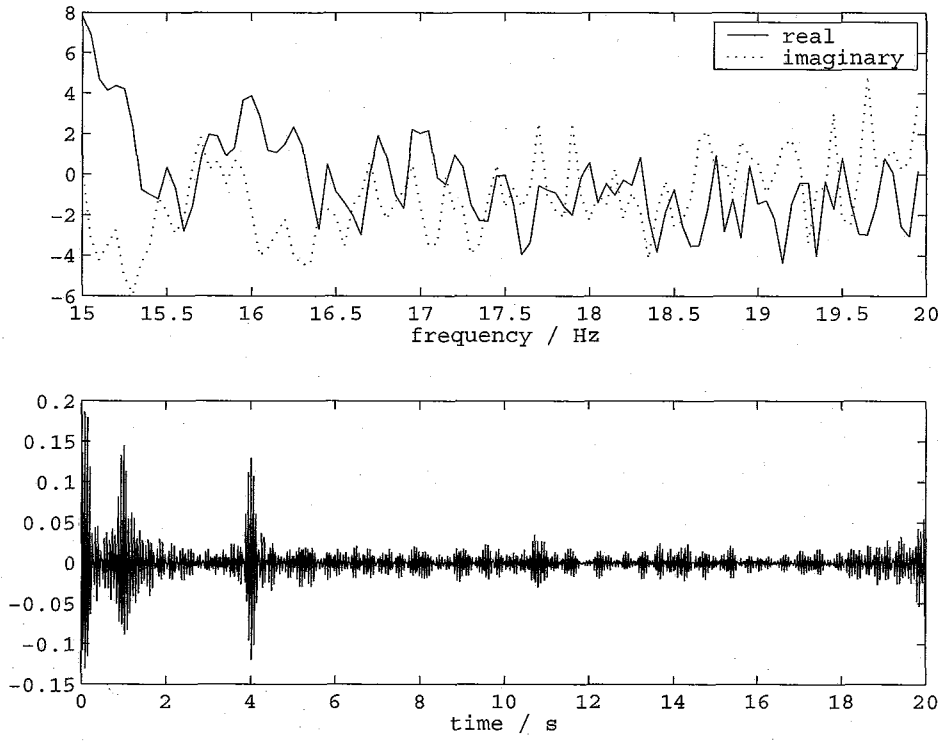

Figure 4.2.3 The synthetic transfer function (top) and the time-domain waveform (bottom) obtained by Fourier transformation.

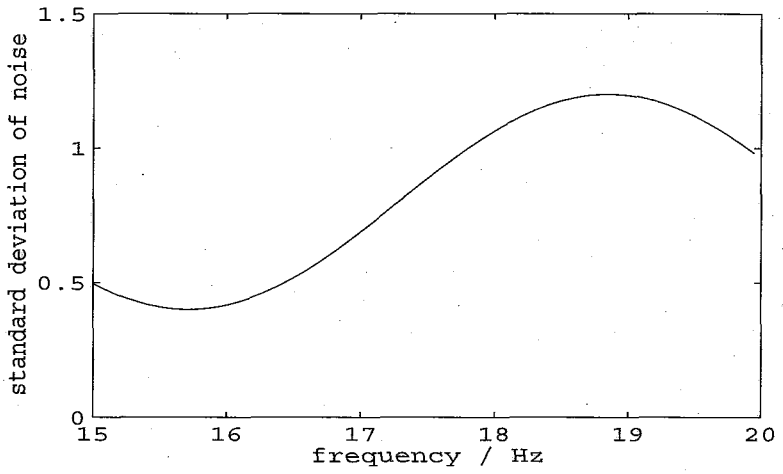

Figure 4.2.4 The frequency dependency of noise amplitude.

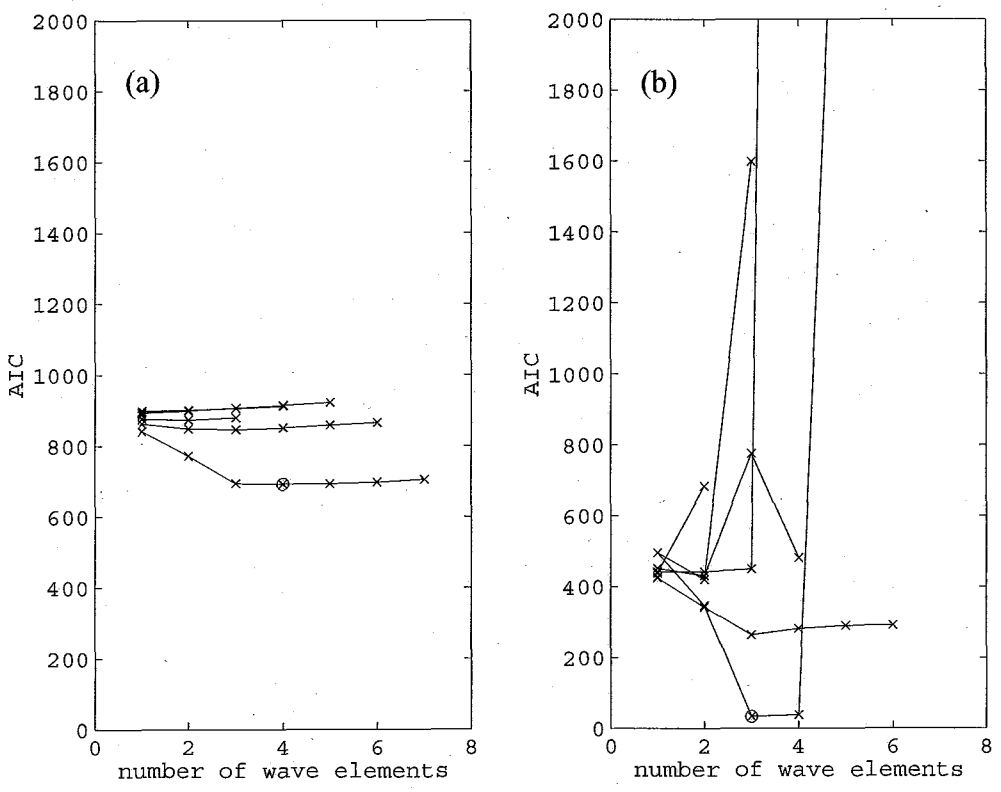

Figure 4.2.5 Two-parameter AIC of all models for the previous method (a) and revised method (b). The markers '×' indicate how AIC changes with number of adopted wave elements while AR order is changed from 1 to 7. The optimum models '○', are (7, 4) for (a) and (7, 3) for (b).

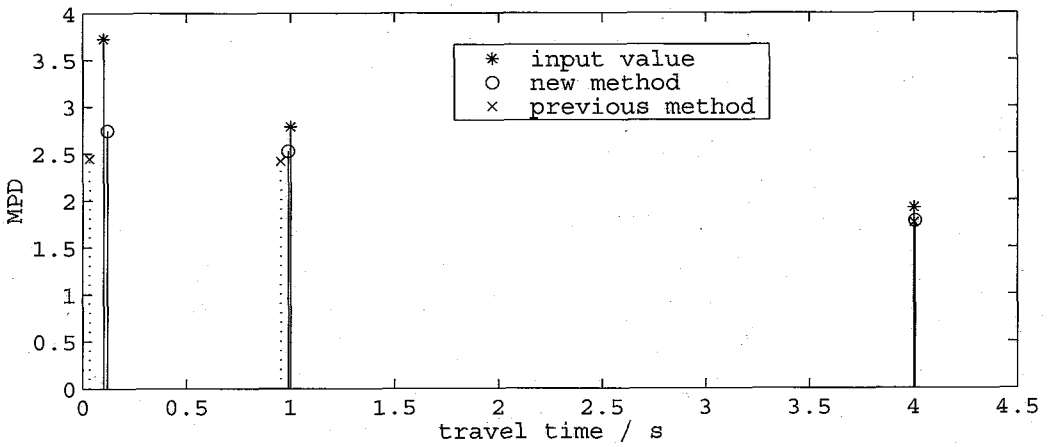

Figure 4.2.6 The results of travel-time estimation by the previous method (×) and the revised method (○) plotted with input values (*).

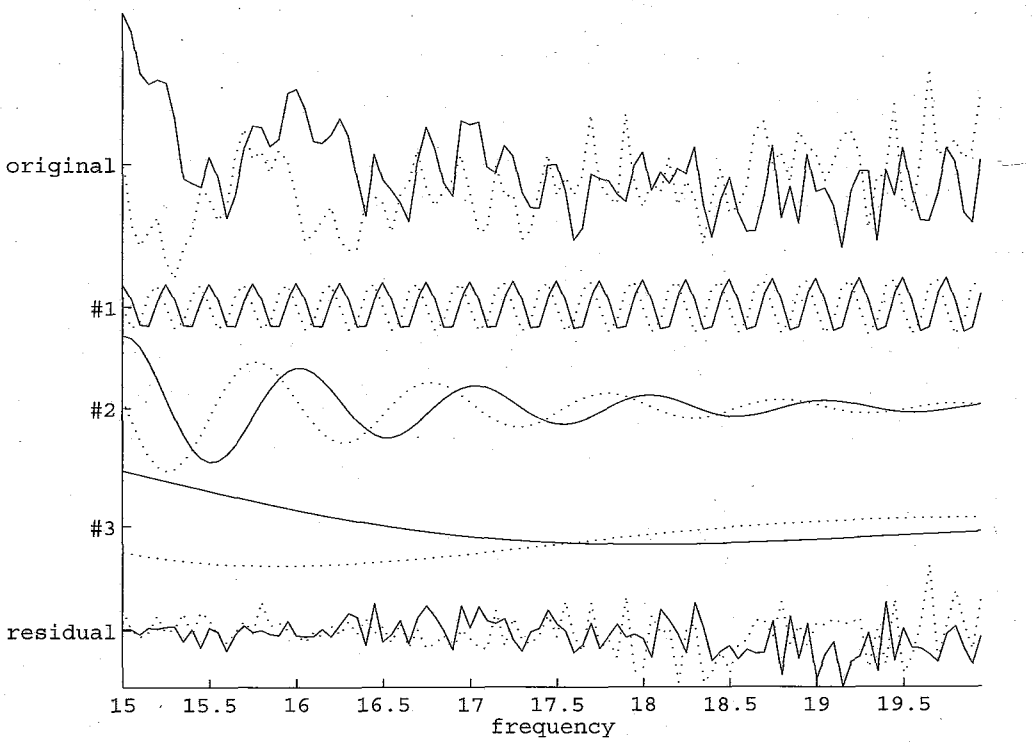

Figure 4.2.7 The decomposed wave elements and the residual which are calculated with the parameters by the revised method. The residual has similar frequency dependency to input noise amplitude.

4.3 Numerical computation of wave fields and frequency wavenumber response characteristics of an isolated linear dynamic system

4.3.1 Intoroduction

The new method we have examined in this paper has been proposed in order to provide a theoretical support for sinusoidal approach in geophysical exploration and also a potential method of analyzing the very accurate data acquired by ACROSS. Whereas there are a number of computation codes to enable us to compute the wave fields under various conditions, there are not ones satisfactory for computing the general wave field within a limited part of a large body with the most general structures in frequency domain[1]. Keeping the possible extension to general cases in mind, we examined the basic nature of this theory in the simplest case: a finite one-dimensional elastic body. Spatial variation of material parameters in the wave equation is converted to a set of several quantities representing separately the continuity and the discontinuity of different orders as a function of space by means of hyperfunctions. With a set of the converted parameters, wave equation described by differential equation is rewritten to a linear system model expressing the external excitation as output and the wave field as an input. This linear equation is converted to an inverse system model expressing the external excitation as input and the wave field as an output in frequency and wavenumber domain. This inverse system model is described by FWR, the frequency and wavenumber response characteristics. Multiplying the excitation in frequency and wavenumber domain to FWR, we obtain the wave field as a dispersion relation. Consequently, any computational procedure is not demanded in treating the boundary conditions at discontinuities in the medium and it is free from grid dispersion.

In the present paper, the computed wave field in frequency domain is converted to that excited by an impulse to demonstrate the validity of the present theory. We also discuss the utility of this theory for practical application in geophysical exploration within the limited frequency range.

4.3.2 Governing wave equation

We start with a wave equation of a one-component one-dimensional elastic body:

$$D_u(t,x)\,u(t,x) = e(t,x) \tag{4.3.1}$$

$$D_u(t,x) = \rho(x)\frac{\partial^2}{\partial t^2} - \frac{\partial}{\partial x}\left\{c(x)\frac{\partial}{\partial x}\right\} \tag{4.3.2}$$

where $u(t,x)$ denotes displacement, $e(t,x)$ external force, $\rho(x)$ density and $c(x)$ elastic constant, respectively. It is assumed that there exist isolated discontinuities in the material properties $\rho(x)$ and

$c(x)$ to describe the heterogeneity of the system. In the new theory, spatial material parameters in the wave equation are converted to a set of coefficients in polynomial expansions which separately represent the continuity and the discontinuity of different orders as a function of space by means of a theory of hyperfunction[2]. With the material parameters converted, Equation (4.3.1) is written to a linear dynamic system model as follows: By representing $u(t,x)$ by Fourier integral,

$$u(t,x) = \int_{-\infty}^{\infty}\int_{-\infty}^{\infty} u(\omega,\kappa)\exp(i\omega t - i\kappa x)d\omega d\kappa$$

We obtain

$$\int_{-\infty}^{\infty} P_L(\omega,\kappa,x)\,u(\omega,\kappa)d\kappa = \int_{-\infty}^{\infty}\delta(x-x')e(\omega,x')dx' \tag{4.3.3}$$

where P_L consists of three terms,

$$P_L(\omega,\kappa,x) = p(\omega,\kappa,x) + \sum_d q_d(\omega,\kappa)H(x-x_d) + \sum_d r_d(\omega,\kappa)\delta(x-x_d) \tag{4.3.4}$$

with

$$p(\omega,\kappa,x) = [\kappa^2 c^{(0)}(x) + i\kappa c^{(1)}(x) - \omega^2\rho^{(0)}(x)] - \sum_d q_d(\omega,\kappa)H(x-x_d)$$
$$q_d(\omega,\kappa) = \kappa^2\Delta c^{(0)}(x_d) + i\kappa\Delta c^{(1)}(x_d) - \omega^2\Delta\rho^{(0)}(x_d)$$
$$r_d(\omega,\kappa) = i\kappa\Delta c^{(0)}(x_d)$$

where ω represents angular frequency, κ wavenumber, $c^{(n)}(x)$ average elastic constant of n-th order derivative, $\Delta c^{(n)}(x)$ jump of elastic constant discontinuity of n-th order derivative, $\rho^{(n)}(x)$ average density of n-th order derivative, $\Delta\rho^{(n)}(x)$ jump of density discontinuity of n-th order derivative and x_d location of the d-th discontinuity. Note that there are the relations $s(x)^2=\rho(x)/c(x)$ and $Z(x)^2=\rho(x)c(x)$ where $s(x)$ and $Z(x)$ represent slowness and impedance, respectively. The first term in (4.3.4) is a continuous function of x as given by the subtraction of the first order discontinuity of material property evaluated to be q_d at $x = x_d$. The second term dependent on q_d is a sequence of step functions, and the third term contains delta function originated from the spatial derivative of the step discontinuity of the material property.

Representing the wave field by particle velocity $v(t,x)$ which is equal to $i\omega u(t,x)$ and expressing $P_L/i\omega$ as P, we have a convenient form to solve the equation as:

$$\int_{-\infty}^{\infty} P(\omega,\kappa,x)\,v(\omega,\kappa)d\kappa = \int_{-\infty}^{\infty}\delta(x-x')e(\omega,x')dx' \tag{4.3.5}$$

4.3.3 Discretizing and solving the equation

To solve the wave equation, ω, κ and x in Equation (4.3.5) are discretized as follows:

$$\omega = m\Delta\omega \quad (-\omega_N \le m\Delta\omega < \omega_N;\ m, \Delta\omega = arbitrary)$$
$$\kappa = k\Delta\kappa \quad (-\kappa_N \le k\Delta\kappa < \kappa_N;\ -N/2 \le k \le N/2-1)$$
$$x = j\Delta x \quad (0 \le j\Delta x < L;\ j = 0,\ \ldots\ ,N-1)$$

where ω_N and κ_N are the Nyquist angular frequency and the Nyquist wavenumber, respectively. Then equation (4.3.5) is rewritten by a set of associated equations of $v(k)$ for each of m as:

$$\sum_k P(m,j,k)v(m,k) = \sum_{j'} \delta(j,j')e(m,j') \qquad (4.3.6\ (a))$$

where $\delta(j,j')$ is Kronecker's delta. This is simply represented by a matrix form:

$$P_m(j,k)v_m(k) = \Delta(j,j')e_m(j') \qquad (4.3.6\ (b))$$

where $\Delta(j,j')$ is an $N\times N$ matrix with $\delta(j,j')$ as each element. Equation (4.3.6) is nothing but a wave equation in discrete form. The wave field $v(k)$ is then solved as follows:

$$v_m(k) = R_m(k,j')e_m(j') \qquad (4.3.7\ (a))$$

where R_m is the frequency wavenumber response characteristics and given by an inverse matrix of P_m:

$$R_m(k,j) = P_m(j,k)^{-1} \qquad (4.3.8\ (a))$$

In order to derive the formula with FWR, we first prepare Fourier transform operators in an $N\times N$ matrix from of $F(k,j)$ with $\exp(-2\pi ijk/N)$ as a (j,k) element and of $I(j,k)$ with $1/N\times\exp(2\pi ijk/N)$ as a (k,j) element, respectively, and then insert $I(j',k')F(k',j')$ between $R_m(k,j')$ and $e_m(j')$ in (4.3.7 (a)) as follows:

$$v_m(k) = R_m(k,k')e_m(k') \qquad (4.3.7\ (b))$$

where $R_m(k,k')$, the FWR is given by multiplying the invrse Fourier transform matrix to (4.3.8 (a)) as follows:

$$R_m(k,k') = R_m(k,j')I(j',k') \qquad (4.3.8\ (b))$$

Once we compute R_m in the sufficiently wide range of m, all necessary computations are finished and we can synthesize any type of representation of wave field only by Fourier transform;. $v(\omega,\kappa)$, $v(\omega,x)$, $v(t,\kappa)$ and $v(t,x)$.

One may raise a question if the inverse matrix with elements containing hyperfunction such as delta function can be calculated. Mathematical proof will be reported somewhere. Anyway, we can do that as shown by the computed result in the next.

4.3.4 Results

In the present computations, we do not devise any absorbing boundary conditions, so the periodic condition with a length of the system is automatically set for the wave field.

(1) Uniform medium

It is easy to depict the FWR for a uniform medium since non-zero values exist only on the two diagonals in the rectangular parallelepiped spanned by ω-, κ- and κ'-axes, as shown in Figure 4.3.1. Multiplying the FWR by an impulsive excitation located at $t=t_0$ and $x=L/8$, a dispersion relation of particle velocity is computed (Figure 4.3.2 (a)). The upper and lower figures in Figure 4.3.2 (a) show the real and imaginary parts of $v(\omega,\kappa)$, respectively. Note that grid dispersion is not existent at all up to the Nyquist wavenumber in the figures as theoretically expected. It is also noted that the first quadrant, $v(\omega,\kappa)$, and the third quadrant, $v(-\omega,-\kappa)$, in Figure 4.3.2 (a) are conjugate and their combination represents the waves propagating leftward. The remaining two quadrants show the waves propagating rightward. The dispersion relation in Figure 4.3.2 (a) is inversely transformed to constitute the wave field in time and space, i.e., a travel time curve as shown in Figure 4.3.2 (b). The length of the medium is L. Since periodic boundary conditions are assumed, the wave propagating leftward, for example, disappears at $x=0$ and appears again from the right side at the next time step. Figure 4.3.2 (c) shows frequency dependence of particle velocity in frequency domain (real part alone is shown) as a function of space. This is the observable of ACROSS. Such a representation of wave field is not popular and appears somewhat unique but it is the essential representation of the ACROSS data

(2) Discontinuities included

Let us consider a simple elastic body with a length of L consisting of the two different segments which are in contact with discontinuities at $x=L/4$ and $3L/4$. The material parameters, $s(x)$ and $Z(x)$ are set as follows:

$$s(x)=\begin{cases} s_1 & (0 \le x \le L/4) \\ s_2 & (L/4 \le x \le 3L/4) \\ s_1 & (3L/4 \le x \le L) \end{cases} \tag{4.3.9}$$

$$Z(x)=\begin{cases} Z_1 & (0 \le x \le L/4) \\ Z_2 & (L/4 \le x \le 3L/4) \\ Z_1 & (3L/4 \le x \le L) \end{cases} \tag{4.3.10}$$

where s_1, s_2 ($=2s_1$), Z_1 and Z_2 ($=1.0005Z_1$) are constant.

Figure 4.3.3 (a) shows how FWR looks like in heterogeneous case. Note that in a non-uniform case even if it is rather simple in its structure, the FWR with three variables becomes too complicated to describe on 3D space, so that only the one on the κ–κ' plane at a certain ω is shown in Figure 4.3.3 (a). There are four spikes in one quadrant indicating the presence of two medium accommodating two resonance wavenumbers in mutual interaction. When we sweep the frequency, there appears a sequence of successive resonance frequencies.

The dispersion relation is shown in Figure 4.3.3 (b). We can see two straight lines, though they are a little vague, suggesting that there are two different phase velocities in the medium. The ravel time curve transformed from Figure 4.3.3 (b) is shown in Figure 4.3.4 (a). We can observe that the two impulses start to propagate towards leftward and rightward exactly from the set point of the initial excitation at $t=t_0$ and $x=L/8$, respectively. Then the waves propagate repeatedly both with reflection at and with transmission through the discontinuity points $x=L/4$ and $3L/4$. Here the periodical boundary conditions are also built in. Figure 4.3.4 (b) shows the ACROSS observable derived from dispersion relation. represents $v(\omega,x)$ converted from the dispersion relation (real part alone is shown), which is ACROSS observable.

Once we obtain the dispersion relation of particle velocity, travel time curves of physical quantities such as displacement ($u(t,x)=v(t,x)/i\omega$) and stress σ ($\sigma(t,x)=c(x)\partial u(t,x)/\partial x=-i\kappa c(x)u(t,x)$) are easily calculated as shown in Figures 4.3.4 (c) and (d), respectively.

4.3.5 Discussion and concluding remarks

The proposed theory appears valid as demonstrated in Figures 4.3.2 ~ 4.3.4, whereas numerical comparison with the analytic solution has not yet been made so far. The comparison with the analytic solution is to be made in order to know the extent of the numerical errors encountered in this theory.

We would like to address computational feasibility of the proposed method. Derivation of FWR, R_m from P_m in Equation (4.3.8) demands the inverse calculation of a very large matrix or the solution of the associated equations with a large degree of freedom. It requires arithmetic operations of $O(N^3)$ for a given ω in a one-dimensional case. Being more practical in a 3D problem, it amounts to $O(N^9)$ for each ω. If we take N=10^2, it becomes $O(10^{18})$. This amount of calculation appears quite feasible, since supercomputers with more than10 Tflops in performance are nowadays easily available. For example, if we utilized a supercomputer Fujitsu PRIMEPOWER HPC2500 with theoretical peak performance of 13.8 Tflops in the Information Technology Center, Nagoya University, which is open to researchers and graduate students throughout Japan, it would take about one day to solve the linear equations for each ω. The computation of the FWR is usually necessary at many discrete frequencies spanning wide range to compute the wave form by Fourier transform of FWR. However, use of SEA (Sompi Event Analysis) allow us to save significantly the number of discrete frequencies to compute FWR for deriving the arrival time and amplitude of isolated wave elements[3,4]. Therefore, we would be able to finalize the whole calculation in dozens of days, whereas it does not appear practical at this moment. However, the present theory of computing wave field in frequency domain would be recognized as useful within a few years, since the progress of computation technology is so fast.

References

[1] M. Kumazawa, K. Tsuruga, N. Shigeta, T. Nakajima and T. Nagai, Treatise of discontinuity in wave equation to derive linear system equation for computation of wave field, *Proceedings of the first International Workshop on "Active Monitoring in the Solid Earth Geophysics"*, 2004.

[2] for example, M. J. Lighthill, *An introduction to Fourier analysis and generalized functions*, Cambridge University Press, 1959.

[3] Y. Hasada, H. Kumagai and M. Kumazawa, Autoregressive modeling of transfer functions in frequency domain to determine complex travel times, *Earth Planets Space*, **53**, 3-11, 2001.

[4] Y. Hasada, M. Kumazawa, K. Tsuruga and T. Kunitomo, Travel time estimation from a transfer function in frequency domain: the revised Sompi event analysis, *JAEA-Research*, 2007-033, 4.2, 120-133, 2007.

Toru Nagai [1], Katsuya Ishii [1] and Mineo Kumazawa [2]

[1] Information Technology Center, Nagoya University,

[2] Tono Geoscientific Research Unit, JAEA

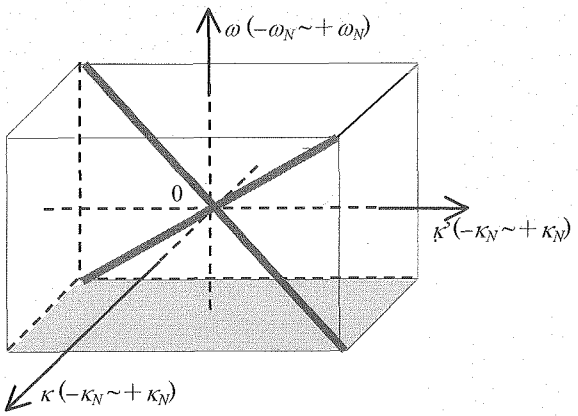

Figure 4.3.1 FWR of a uniform medium within the Nyquist range both in frequency and in wavenumbers.

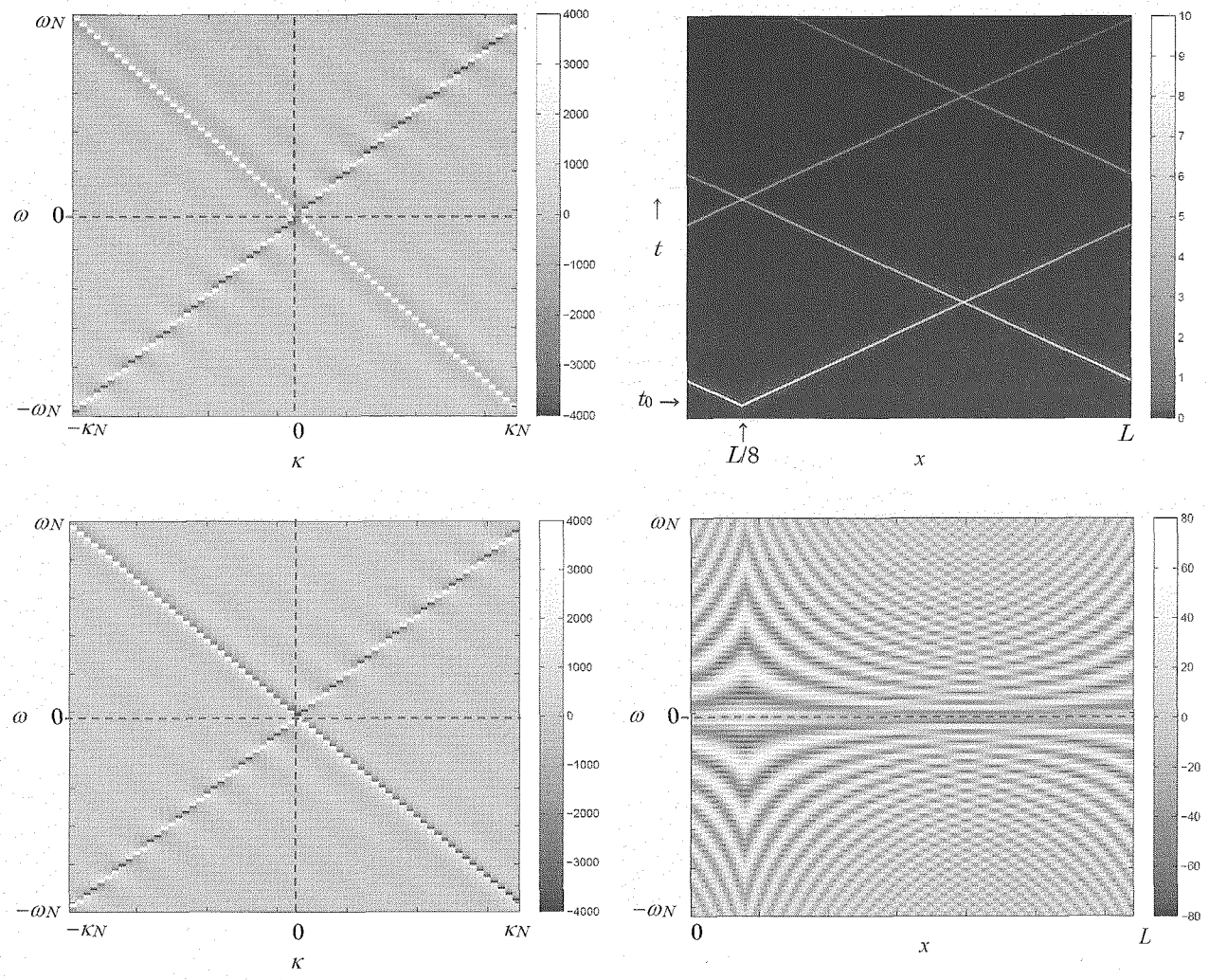

Figures 4.3.2 (a) Dispersion relation of particle velocity (left). The upper figure shows the real part of while the lower the imaginary part. (b) Travel time curve of particle velocity (top right). (c) Particle velocity in the space and frequency domains (bottom right). Note that $v(\omega, x)$ is ACROSS observable and that the real part alone is shown.

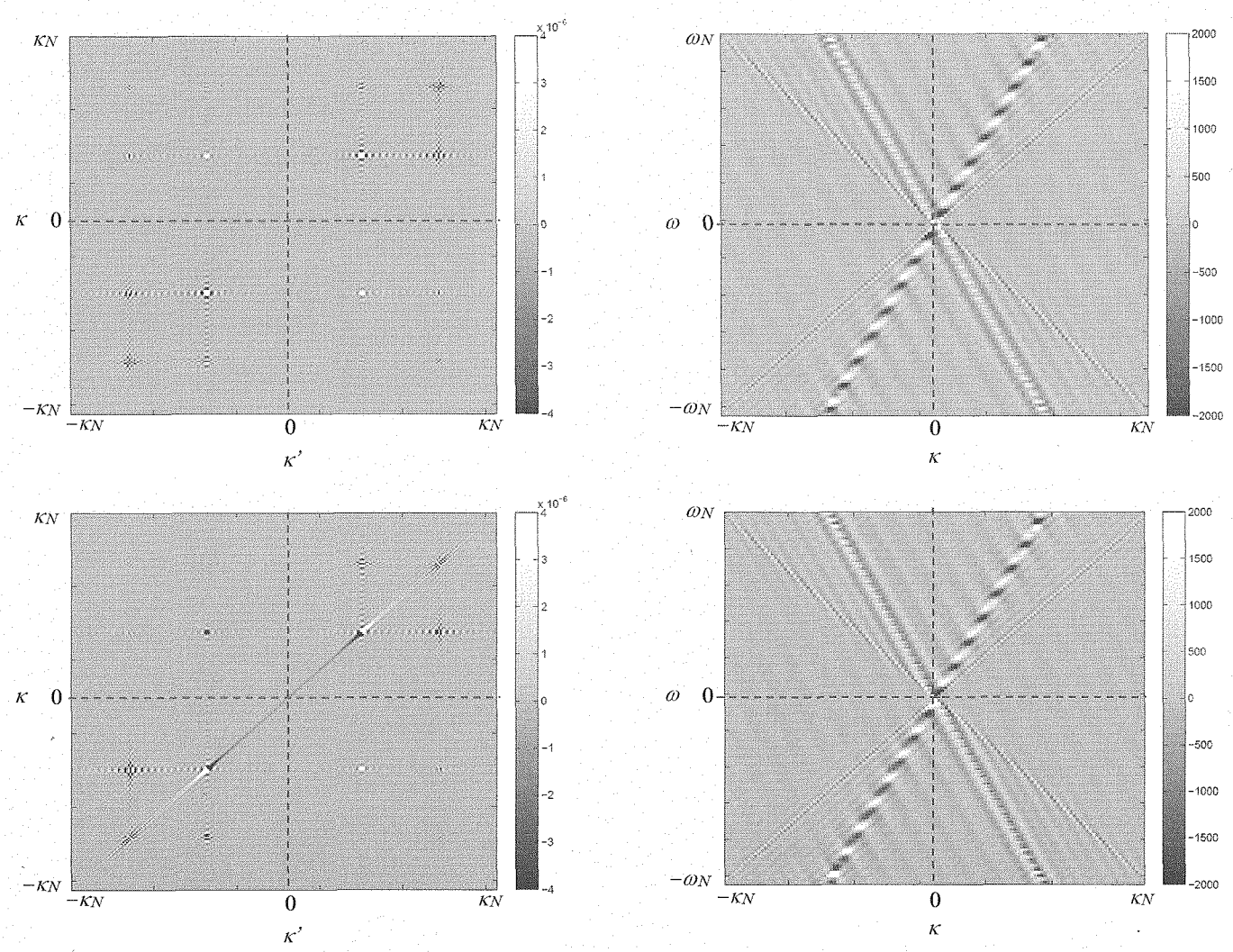

Figures 4.3.3 (a) FWR on the κ-κ' plane at a certain ω (left). The upper figure shows the real part of FWR while the lower the imaginary part. (b) Dispersion relation of particle velocity (right). The upper figure shows the real part of $\nu(\omega,\kappa)$ while the lower the imaginary part

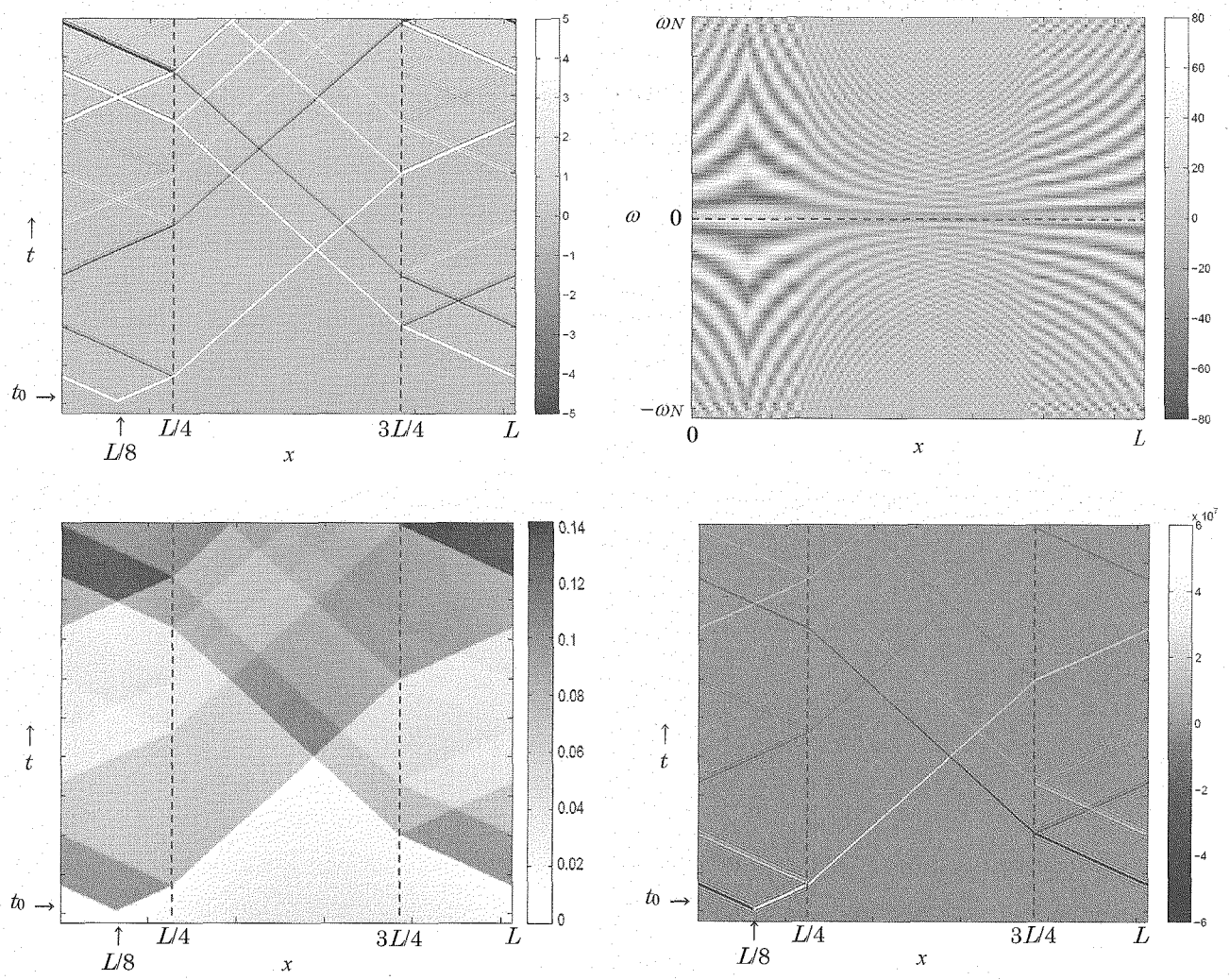

Figures 4.3.4 (a) Travel time curve of particle velocity (top left). Since the impedance contrast is set small (0.05% as shown in Equation (4.3.10)), the induced impulses transmit through the boundary many times in association with the generation of small amplitude reflection waves. (b) Particle velocity in the space and frequency domains (top right). Note that $v(\omega, x)$ is ACROSS observable and that the real part alone is shown. (c) Travel time curve of displacement (bottom left). Note that the center of gravity of the medium initially at rest starts to move with a constant velocity on impulse excitation, although it is difficult to confirm it quantitatively with this figure. (d) Travel time curve of stress (bottom right). Note that two stress impulses started at the point of excitation have opposite signs. This is contrasted to the velocity impulses shown in Figure (a).

5. Target of constant monitoring

5.1 Proposal: Detection of transient phenomena due to the structure sensitivity of rocks in the crust and uppermantle

5.1.1 Targets of constant monitoring

The most urgent target of our concerns is the constant monitoring of the physical states at and around the expected focal region of disastrous earthquakes in order to detect any diagnostic information useful for the prediction of the earthquakes. Before going to our ultimate target, however, we need to discuss the two types of backgrounds that would enable us to trace a reasonable approach towards our target. One is the tectonic environment of the relevant region, another is the physical processes leading to the time-evolution of the possible observables by remote monitoring observation.

Geologically active regions such as subduction zones are characterized by relatively short temporal variations of the crustal deformations associated with occurrence of earthquakes, movements of active faults and volcanic activities. Typical examples of such temporal variations other than the seismic and volcanic activities are the slow slip events (e.g. [1, 2]) and fluctuations in convergent rate of plate motions that are recently revealed by dense GPS networks (GEONET, Geographycal Survey Institute). In addition, deep non-volcanic tremors recognized in southwest Japan occurred intermittently to distribute along the strike of the subducting slab of Philippine Sea Plate (e.g. [3,5]). Intermittent occurrence of nonvolcanic deep tremors and associated slow slip events are confirmed to exist almost all subduction zones under some paticular conditions. These phenomena are thought to be associated with the movement of super critical fluid that could be released by the dehydration processes from the subducting slab.

Physical conditions of seismogenic regions have not been clarified in detail yet, but we have several models that may be useful to deepen our understandings. Whereas the deep-seated solid rocks had been considered traditionally quite stable without any significant change in their physical properties within a short time scale, our models, for example, have evolved to include the presence of variability and instability as a consequence of very small amount of 'water' contained in the textures of solid rocks as polycrystalline aggregates. The relevant physical characteristics is called 'structural sensitivity' in this paper by referring to the solid state physics as will be explained in detail later. The object of direct observation by ACROSS is addressed to 'wave-scattering sources' or shortly 'scatterers' in this paper just for convenience. This does not means to exclude the possible time-delay of wave propagation through a certain spatial distance from our research works.

Another important target of active monitoring is the stability of geologic environment underground constructions. One of the examples is the reservoirs of high-level radioactive wastes for

isolation. Whatever the geology of the site is, the reservoirs are surrounded by the polycrystalline aggregates containing water. Therefore, it is inevitable to concern with the 'structural sensitive scatterers' in this case, so it is useful to consider the relevant problems collectively. In this section, we discuss the possibilities to detect the transient as well as chronic variation caused by the structure sensitiveness, particularly associated with the movement of fluid phases (supercritical water, carbon dioxide, and etc.) expected in the crust and upper mantle of the Earth.

5.1.2 Structure sensitiveness of polycrystalline composite containing fluid

(1) Examples of Structure Sensitive Property

A relatively small volume fraction of "impurity" or distributed "heterogeneity" in a medium frequently plays an important role of whole mechanical behavior of the medium for chemical reactions, plastic deformations, and so on. Such phenomenon is recognized as the mechanism governed by the "structure sensitive" properties of the medium.

It is well known that a small amount of water causes a large decrease of the strength of rocks. The process that controls such strong changes of strength is thought to be the stress corrosion cracking, in a relatively shallow crustal condition. These mechanisms are typical examples of the structure sensitive characteristics of the silicate rocks.

(2) Microscopic View of the Structure Sensitiveness

In a dynamic behavior in the crust and upper mantle, property of small amount of special material sometimes controls whole process of the medium. For example, a small amount of water causes a large decrease of the strength of rocks. This phenomenon is normally understood as the stress corrosion mechanism, that is the hydrogen ions of water easily cut the Si-O bonds of silicate minerals in the crust and upper mantle condition. Another example will be observed in the permeable flow of fluids (volatiles) within the crust, in which the permeability depends strongly on the wetness and contiguity of pore spaces at the grain boundaries, joint structures and so on.

(3) Structure Sensitive Bodies

The term "structure sensitive" which has been used in material science is used here in more wide range of scales, from grain size to a few tens of kilometers. In addition, the "structure sensitive body" can be recognized as the temporal variations of the "scattering sources" among the distributed heterogeneities in a medium (e.g. [6]).

. In the crust and upper mantle, typical candidates of the "structure sensitive bodies" are (1) abnormally localized regions such as magma chamber beneath active volcanoes, and deeper extension of active faults, (2) beneath the seismogenic regions related to brittle-ductile transitions,

and (3) deeper part of sticked region of subducting plate boundaries (i.e. nearby regions of asperities at the subduction boundaries), and etc.

Networks of cracks and pathways of volatiles in surrounding rocks of a magma chamber can sensitively control the changes of volcanic activities on the migration of volcanic gasses, although the actual structure of the network could not be recognized. However, the scattering properties both for elastic and electromagnetic waves will largely be depend on the variations of the migrating gasses. The region beneath the active faults will be similar in terms of the structure sensitiveness due to the localization of deformations (See Figure 5.1.1(a) and (b)).

Temporal variations of scattering properties for elastic waves at brittle-ductile transition zone will not simply be expected, because it may need additional conditions such as the criticality of stress state, magnitude of heterogeneity of the medium, and so on.

Intermittent occurrences of the slip events are observed by dense GPS networks and these are attributed to the temporal changes of the friction conditions of fault surfaces and gauges along the plate subducting boundaries in surrounding regions of the asperities. It seems likely that the pore pressures could change with accumulated stress during inter seismic periods. Heterogeneous distributions of pore pressures can easily affect the friction conditions due to geometrical roughness of the fault surface and changes of mechanical properties of fault gauge material, although the amount of the reflectivity (or scattering properties) for elastic waves remain uncertain.

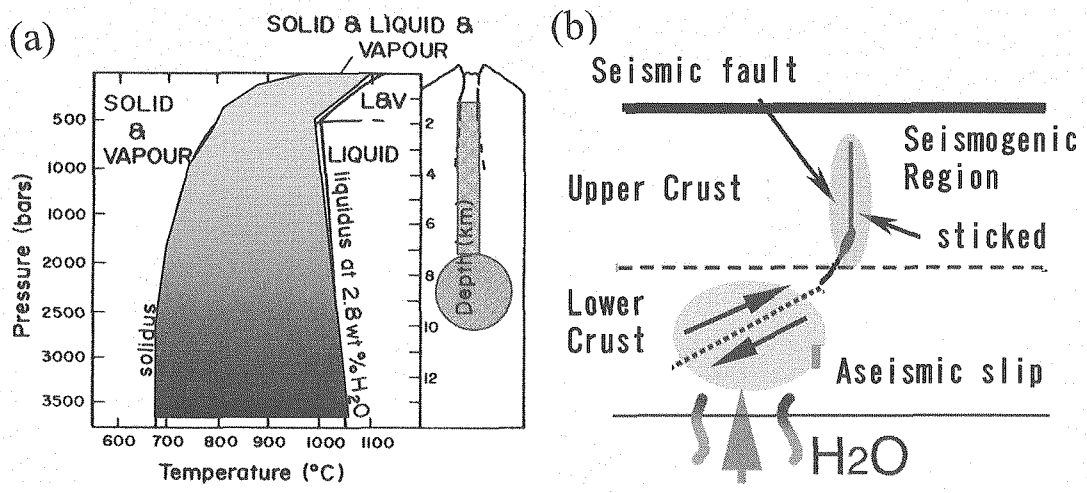

Figure 5.1.1. Examples of distribution of structure sensitive bodies; (a) Near magma chamber: Solid-Liquid-Vapor field for an andesitic magma with 2.8 wt% H_2O (After Burnham, 1972). (b)Aseismic slip beneath seismic faults; Slip is enhanced by super critical water beneath sticked seismic fault in the seismogenic region.

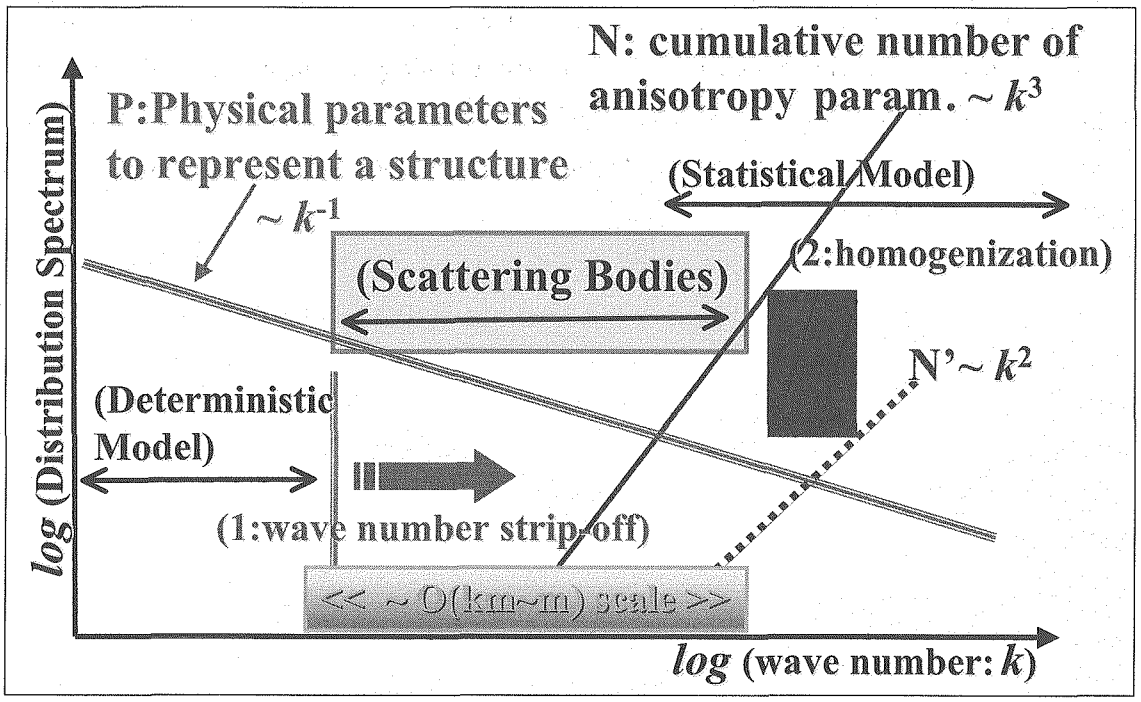

Figure 5.1.2. Logarithmic distribution spectrum of heterogeneities as a function of log (wave number) expected in the crust and upper mantle. Modeling of scattering bodies can be attributed between deterministic and statistical models.

5.1.3 Observables of structure sensitive bodies

Observable phenomena that cause temporal variations of stress field related to generations of earthquakes and volcanic eruptions could be mainly the reflected wave from "scattering sources". The heterogeneity in the lithosphere originated from both stress state and heterogeneous distribution of fluid-bearing rocks can be the "scattering sources". Temporal variation of the "scattering sources" due to the structure sensitivity of rocks is an essential characteristics of seismogenic regions as well as the active volcanic regions.

The spatial scale of the heterogeneity can be represented by deterministic models for sufficiently small wave number, while one needs to introduce statistical models for large wave number. Number of physical parameters to represent structure heterogeneity could be inversely proportional to the wave number, whereas number of anisotropy parameters would be proportional to 3rd power of wave number so that statistical models can only be used to represent heterogeneous structure with large wave number (Figure 5.1.2.). In case of monitoring by elastic wave, our targets of tectonically interesting are mostly between the two limiting cases. The scattering bodies of meters to tens of kilometers should be modeled with special care due to complex interactions among scaterers.

Among many structure sensitive phenomena, probable changes in the reflected seismic or electromagnetic signals are expected in the temporal variations of impedance and anisotropic dispersion of the transmitted signals in the subduction zone where the "scattering sources" are evolving associated with the movement of the fluid mainly composed of supercritical water in the crust and upper mantle conditions.

The active geophysical monitoring would be the essential tool to detect and clarify such an evolving process that governed by the "structure sensitivity of rocks" in the crust and upper mantle. Recently discovered slow slip events and deep non-volcanic tremors in the subduction zone could be one of the most challenging targets to clarify their characteristics by using the active monitoring techniques.

(1) Scattering Sources by Structure Sensitive Bodies

It is noteworthy to point out that the scattering sources are not always structure sensitive, because all heterogeneities in the lithosphere can scatter the elastic and electromagnetic waves.

As the rocks are composed of polycrystalline minerals, the macroscopical material properties, such as electromagnetic (dielectric coefficients) and elastic properties under high pressures and high temperatures conditions, normally insensitive to the small stress changes during the dynamical processes in the crust and upper-mantle.

Although the Moho discontinuity and the upper surface of the slab seem to be the most strong reflection boundary in the subduction zones, these heterogeneities would not be "structure sensitive" but material boundaries. Relatively short temporal variations of such boundaries are not expected. Once fluids were introduced into such reflection boundaries, however, the scattering properties (reflectivity or impedance, and complex dielectric coefficients) will strongly be affected due to the presence of water.

(2) Anisotropy and Dispersion of Structure Sensitive Bodies

Main characteristic properties of the structure sensitive bodies are anisotropy due to orientation distribution of microcracks and dispersion due to the attenuation. Both properties are observable macroscopically, because the orientation distribution of microcracks and permeable structure due to network of cracks and pores can be affected by the deformation process and stress orientation in a media.

There are two anisotropies: one is azimuthal and another is polarization. The former includes the anisotropic orientation distribution of microcracks due to geological evolution of tectonic stresses that could only change with long time scale (i.e. more than thousands of years). The latter can be strongly affected by the local deformation and stress state and possible to change with time.

Polarization anisotropy is likely to change with time associated to the movement of fluid through network of pores and cracks so that the impedance of scattering source can easily change with time.

The dispersion of transmitted waves can also change easily with the re-distribution of fluids in the network of pores and cracks. As the mechanisms that can produce the dispersion are so complex that we need to investigate more in detail in future.

(3) Temporal Variations of Reflectors at Subducting Boundary

A seismic reflector at the subducting boundary of the Philippine Sea Plate was clearly identified by the Tokai seismic experiment (e.g. [7~10]). Estimated depth of the reflector is 30 ~ 50 km depending on the model. It is suggested that the deeper extension of the Tokai Earthquake fault can be a good reflector, although the reflective property is not clearly understood. If the reflection could be caused by high pore pressures due to the geometrical roughness of the boundary, time scale of the variation of reflective property could be similar to the recurrence time of the Tokai Earthquake (~100 years). The active monitoring of this reflector is one of the most exciting target to investigate in further detail.

5.1.4 Discussions and conclusions

We discussed here the possible characteristics of the temporal variations of scattering sources, particularly focused on the scattering properties due to the structure sensitive bodies.

Typical candidates of the "structure sensitive bodies" are discussed for three types of the scattering sources: (1) abnormally localized regions such as magma chamber beneath active volcanoes, and deeper extension of active faults, (2) beneath the seismogenic regions related to brittle-ductile transitions, and (3) deeper part of sticked region of subducting plate boundaries (i.e. nearby regions of asperities at the subduction boundaries), and etc.

Observable properties for the three types of the scattering sources that are caused by temporal variations of stress field related to generations of earthquakes and volcanic eruptions can be modeled through analyses of the transmitted elastic and electromagnetic waves. The heterogeneity in the lithosphere originated from both stress state and heterogeneous distribution of fluid included rocks can be the "scattering sources" (eg. [6, 11]). Temporal variation of the "scattering sources" due to the structure sensitivity is an essential characteristics of seismogenic regions as well as the active volcanic regions.

It is pointed out that the scattering sources are not always structure sensitive, because all heterogeneities in the lithosphere can scatter the elastic and electromagnetic waves.

Polarization anisotropy and dispersion of transmitted waves are candidates for the observable properties of the temporal variations of scattering sources due to the structure sensitive bodies, however, the mechanisms governed to emerge these phenomena have not clearly understood.

The actual changes of the polarization anisotropy and dispersion relation depend on the processes of the movement of water vapor (or the fluid mainly composed of supercritical water) through the

networks of cracks and pores, so that we need to develop models and analysis methods for the properties of scattering sources.

The quantitative estimates for the possibility to detect the temporal changes of scattering properties by the structure sensitive bodies await for the future investigation.

Acknowledgment

We thank all the workers interested in the active monitoring of the underground for their enthusiastic discussions on the relevant subjects.

References

[1] Hirose, H., K. Hirahara, F. Kimata, N. Fujii & S. Miyazaki, A slow thrust slip event following the two 1996 Hyuganada earthquakes beneath the Bungo channel, southwest Japan, Geophys. Res. Lett., 26, 3237-3240, 1999.

[2] Dragert, H., Wang, K. & James, T. S., A silent slip event on the deeper Cascadia subduction interface. Science 292, 1525–1528, 2001.

[3] Obara, K., Nonvolcanic deep tremor associated with subduction in southwest Japan, Science 296, 1679–1681, 2002.

[4] Rogers, G., and H. Dragert, Episodic tremor and slip on the Cascadia subduction zone: The chatter of silent slip, Science, 300, 1942– 1943, 2003.

[5] Obara, K., Hitoshi Hirose, Fumio Yamamizu, and Keiji Kasahara, Episodic slow slip events accompanied by non-volcanic tremors in southwest Japan subduction zone, GRL., vol. 31, L23602, doi:10.1029/2004GL020848, 2004.

[6] Sato, H. and M. C. Fehler, *Seismic Wave Propagation and Scattering in the Heterogeneous Earth*, Springer-Verlag, New York, 1998.

[7] Iidaka, T., T. Iwasaki, T. Takeda, T. Moriya, I. Kumakawa, E. Kurashimo, T. Kawamura, F. Yamazaki, K. Koike and G. Aoki: Configuration of subducting Philippine Sea plate and crustal structure in the central Japan region. Geophy. Res. Letters, 30, No. 5, 1219-1222, 2003.

[8] Kasahara, J., K. Tsuruga, Y. Hasada, K. Yamaoka, N. Fujii, Y. Yoshida, T. Kunitomo, and M. Kumazawa, A proposal of imaging of the plate boundary using the active monitoring method, in "Proc. International workshop on Active Monitoring in the solid Earth geophysics",(S2-03), 44-48, Mizunami, Japan, 2004.

[9] Tsuruga, K., J. Kasahara, H. Mikada, K. Yamaoka, and N. Fujii, Mapping non-asperities and continuous, active monitoring of the interior of the Earth's crust. Jour. of Geogra., 115(No.1), 51-71, 2006. (In Japanese with English abstract)

[10] Kasahara, J., K. Tsuruga, H. Mikada, K. Yamaoka, and N. Fujii, Time Lapse Approach in the Study of Earthquake Generation -Geophysical Exploration of Asperities-Reflectors System (EARS) for Interplate Earthquake Generation along a Subducting Oceanic Plate, BUTSURI-TANSA, Vol.59, No.6, 300-XX, 2007.

[11] Fujii, N. and M. Kumazawa, Detection of Transient Phenomena Due to the Structure Sensitivity of Rocks in the Crust and Uppermantle, in "Proc. International workshop on Active Monitoring in the solid Earth geophysics", (S7-P05), 353-354, Mizunami, Japan, 2004.

[12] Fujii, N., V. Korneev, J. Kasahara, H. Higashihara, S. Goldin, I. Chichinin, R. Unger, M. Zhdanov, V. Seleznev and M. Kumazawa, First International Workshop on 'Active Monitoring in the Solid Earth Geophysics', Trans. EOS, vol.86, No.91, 92-94, March 2005. (IWAM04): (June 30 - July 2, 2004 in Mizunami city, Japan), (paper ID. 2004ES000884R)

Naoyuki FUJII and Mineo KUMAZAWA
Tono Geoscientific Research Unit, JAEA

Acknowledgement

The present program was supported by Tono Geoscience Center of PNC (Power Reactor and Nuclear Fuel Development Corporation) that subsequently reorganized to JNC (Japan Nuclear Cycle Development Institute), and further to JAEA (Japan Atomic Energy Agency). The research workers of ACROSS Research Team have been supported by many personals (past and present) of Tono Geoscience Center and Horonobe Underground Research Laboratory; Minoru Yamakawa, Kazuhiro Aoki, Noboru Nakatsuka, Tatsumi Hanaki, Shinichi Yamasaki, Seietsu Takeda, Naotaka Shigeta, Tatsuo Fukushima, Tsuneari Ishimaru, Osamu Fujiwara, Tsuyoshi Nohara, Akira Takami, Kazuyuki Matsusue, Noboru Furukawa, Yasunori Abe, Masaru Nakamura, Tatsuo Saito and many others. We also thank to Hiromichi Higashihara of JCEAM (Japanese Consortium of Earth's Active Monitoring) for his advice and encouragement on the present work and also Katsuro Ogawa and Koshun Yamaoka at Nagoya University (now at the University of Tokyo) for their cooperation.

We also thank Dr. Takanobu Kamataki for his editorial works on this publication.

Appendix: Authors of the report

1. Introduction

Mineo KUMAZAWA[1], Takahiro KUNITOMO[1]
and Takahiro NAKAJIMA[1]

2. Seismic ACROSS

2.1 Overview of Seismic ACROSS and its development

Takahiro KUNITOMO[1] and Mineo KUMAZAWA[1]

2.2 Transmitting and receiving technologies of the Seismic ACROSS

Takahiro KUNITOMO[1] and Mineo KUMAZAWA[1]

2.3 Field examples at the Tono mine ACROSS experimental site

Takahiro KUNITOMO[1] and Mineo KUMAZAWA[1]

2.4 A dense seismic array for acquisition of high quality data in the ACROSS observation

Kayoko TSURUGA[2], Takahiro KUNITOMO[1],
Yoko HASADA[3], Mineo KUMAZAWA[1],
Naotaka SHIGETA[4] and Junzo KASAHARA[5]

3. EM-ACROSS

3.1 Overview of EM-ACROSS and its development

Takahiro NAKAJIMA[1], Mineo KUMAZAWA[1],
Naotaka SHIGETA[4], Takahiro KUNITOMO[1],
Hiromichi NAGAO[6] and Hiroshi MATSUMOTO[7]

3.2 Long-term operation of the EM-ACROSS and derived transfer function in the diffusion field region

Takahiro NAKAJIMA[1], Takahiro KUNITOMO[1],
Hiromichi NAGAO[6], Mineo KUMAZAWA[1]
and Naotaka SHIGETA[4]

3.3 Complex dielectric permittivity spectroscopy using ACROSS measurement system

Hiroshi MATSUMOTO[7], Naotaka SHIGETA[4],
Mineo KUMAZAWA[1] and Takahiro NAKAJIMA[1]

4. Theory of data analysis and modeling

4.1 Optimum weighted stacking method for acquisition of the ACROSS transfer functions having the maximum signal-to-noise ratio

Hiromichi NAGAO[6], Takahiro NAKAJIMA[1],

Mineo KUMAZAWA[1] and Takahiro KUNITOMO[1]

4.2 Travel time estimation from a transfer function in frequency domain: the revised Sompi event analysis

Yoko HASADA[3], Mineo KUMAZAWA[1],
Kayoko TSURUGA[2] and Takahiro KUNITOMO[1]

4.3 Numerical computation of wave fields and frequency wavenumber response characteristics of an isolated linear dynamic system

Toru NAGAI[8], Katsuya Ishii[8]
and Mineo KUMAZAWA[1]

5. Target of constant monitoring in the Earth's interiors: Transient phenomena due to the structure sensitivity of polycrystalline rocks

Naoyuki FUJII[1] and Mineo KUMAZAWA[1]

[1] Invited Researcher of Tono Geoscientific Research Unit, Japan Atomic Energy Agency
[2] Invited Researcher of Science and Technology for Earthquake Environments' project lead by Japan Nuclear Cycle Development Institute (now Japan Atomic Energy Agency), now at The University of Tokyo
[3] Invited Researcher of Science and Technology for Earthquake Environments' project lead by Japan Nuclear Cycle Development Institute (now Japan Atomic Energy Agency), now at Nagoya University
[4] Horonobe Underground Research Unit, Geological Isolation Research and Development Directorate, JAEA
[5] Invited Researcher of Science and Technology for Earthquake Environments' project lead by Japan Nuclear Cycle Development Institute (now Japan Atomic Energy Agency), now at Japan Continental Shelf Survey, Co. Ltd., Japan
[6] Invited Researcher of Science and Technology for Earthquake Environments' project lead by Japan Nuclear Cycle Development Institute (now Japan Atomic Energy Agency), now at Japan Agency for Marin-Earth Science and Technology
[7] Post-Doctoral Fellow of Japan Nuclear Cycle Development Institute (now Japan Atomic Energy Agency), now at Toyama University
[8] Nagoya University

This is a blank page.

国際単位系（SI）

表１．SI 基本単位

基本量	SI 基本単位	
	名称	記号
長さ	メートル	m
質量	キログラム	kg
時間	秒	s
電流	アンペア	A
熱力学温度	ケルビン	K
物質量	モル	mol
光度	カンデラ	cd

表２．基本単位を用いて表されるSI組立単位の例

組立量	SI 基本単位	
	名称	記号
面積	平方メートル	m^2
体積	立法メートル	m^3
速さ，速度	メートル毎秒	m/s
加速度	メートル毎秒毎秒	m/s^2
波数	毎メートル	m^{-1}
密度（質量密度）	キログラム毎立法メートル	kg/m^3
質量体積（比体積）	立法メートル毎キログラム	m^3/kg
電流密度	アンペア毎平方メートル	A/m^2
磁界の強さ	アンペア毎メートル	A/m
（物質量の）濃度	モル毎立方メートル	mol/m^3
輝度	カンデラ毎平方メートル	cd/m^2
屈折率	（数の）1	1

表５．SI 接頭語

乗数	接頭語	記号	乗数	接頭語	記号
10^{24}	ヨタ	Y	10^{-1}	デシ	d
10^{21}	ゼタ	Z	10^{-2}	センチ	c
10^{18}	エクサ	E	10^{-3}	ミリ	m
10^{15}	ペタ	P	10^{-6}	マイクロ	μ
10^{12}	テラ	T	10^{-9}	ナノ	n
10^{9}	ギガ	G	10^{-12}	ピコ	p
10^{6}	メガ	M	10^{-15}	フェムト	f
10^{3}	キロ	k	10^{-18}	アト	a
10^{2}	ヘクト	h	10^{-21}	ゼプト	z
10^{1}	デカ	da	10^{-24}	ヨクト	y

表３．固有の名称とその独自の記号で表されるSI組立単位

組立量	SI 組立単位			
	名称	記号	他のSI単位による表し方	SI基本単位による表し方
平面角	ラジアン(a)	rad		$m \cdot m^{-1}=1$(b)
立体角	ステラジアン(a)	sr(c)		$m^2 \cdot m^{-2}=1$(b)
周波数	ヘルツ	Hz		s^{-1}
力	ニュートン	N		$m \cdot kg \cdot s^{-2}$
圧力，応力	パスカル	Pa	N/m^2	$m^{-1} \cdot kg \cdot s^{-2}$
エネルギー，仕事，熱量	ジュール	J	N・m	$m^2 \cdot kg \cdot s^{-2}$
工率，放射束	ワット	W	J/s	$m^2 \cdot kg \cdot s^{-3}$
電荷，電気量	クーロン	C		s・A
電位差（電圧），起電力	ボルト	V	W/A	$m^2 \cdot kg \cdot s^{-3} \cdot A^{-1}$
静電容量	ファラド	F	C/V	$m^{-2} \cdot kg^{-1} \cdot s^4 \cdot A^2$
電気抵抗	オーム	Ω	V/A	$m^2 \cdot kg \cdot s^{-3} \cdot A^{-2}$
コンダクタンス	ジーメンス	S	A/V	$m^{-2} \cdot kg^{-1} \cdot s^3 \cdot A^2$
磁束	ウエーバ	Wb	V・s	$m^2 \cdot kg \cdot s^{-2} \cdot A^{-1}$
磁束密度	テスラ	T	Wb/m^2	$kg \cdot s^{-2} \cdot A^{-1}$
インダクタンス	ヘンリー	H	Wb/A	$m^2 \cdot kg \cdot s^{-2} \cdot A^{-2}$
セルシウス温度	セルシウス度(d)	℃		K
光束	ルーメン	lm	cd・sr(c)	$m^2 \cdot m^{-2} \cdot cd=cd$
照度	ルクス	lx	lm/m^2	$m^2 \cdot m^{-4} \cdot cd=m^{-2} \cdot cd$
（放射性核種の）放射能	ベクレル	Bq		s^{-1}
吸収線量，質量エネルギー分与，カーマ	グレイ	Gy	J/kg	$m^2 \cdot s^{-2}$
線量当量，周辺線量当量，方向性線量当量，個人線量当量，組織線量当	シーベルト	Sv	J/kg	$m^2 \cdot s^{-2}$

(a)ラジアン及びステラジアンの使用は、同じ次元であっても異なった性質をもった量を区別するときの組立単位の表し方として利点がある。組立単位を形作るときのいくつかの用例は表４に示されている。
(b)実際には、使用する時には記号rad及びsrが用いられるが、習慣として組立単位としての記号“１”は明示されない。
(c)測光学では、ステラジアンの名称と記号srを単位の表し方の中にそのまま維持している。
(d)この単位は、例としてミリセルシウス度m℃のようにSI接頭語を伴って用いても良い。

表４．単位の中に固有の名称とその独自の記号を含むSI組立単位の例

組立量	SI 組立単位		
	名称	記号	SI 基本単位による表し方
粘度	パスカル秒	Pa・s	$m^{-1} \cdot kg \cdot s^{-1}$
力のモーメント	ニュートンメートル	N・m	$m^2 \cdot kg \cdot s^{-2}$
表面張力	ニュートン毎メートル	N/m	$kg \cdot s^{-2}$
角速度	ラジアン毎秒	rad/s	$m \cdot m^{-1} \cdot s^{-1}=s^{-1}$
角加速度	ラジアン毎平方秒	rad/s^2	$m \cdot m^{-1} \cdot s^{-2}=s^{-2}$
熱流密度，放射照度	ワット毎平方メートル	W/m^2	$kg \cdot s^{-3}$
熱容量，エントロピー	ジュール毎ケルビン	J/K	$m^2 \cdot kg \cdot s^{-2} \cdot K^{-1}$
質量熱容量（比熱容量），質量エントロピー	ジュール毎キログラム毎ケルビン	J/(kg・K)	$m^2 \cdot s^{-2} \cdot K^{-1}$
質量エネルギー（比エネルギー）	ジュール毎キログラム	J/kg	$m^2 \cdot s^{-2} \cdot K^{-1}$
熱伝導率	ワット毎メートル毎ケルビン	W/(m・K)	$m \cdot kg \cdot s^{-3} \cdot K^{-1}$
体積エネルギー	ジュール毎立方メートル	J/m^3	$m^{-1} \cdot kg \cdot s^{-2}$
電界の強さ	ボルト毎メートル	V/m	$m \cdot kg \cdot s^{-3} \cdot A^{-1}$
体積電荷	クーロン毎立方メートル	C/m^3	$m^{-3} \cdot s \cdot A$
電気変位	クーロン毎平方メートル	C/m^2	$m^{-2} \cdot s \cdot A$
誘電率	ファラド毎メートル	F/m	$m^{-3} \cdot kg^{-1} \cdot s^4 \cdot A^2$
透磁率	ヘンリー毎メートル	H/m	$m \cdot kg \cdot s^{-2} \cdot A^{-2}$
モルエネルギー	ジュール毎モル	J/mol	$m^2 \cdot kg \cdot s^{-2} \cdot mol^{-1}$
モルエントロピー，モル熱容量	ジュール毎モル毎ケルビン	J/(mol・K)	$m^2 \cdot kg \cdot s^{-2} \cdot K^{-1} \cdot mol^{-1}$
照射線量（X線及びγ線）	クーロン毎キログラム	C/kg	$kg^{-1} \cdot s \cdot A$
吸収線量率	グレイ毎秒	Gy/s	$m^2 \cdot s^{-3}$
放射強度	ワット毎ステラジアン	W/sr	$m^4 \cdot m^{-2} \cdot kg \cdot s^{-3}=m^2 \cdot kg \cdot s^{-3}$
放射輝度	ワット毎平方メートル毎ステラジアン	$W/(m^2 \cdot sr)$	$m^2 \cdot m^{-2} \cdot kg \cdot s^{-3}=kg \cdot s^{-3}$

表６．国際単位系と併用されるが国際単位系に属さない単位

名称	記号	SI 単位による値
分	min	1 min=60s
時	h	1h =60 min=3600 s
日	d	1 d=24 h=86400 s
度	°	1° =(π/180) rad
分	’	1’ =(1/60)° =(π/10800) rad
秒	”	1” =(1/60)’ =(π/648000) rad
リットル	l、L	1l=1 $dm^3=10^{-3}m^3$
トン	t	1t=10^3 kg
ネーパ	Np	1Np=1
ベル	B	1B=(1/2)ln10(Np)

表７．国際単位系と併用されこれに属さない単位でSI単位で表される数値が実験的に得られるもの

名称	記号	SI 単位であらわされる数値
電子ボルト	eV	$1eV=1.60217733(49) \times 10^{-19}J$
統一原子質量単位	u	$1u=1.6605402(10) \times 10^{-27}kg$
天文単位	ua	$1ua=1.49597870691(30) \times 10^{11}m$

表８．国際単位系に属さないが国際単位系と併用されるその他の単位

名称	記号	SI 単位であらわされる数値
海里		1海里=1852m
ノット		1ノット=1海里毎時=(1852/3600)m/s
アール	a	1 a=1 $dam^2=10^2m^2$
ヘクタール	ha	1 ha=1 $hm^2=10^4m^2$
バール	bar	1 bar=0.1MPa=100kPa=1000hPa=10^5Pa
オングストローム	Å	1 Å=0.1nm=10^{-10}m
バーン	b	1 b=100$fm^2=10^{-28}m^2$

表９．固有の名称を含むCGS組立単位

名称	記号	SI 単位であらわされる数値
エルグ	erg	1 erg=10^{-7} J
ダイン	dyn	1 dyn=10^{-5}N
ポアズ	P	1 P=1 dyn・s/cm^2=0.1Pa・s
ストークス	St	1 St =1$cm^2/s=10^{-4}m^2/s$
ガウス	G	1 G ^10^{-4}T
エルステッド	Oe	1 Oe ^(1000/4π)A/m
マクスウェル	Mx	1 Mx ^10^{-8}Wb
スチルブ	sb	1 sb =1cd/$cm^2=10^4cd/m^2$
ホト	ph	1 ph=10^4lx
ガル	Gal	1 Gal =1cm/$s^2=10^{-2}m/s^2$

表10．国際単位に属さないその他の単位の例

名称	記号	SI 単位であらわされる数値
キュリー	Ci	1 Ci=3.7×10^{10}Bq
レントゲン	R	1 R = 2.58×10^{-4}C/kg
ラド	rad	1 rad=1cGy=10^{-2}Gy
レム	rem	1 rem=1 cSv=10^{-2}Sv
X線単位		1X unit=1.002×10^{-4}nm
ガンマ	γ	1γ=1 nT=10^{-9}T
ジャンスキー	Jy	1 Jy=$10^{-26}W \cdot m^{-2} \cdot Hz^{-1}$
フェルミ		1 fermi=1 fm=10^{-15}m
メートル系カラット		1 metric carat = 200 mg = 2×10^{-4}kg
トル	Torr	1 Torr = (101 325/760) Pa
標準大気圧	atm	1 atm = 101 325 Pa
カロリー	cal	
ミクロン	μ	1 μ =1μm=10^{-6}m

（第７版，1998年改訂）